

博士論文（要約）

A Study on Application of  
Persistent Homology to  
Nonlinear Time Series  
Analysis

（非線形時系列解析に対するパーシステント・  
ホモロジーの応用に関する研究）

辻 祥太郎



# Abstract

Persistent homology is a concept used in the field of topological data analysis. Homology groups represent the topological features of a shape: connected components, holes, voids, and so on. On computers, a shape is often given as a point cloud. A growing sequence of a shape, or a filtered simplicial complex is constructed from a point cloud. Persistent homology groups represent the appearance and the disappearance of the topological features of a filtered simplicial complex.

The nonlinear time series analysis provides a method to reconstruct an orbit in the phase space from an observed time series. The method is called attractor reconstruction. Attractor reconstruction is achieved with delay-coordinates. Delay-coordinates map observed values into a vector which consists of time delayed values.

The combination of persistent homology and attractor reconstruction enables us to compute the shape of an orbit. The topological features of reconstructed attractors are used to detect such dynamical properties as the periodicity of the observed signal or to classify the signals.

It is needed to select the time delay of delay-coordinates. The thesis investigated a criterion to select the delay and observed the behavior of the criterion applied to periodic signals and chaotic signals. The thesis proposed an index called the most significant death value (MSDV) and the criterion that the delay that maximizes an MSDV should be selected. The thesis observed that the criterion was effective for several non-chaotic signals with periodicity. However, the criterion was not effective for several chaotically periodic signals. The thesis compared the criterion with the mutual information, which is a method widely used to select the delay. The criterion produced the results better than the mutual information. Although the results did not give a complete solution, it may give us an insight to use the combination of persistent homology and attractor reconstruction.

The computation of the persistent homology of more than thousand points sometimes takes more than a day. It also takes more than hundred gigabytes of memory. The thesis proposed a method to make the computational time faster and the computational space smaller as long as the input is a continuous curve. The input time series was assumed to be continuous and the curve was assumed to be given as a set of sampled points. The proposed method obtained the line segments approximating to the given curve and computed the persistent homology of the line segments, instead of the points. The computational time of the proposed method was made ten times or more faster and its computational space was made ten times or more smaller. The proposed method also smoothed out the noise of data. It is obvious that these results are useful for the

practical applications of the combination of persistent homology and attractor reconstruction.

**Keywords:** persistent homology, attractor reconstruction, delay-coordinates, Takens' theorem, Vietoris-Rips complex.

# Preface

This thesis presents the studies on the combination of persistent homology and attractor reconstruction. The thesis is the fruits of my efforts to make the combination practical. The research was like a play without plot. The motive for the research was simply interest. I learnt the algebraic topology in a lecture four years ago. I have got interested in computing the homology groups of data, instead of computing the homology groups of topological spaces by hand. Then I encountered persistent homology, namely a computational method of homology. I knew the concept of attractor reconstruction in the current laboratory. It was natural that I came up with their combination. Although several researchers have already proposed the combination and its applications, I was interested in the behavior of the method for periodic signals and chaotic signals. This study is presented in Chapter 3. While I was working on the study, I suffered from the long time of computing the persistent homology. I solved this obstacle with the simple idea for continuous time series data. The computational time was made faster with an approximation method. The second study is presented in Chapter 4.

Chapter 2 introduces the mathematical foundations of the concepts used in the studies. Section 2.1 offers the definitions and the explanations on persistent homology and related concepts. Section 2.2 explains the concept of attractor reconstruction and Takens' theorem. Section 2.3 provides the definition of Bézier curves and the method for fitting them to sampled points. Chapter 3 and Chapter 4 gives the methods and the results of my studies. Chapter 3 explains the study of persistent homology and attractor reconstruction. Chapter 4 explains the study that speeds up the computation of persistent homology of continuous curves. Finally Chapter 5 presents the conclusion of the thesis.

I would like to express gratitude to my supervisor Professor Kazuyuki Aihara for his support for my research. It goes without saying that his support was important. I would like to thank the referees for my doctoral thesis: Professor Satoru Iwata, Professor Tomonori Sei, Professor Takaaki Ohnishi, and Professor Hiroshi Kori. They gave me useful comments for revising my thesis. I thank the rest of the members of the Aihara Laboratory. Finally, I thank the University of Tokyo–NEC Future AI scholarship for financial support.

Shotaro Tsuji  
Tokyo, Japan, 2019.

# Contents

<b>1</b>	<b>Introduction</b>	<b>1</b>
1.1	Overview to Topics . . . . .	2
1.1.1	Differential Equations . . . . .	2
1.1.2	Method of Delays . . . . .	8
1.1.3	Homology and Topological Persistence . . . . .	10
1.2	Related Work . . . . .	20
1.2.1	Information Extracted from Dynamical Systems . . . . .	20
1.2.2	Topology of Attractors . . . . .	22
1.2.3	Speeding up the Computation of Persistent Homology . . . . .	24
1.2.4	Selection of the Delay Time . . . . .	25
1.3	Contribution of the Thesis . . . . .	26
<b>2</b>	<b>Mathematical Foundations</b>	<b>28</b>
2.1	Persistent Homology for Topological Data Analysis . . . . .	28
2.1.1	Simplex . . . . .	29
2.1.2	Simplicial Complex . . . . .	31
2.1.3	Chain Complex . . . . .	33
2.1.4	Homology Group . . . . .	39
2.1.5	Persistent Homology . . . . .	41
2.1.6	Persistence Diagram . . . . .	54
2.1.7	Čech Complex and Vietoris-Rips Complex . . . . .	55
2.1.8	Witness Complex . . . . .	57
2.1.9	Stability . . . . .	58
2.2	Attractor Reconstruction and Takens' Theorem . . . . .	59
2.3	Bézier Curve and Its Fitting . . . . .	60
<b>3</b>	<b>Attractor Reconstruction and Persistent Homology</b>	<b>63</b>
3.1	Proposed Criterion . . . . .	64
3.2	Methods . . . . .	67
3.2.1	Materials . . . . .	67
3.2.2	Procedure . . . . .	68
3.3	Results . . . . .	68
3.4	Discussion . . . . .	69
3.4.1	Dynamical Systems . . . . .	69
3.4.2	Japanese Vowel /a/ . . . . .	71
3.4.3	Comparison with Mutual Information . . . . .	72

<b>4 Vietoris-Rips Complex of Line Segments</b>	<b>80</b>
4.1 Proposed Methods . . . . .	81
4.1.1 Getting Approximating Line Segments . . . . .	81
4.1.2 Vietoris-Rips Complex of Line Segments . . . . .	81
4.2 Results and Discussion . . . . .	82
4.2.1 Irrational Flow on 2-torus . . . . .	82
4.2.2 Japanese Vowels . . . . .	83
<b>5 Conclusion</b>	<b>87</b>
<b>Bibliography</b>	<b>88</b>

# List of Figures

1.1	The harmonic oscillator ( $k/m = 1$ ). (a) The vector field of Equation (1.1.7) and (b) the solution with initial condition $(x_0, y_0) = (1, 0)$ . The color scale indicates the time. The solution was numerically developed with the fourth order Runge-Kutta method. The step size was set to 0.01 and the number of the steps was 630.	4
1.2	The damped oscillator ( $\omega = 1, \alpha = 0.5$ ). (a) The vector field of Equation (1.1.10) and (b) the solution with initial condition $(x_0, y_0) = (1, 0)$ . The color scale indicates the time. The solution was numerically developed with the fourth order Runge-Kutta method. The step size was set to 0.01 and the number of the steps was 2000.	5
1.3	The van der Pol equation ( $\mu = 1$ ). (a) The vector field of the van der Pol equation, (b) the solution of the van der Pol equation with the initial condition $(v_0, w_0) = (0.1, 0)$ , and (c) the solution with the initial condition $(v_0, w_0) = (-2, -2)$ . The color scale indicates the time. The solutions were developed with the fourth order Runge-Kutta method. The step size was set to 0.01 and the number of the steps was 4000.	7
1.4	The Lorenz attractor numerically developed by the fourth order Runge-Kutta method, where the step size was set to 0.01 and the initial condition was $(x, y, z) = (1, 1, 0)$ . The color scale indicates the time.	8
1.5	The projections of Lorenz attractor. The Lorenz attractor shown in Figure 1.4 is projected onto (a) the $xy$ -plane, (b) the $xz$ -plane, and (c) the $yz$ -plane. The color scale indicates the time. The first 20000 points were omitted because they were not in the attractor.	9
1.6	The Lorenz attractor numerically developed by the fourth order Runge-Kutta method, where the step size was set to 0.01 and the initial condition was the point $(x, y, z) = (1, 1.00001, 0)$ . The color scale indicates the time.	10
1.7	The comparison of two orbits of the Lorenz system with different initial conditions from $t = 0$ to $t = 300$ . The purple line is the $x$ -coordinate of the orbit with the initial condition $(x, y, z) = (1, 1, 0)$ and the green line is the $x$ -coordinate of the orbit with the initial condition $(x, y, z) = (1, 1.00001, 0)$ .	11
1.8	A successful case of a reconstructed Lorenz attractor: The time delay and the embedding dimension were set to $a = 10$ and $n = 3$ . The color scale indicates the time.	12

1.9	A reconstructed Lorenz attractor: The time delay and the embedding dimension were set to $a = 1$ and $n = 3$ . The color scale indicates the time. . . . .	12
1.10	A reconstructed Lorenz attractor: The time delay and the embedding dimension were set to $a = 100$ and $n = 3$ . The color scale indicates the time. . . . .	13
1.11	Examples of simplices. . . . .	13
1.12	The condition of simplicial complices: (a) A simplicial complex. (b) A shape which is not a simplicial complex. . . . .	14
1.13	An example of triangulation. A circle (a) is homeomorphic to a simplicial complex (b). . . . .	15
1.14	The boundary of a simplicial complex: (a) A simplicial complex, and (b) the boundary of the simplicial complex. The numbers 0, 1, 2, and 3 are the labels of the vertices. . . . .	15
1.15	Sublevel sets of a function and topological persistence. A continuous function and the threshold values of sublevel sets (left) and the sublevel sets of the thresholds (right). . . . .	17
1.16	An example of the growing of the Vietoris-Rips complex. (a,c,e,g) The points and the balls. (b,d,f,h) The Vietoris-Rips complices. . . . .	19
1.17	The persistence diagrams of the Vietoris-Rips complex in Figure 1.16. The horizontal axis indicates the birth scale and it ranges from 0 to 1. The vertical axis indicates the death scale; it ranges from 0 to 1 and it have an additional tick which indicates infinity. A grid is added to help people to read the values. . . . .	20
3.1	The signal and its FFT spectrum of the Japanese vowel /a/. . . . .	69
3.2	The $x$ -coordinate and its FFT spectrum of the limit cycle of the van der Pol equation ( $\mu = 10$ ). . . . .	70
3.3	The $x$ -coordinate and its FFT spectrum of the Rössler attractor. . . . .	71
3.4	The $x$ -coordinate and its FFT spectrum of the Lorenz attractor. . . . .	72
3.5	Most significant death values of the harmonic oscillator. The horizontal axis represents the delay divided by the period $T = 628$ , and the vertical axis the most significant death values. The lowest line is the case of embedding dimension two. The embedding dimension is in an increasing order. The x marks plotted in the graph represent the points where $a = \frac{1}{n} \frac{T}{2}$ . (Copyright©2019 IEICE, (Tsuji and Aihara, 2019a: Figure 9)) . . . . .	73
3.6	Most significant death values of the van der Pol system with $\mu = 10$ . The horizontal axis represents the delay divided by the period $T = 1908$ , and the vertical axis the most significant death values. The lowest line is the case of embedding dimension two. The embedding dimension is in an increasing order. The x marks plotted in the graph represent the points where $a = \frac{1}{n} \frac{T}{2}$ . (Copyright©2019 IEICE, (Tsuji and Aihara, 2019a: Figure 10)) . . . . .	73

3.7	Most significant death values of the Rössler attractor. The vertical axis represents the delay divided by the characteristic period $T = 625$ , and the horizontal axis the most significant death values. The lowest line is the case of embedding dimension two. The embedding dimension is in an increasing order. The x marks plotted in the graph represent the points where $a = \frac{1}{n} \frac{T}{2}$ . (Copyright©2019 IEICE, (Tsuiji and Aihara, 2019a: Figure 11)) . . . .	74
3.8	Most significant death values of the Lorenz attractor. The vertical axis represents the delay divided by the characteristic period $T = 58$ , and the horizontal axis the most significant death values. The lowest line is the case of embedding dimension two. The embedding dimension is in an increasing order. The x marks plotted in the graph represent the points where $a = \frac{1}{n} \frac{T}{2}$ . (Copyright©2019 IEICE, (Tsuiji and Aihara, 2019a: Figure 12)) . . . .	74
3.9	Most significant death values of the Japanese Vowel /a/. The horizontal axis is the delay divided by the characteristic period $T = 170$ , and the vertical axis the most significant death values. The lowest line is the case of embedding dimension two. The embedding dimension is in an increasing order. The x marks plotted in the graph represent the points where $a = \frac{1}{n} \frac{T}{2}$ . (Copyright©2019 IEICE, (Tsuiji and Aihara, 2019a: Figure 13)) . . . .	74
3.10	A reconstructed trajectory of the harmonic oscillator with delay time $a = 62$ and embedding dimension $n = 5$ . The axes of this plot represent principal components and the color scale indicates the time. This delay was chosen to satisfy the equation $an = T/2$ . (Copyright©2019 IEICE, (Tsuiji and Aihara, 2019a: Figure 14)) .	75
3.11	A reconstructed limit cycle of the van der Pol system with delay time $a = 191$ and embedding dimension $n = 5$ . The axes of this plot represent principal components and the color scale indicates the time. This delay was chosen to satisfy the equation $a = T/2$ . (Copyright©2019 IEICE, (Tsuiji and Aihara, 2019a: Figure 15)) .	75
3.12	A reconstructed Rössler attractor with delay time $a = 62$ and embedding dimension $n = 5$ . The axes of this plot represent principal components and the color scale indicates the time. This delay was chosen to satisfy the equation $an = T/2$ . (Copyright©2019 IEICE, (Tsuiji and Aihara, 2019a: Figure 16)) . . . . .	75
3.13	A reconstructed Rössler attractor with delay time $a = 198$ and embedding dimension $n = 5$ . The axes of this plot represent principal components and the color scale indicates the time. This delay attains the first peak of the graph. (Copyright©2019 IEICE, (Tsuiji and Aihara, 2019a: Figure 17)) . . . . .	76
3.14	A reconstructed Rössler attractor with delay time $a = 125$ and embedding dimension equal $n = 5$ . The axes of this plot represent principal components and the color scale indicates the time. (Copyright©2019 IEICE, (Tsuiji and Aihara, 2019a: Figure 18)) .	76
3.15	A reconstructed Rössler attractor with delay time $a = 125$ and embedding dimension $n = 10$ . The axes of this plot represent principal components and the color scale indicates the time. (Copyright©2019 IEICE, (Tsuiji and Aihara, 2019a: Figure 19)) .	76

3.16	A reconstructed Lorenz attractor with delay time $a = 6$ and embedding dimension $n = 5$ . The axes of this plot represent principal components and the color scale indicates the time. This delay was chosen to satisfy the equation $an = T/2$ . (Copyright©2019 IEICE, (Tsuiji and Aihara, 2019a: Figure 20)) . . . . .	77
3.17	A reconstructed Lorenz attractor with delay time $a = 22$ and embedding dimension $n = 5$ . The axes of this plot represent principal components and the color scale indicates the time. This delay was chosen to the delay attains the maximum of the MSDV. (Copyright©2019 IEICE, (Tsuiji and Aihara, 2019a: Figure 21)) .	77
3.18	A reconstructed attractor of Japanese vowel /a/. The delay time was $a = 12$ and the embedding dimension was $n = 10$ . The axes of this plot represent principal components and the color scale indicates the time. This delay was chosen to maximize the most significant death value. (Copyright©2019 IEICE, (Tsuiji and Aihara, 2019a: Figure 22)) . . . . .	77
3.19	First persistence diagram of a reconstructed attractor of the Japanese vowel /a/. The delay time was $a = 12$ and the embedding dimension was $n = 10$ . This delay was chosen to maximize the most significant death value. The horizontal axis represents the birth filtration value and the vertical axis the death filtration value. (Copyright©2019 IEICE, (Tsuiji and Aihara, 2019a: Figure 23)) .	78
3.20	Plots of mutual information versus delay. The horizontal axis represents the delay normalized by the period or the characteristic period and the vertical axis the mutual information between $x(t)$ and $x(t + a)$ . A “+” mark represents the first minimum on the graph. . . . .	79
4.1	Comparison of the performance of the ordinary method and the proposed method. . . . .	84
4.2	Bottleneck distance between the original data of 2-torus and the noised data of that. The left-side blank bars show the distances between the original and the ordinary Vietoris-Rips complex of the noised data. The right-side hatched bars show the distances between the original and the Vietoris-Rips complex of the segments fitted to the noised data ©2019 IEEE. . . . .	85

# List of Tables

1.1	The persistence pairs of the Vietoris-Rips complex in Figure 1.16.	20
2.1	Persistence pairs in Example 2.1.47 . . . . .	54
4.1	Performance comparison of computing the persistent homology of speech signals ©2019 IEEE. . . . .	86
4.2	The comparison of the bottleneck distances between the ordinary method and the proposed method (left) and those between the ordinary method and the witness complex (right) ©2019 IEEE. .	86

# Chapter 1

## Introduction

Dynamics occurs everywhere. In physics, the motion of an object is described by differential equations. In biology, the behavior of cells is also described by differential equations. In other fields, such as climatology, sociology, economics, etc., differential equations are used to make a model of a phenomenon. If it is not easy to describe phenomena as differential equations, it may be governed by some differential equations.

A set of observed time series data is given but the differential equations that govern them are unknown. The observed time series data may not be governed by the same differential equations; different phenomena may be observed as time series data. How we can distinguish the observed time series data from each other?

Suppose that observed time series data is an orbit of an ordinary differential equation. Information at several scales can be acquired from an orbit. At local scale, the Lyapunov exponent and the fractal dimensions reflect the characteristics of the differential equations. At middle scale, the branched manifold, which is a projection of an attractor made by identifying two orbits if they become equal as the time approaches infinity, provides the behavior of orbits. At global scale, the embedding manifold, which encloses an orbit, gives a clue to the structure of the differential equation.

The aim of this thesis is to provide practical means of extracting the global information of an orbit. The topology of the embedding manifold of an orbit is extracted. Researchers have investigated such method. In last five years, persistent homology groups have been used to extract the topology of embedding manifolds. Persistent homology groups are the homology groups with topological persistence. Homology groups are topological invariants of a space and they represent the connected components, the holes, the voids, and higher dimensional holes of the given space. Topological persistence is a notion how long each topological entity lives as the space changes.

The computation of the persistent homology groups of observed time series data relies on the delay-coordinate space. The observed time series data is mapped into the delay-coordinate space in order to reconstruct the shape of the orbit in the original phase space. The delay-coordinate space has two parameters: the delay time and the embedding dimension. It is important to select the proper delay time and the proper embedding dimension. If improper parameters are selected, the shape of the orbit is not reconstructed. This thesis

attempts to find a criterion to select the delay time when periodic or recurrent time series data is given. Although the embedding dimension is also important and they relate to each other, I focused on the delay time only.

There is another problem. The computational time and space required to compute persistent homology groups are quite long and large. This thesis proposes a method to reduce them provided that the input is a smooth curve. It requires more than ten times shorter time and smaller space.

The works in this thesis realize the practical use of the persistent homology groups of time series data.

Section 1.1 gives a brief and illustrated introduction on differential equations, the delay-coordinates, and persistent homology. It is wished that the section help readers to understand what will be handled in the thesis by intuition. Section 1.2 provides brief reviews on related works. It shows a brief history of computing the homology of attractors. It also shows applications and problems of persistent homology and delay-coordinates in recent years. Section 1.3 summarizes the contribution of this thesis.

## 1.1 Overview to Topics

### 1.1.1 Differential Equations

Differential equations are equations which contains the derivatives of the variables. Although there are several forms of differential equations, the simplest form is shown here:

$$\frac{dx}{dt} = f(x), \quad (1.1.1)$$

where  $x \in \mathbb{R}^d$  and  $f : \mathbb{R}^d \rightarrow \mathbb{R}^d$ . The differential equations in this form are called autonomous systems. The set of pairs  $(x, f(x))$  is called the vector field of the differential equations. By integrating the differential equation with an initial condition  $x_0 = x(t_0)$ , we obtain a curve starting from the point  $x_0$ , which is called an orbit.

On computers, numerical methods are used to solve differential equations. The simplest and most basic method is the explicit Euler method (Strogatz, 2014: p. 32). The idea of the explicit Euler method is to use the difference of the variable as an approximation to the derivative. Let  $h$  be a step size. The difference of the variable  $x$  in Equation (1.1.1) which is an approximation to  $dx/dt$  is written as

$$\frac{dx}{dt}(t) \approx \frac{x(t+h) - x(t)}{h}. \quad (1.1.2)$$

Let  $t_0$  be the initial time and let  $t_n = hn + t_0$ . We obtain the following difference equation from Equation (1.1.1) and Equation (1.1.2):

$$x(t_{n+1}) = x(t_n) + hf(x(t_n)). \quad (1.1.3)$$

By solving Equation (1.1.3), a numerical solution of Equation (1.1.1), which is an approximation to an orbit, is obtained.

Because the numerical solution of the Euler method has the error on the order of  $O(h)$ . It is common to use more accurate methods. The fourth order

Runge-Kutta method (Strogatz, 2014: p33) is often employed. It is defined as follows. Let  $x_n = x(t_n)$ . Define the following four numbers:

$$\begin{cases} k_1 &= hf(x_n), \\ k_2 &= hf(x_n + \frac{k_1}{2}), \\ k_3 &= hf(x_n + \frac{k_2}{2}), \\ k_4 &= hf(x_n + k_3). \end{cases} \quad (1.1.4)$$

The difference equation of the Runge-Kutta method is defined as

$$x_{n+1} = x_n + \frac{1}{6}(k_1 + 2k_2 + 2k_3 + k_4). \quad (1.1.5)$$

The error of the solution of the Runge-Kutta method is on the order of  $O(h^4)$ .

Several examples of ordinary differential equations are introduced in order to help the readers to understand this thesis. Some of the systems introduced below appear in later chapters.

The first example is the harmonic oscillator, which represents the motion of a mass on a spring. One side of the spring is fixed and another side has a mass  $m$ . Suppose that the spring is an ideal spring. Let  $x$  denote the displacement of the mass from the fixed side of the spring. From the Newton's equation and the Fooke's law, we obtain the following equation:

$$m \frac{d^2x}{dt^2} = -kx. \quad (1.1.6)$$

By dividing the both side of the equation above by  $m$  and introducing a new variable  $y = dx/dt$ , we obtain the differential equations

$$\begin{cases} \frac{dx}{dt} &= y, \\ \frac{dy}{dt} &= -\frac{k}{m}x. \end{cases} \quad (1.1.7)$$

The vector field of Equation (1.1.7) is shown in Figure 1.1a.

The solution of this system can be obtained by hand. It is written as

$$x(t) = A \cos\left(\sqrt{\frac{k}{m}}t\right) + B \sin\left(\sqrt{\frac{k}{m}}t\right), \quad (1.1.8)$$

where  $A$  and  $B$  are constants determined by the initial conditions.

Figure 1.1b shows a numerical solution of Equation (1.1.7), where  $k/m = 1$ . The initial condition is set to  $(x_0, y_0) = (1.0, 0.0)$ . The orbit is a circle as the exact solution in Equation (1.1.8) says.

The damped oscillator is a system modified from the harmonic oscillator. The frictional force proportional to the velocity is added. A damping term is added to Equation (1.1.6):

$$\frac{d^2x}{dt^2} + \alpha \frac{dx}{dt} + \omega^2 x = 0, \quad (1.1.9)$$

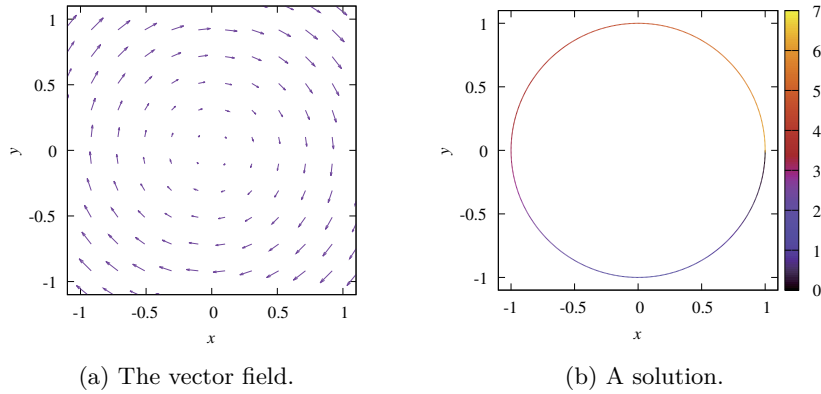


Figure 1.1: The harmonic oscillator ( $k/m = 1$ ). (a) The vector field of Equation (1.1.7) and (b) the solution with initial condition  $(x_0, y_0) = (1, 0)$ . The color scale indicates the time. The solution was numerically developed with the fourth order Runge-Kutta method. The step size was set to 0.01 and the number of the steps was 630.

where the parameter  $\alpha$  is a positive real value. The equation above is rewritten as

$$\begin{cases} \frac{dx}{dt} = y, \\ \frac{dy}{dt} = -\omega^2 x - \alpha y. \end{cases} \quad (1.1.10)$$

The vector field of Equation (1.1.10) is shown in Figure 1.2a. The arrows spiral to the origin, which means orbits go to the origin as the time increases.

Although this system can be solved algebraically, I show only a numerical solution in Figure 1.2b. The amplitude of oscillation decreases as the time goes. The shape of an orbit is different from the harmonic oscillator. It spirals to the origin.

Balthasar van der Pol (Van der Pol, 1926) thought that the case where the sign of the second term of Equation (1.1.9) is reversed. In this case, the amplitude of an orbit increases to infinity as the time approaches to infinity. Such behavior is physically unrealizable. Hence he replaced the parameter  $\alpha$  by the expression  $\alpha - 3\gamma x^2$ , where  $\gamma$  is a positive real value. This replacement makes the value of the second term positive at a certain amplitude. The equation obtained is shown below:

$$\frac{d^2 x}{dt^2} - (\alpha - 3\gamma x^2) \frac{dx}{dt} + \omega^2 x = 0. \quad (1.1.11)$$

By changing the units of the variables with the equations

$$\begin{cases} \omega t = t', \\ x = \sqrt{\frac{\alpha}{3\gamma}} v, \end{cases} \quad (1.1.12)$$

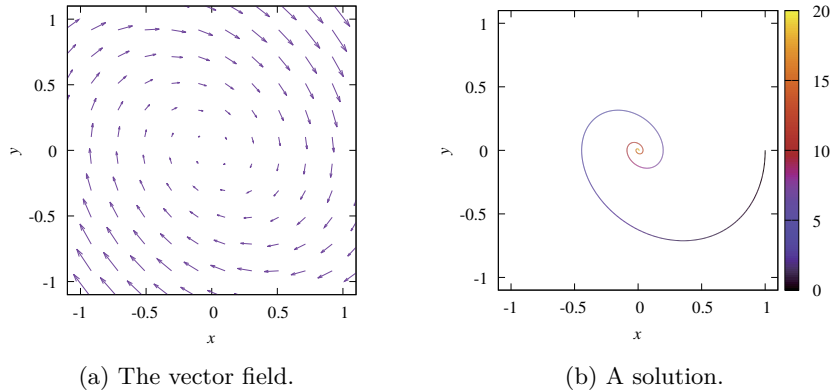


Figure 1.2: The damped oscillator ( $\omega = 1$ ,  $\alpha = 0.5$ ). (a) The vector field of Equation (1.1.10) and (b) the solution with initial condition  $(x_0, y_0) = (1, 0)$ . The color scale indicates the time. The solution was numerically developed with the fourth order Runge-Kutta method. The step size was set to 0.01 and the number of the steps was 2000.

and letting  $\mu = x/\omega$ , we obtain the differential equation

$$\frac{d^2v}{dt^2} - \mu(1 - v^2)\frac{dv}{dt} + v = 0. \quad (1.1.13)$$

This equation is rewritten as

$$\begin{cases} \frac{dv}{dt} = w, \\ \frac{dw}{dt} = \mu(1 - v^2)w - v. \end{cases} \quad (1.1.14)$$

The vector field of Equation (1.1.14) with  $\mu = 1.0$  is shown in Figure 1.3a.

The van der Pol system has the notable property; it has a certain set called attractor to which the orbits approach. Figure 1.3b shows the attractor of the van der Pol system. This type of attractor is called limit cycle because it is a periodic orbit and is the limit of an orbit as the time approaches to infinity. An orbit with an other initial condition is also attracted to this limit cycle. For example, Figure 1.3c shows an orbit starts from the point  $(v, w) = (-2.0, -2.0)$ . What does cause such behavior?

First, it is important to know the vector field around the fixed points. The fixed points are where orbits on them do not move. The value of the vector field on a fixed point is zero. The van der Pol system has one fixed point: the origin.

Because it is difficult to know the behavior of nonlinear differential equations, we linearize the vector field around fixed points. From Taylor's theorem, the linear approximation at the point  $x_*$  of the right-hand side Equation (1.1.1) is

$$f(x) = f(x_*) + J_{x_*}f(x - x_*) + o(|x - x_*|), \quad (1.1.15)$$

where  $J_{x_*}f$  is the Jacobian of  $f$  at  $x_*$  and the little o notation. Since  $x_*$  is a

fixed point, the linear approximation of Equation (1.1.1) is written as

$$\frac{dx}{dt} \approx J_{x_*} f(x - x_*). \quad (1.1.16)$$

By some calculation, we obtain the linear approximation of the van der Pol system at the origin:

$$\begin{cases} \frac{dv}{dt} = w, \\ \frac{dw}{dt} = -v + \mu w. \end{cases} \quad (1.1.17)$$

In the cases where  $\mu > 0$ , the values of solution of Equation (1.1.17) increase as the time increases. The orbits starting from the points inside the limit cycle approach to the limit cycle.

Although I do not enter the details, in order to prove the existence of the limit cycle, the nullclines and Poincaré-Bendixson theorem are needed (Strogatz, 2014: p. 150). The nullclines are the sets such that each coordinate of the vector field is zero. For example, from Equation (1.1.14), the nullclines of the van der Pol system are the curves  $w = 0$  and  $w = v/\mu(1 - v^2)$ . It is easy to know to the direction of the orbits on the nullclines. Poincaré-Bendixson theorem states that if a compact subset in a plane has no fixed point then there is a limit cycle.

The harmonic oscillator and the van der Pol system have periodic solutions. Below I introduce differential equations which have the orbits that are not periodic but pass near to the points where they have already passed. The most famous system with such property is the Lorenz system (Lorenz, 1963).

The Lorenz system originates from a problem of fluid mechanics. It is a simplification of partial differential equations which are derived to study a convection in a layer of fluid of a uniform depth. Prior to Lorenz, Saltzman (1962) derived ordinary differential equations from that partial differential equations by expanding the functions in double Fourier series. Then Lorenz truncated them and obtained the following differential equations, called the Lorenz system.

$$\begin{cases} \frac{dx}{dt} = -\sigma x + \sigma y, \\ \frac{dy}{dt} = -xz + rx - y, \\ \frac{dz}{dt} = xy - bz, \end{cases} \quad (1.1.18)$$

where  $\sigma$ ,  $r$ , and  $b$  are parameters. The parameter  $r$  is related to the Reyleigh number.

For all values of the parameters, the Lorenz system has a fixed point at the origin:  $(0, 0, 0)$ . If  $r > 1$  holds, it has two more fixed points:

$$(\sqrt{b(r-1)}, \sqrt{b(r-1)}, r-1), (-\sqrt{b(r-1)}, -\sqrt{b(r-1)}, r-1).$$

It is known that when the parameters are  $\sigma = 10$ ,  $r = 28$ , and  $b = 8/3$  the orbits exhibit interesting behavior. Figure 1.4 shows an orbit which starts from the point  $(x, y, z) = (1, 1, 0)$ . Figure 1.5a, Figure 1.5b, and Figure 1.5c shows the orbit projected to the  $xy$ -plane, the  $xz$ -plane, and the  $yz$ -plane respectively.

The orbit in Figure 1.4 stays in a certain region. In fact this region is an attractor, called the Lorenz attractor. It attracts the orbits starting from nearby points except on the  $z$ -axis.

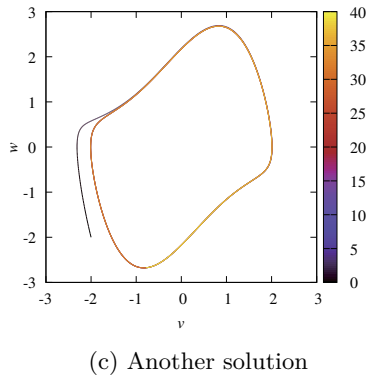
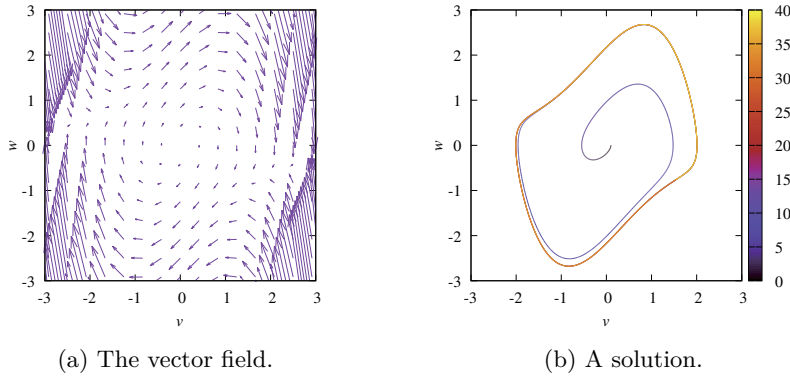


Figure 1.3: The van der Pol equation ( $\mu = 1$ ). (a) The vector field of the van der Pol equation, (b) the solution of the van der Pol equation with the initial condition  $(v_0, w_0) = (0.1, 0)$ , and (c) the solution with the initial condition  $(v_0, w_0) = (-2, -2)$ . The color scale indicates the time. The solutions were developed with the fourth order Runge-Kutta method. The step size was set to 0.01 and the number of the steps was 4000.

The Lorenz attractor has two large holes. The fixed points except the origin, which is located approximately at  $(8.46, 8.46, 27)$  and  $(-8.46, -8.46, 27)$  in this case, is in the holes. It can be considered that the holes of an attractor correspond to the fixed points.

More precisely, there should be one more hole in the attractor. On the  $z$ -axis, from Equation (1.1.18) the vector field of the Lorenz system is written as follows:

$$\begin{cases} \frac{dx}{dt} = 0, \\ \frac{dy}{dt} = 0, \\ \frac{dz}{dt} = -bz. \end{cases} \quad (1.1.19)$$

The points on the  $z$ -axis cannot go out of the  $z$ -axis and they sink down to the origin since  $dz/dt = -bz$  if  $b > 0$ . Although the origin is outside the attractor,

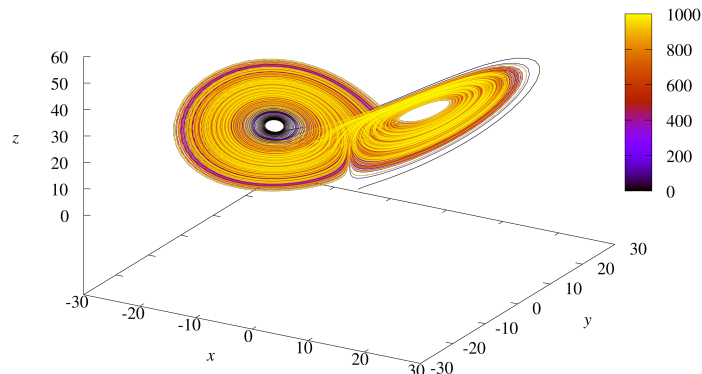


Figure 1.4: The Lorenz attractor numerically developed by the fourth order Runge-Kutta method, where the step size was set to 0.01 and the initial condition was  $(x, y, z) = (1, 1, 0)$ . The color scale indicates the time.

it can be considered that the  $z$ -axis is a fixed point of the attractor.

It is worth noting that the Lorenz attractor is an example of strange attractors. A strange attractor is an attractor which is sensitive to initial conditions (Strogatz, 2014: p. 333). Figure 1.7 shows two orbits with different initial conditions developed from  $t = 0$  to  $t = 300$ . Two lines are the values of the  $x$ -coordinate of the orbits. The purple line has the initial condition  $(x_0, y_0, z_0) = (1, 1, 0)$  and the green line has the initial condition  $(x_0, y_0, z_0) = (1, 1.00001, 0)$ . The slight difference of initial conditions makes different development of the orbits. The two lines in Figure 1.7 have almost the same value until  $t = 25$ . After that time they take different values but they exhibit the similar behavior.

The two orbits make the similar shapes in the phase space. Figure 1.6 shows the orbit with the initial condition  $(x_0, y_0, z_0) = (1, 1.00001, 0)$ . Compared to Figure 1.4, two orbits are attracted into the same attractor. Thus the shape of an orbit in the phase space can be used to characterize and to identify time series data.

This thesis focuses on the topology of orbits. Persistent homology is employed for computing the topology. It is a variant of homology groups, which summarizes the information of the holes of a shape. Before giving a brief introduction of persistent homology, the methods of delays is introduced in order to recover orbits from observed time series data.

### 1.1.2 Method of Delays

Through the examples introduced in the previous section, the shape of an orbit in the phase space seems to be useful to distinguish time series data. Suppose the following situation: We observe time series data with certain measuring machine; and the observed data may be a projection from the phase space. In such a situation, we have to succeed in reconstructing the shape of an orbit in the original phase space.

The method of delays or attractor reconstruction enables us to obtain the shapes of orbits equivalent to the original shapes. The delay-coordinates defined below are used to lift the observed time series up into a higher dimensional

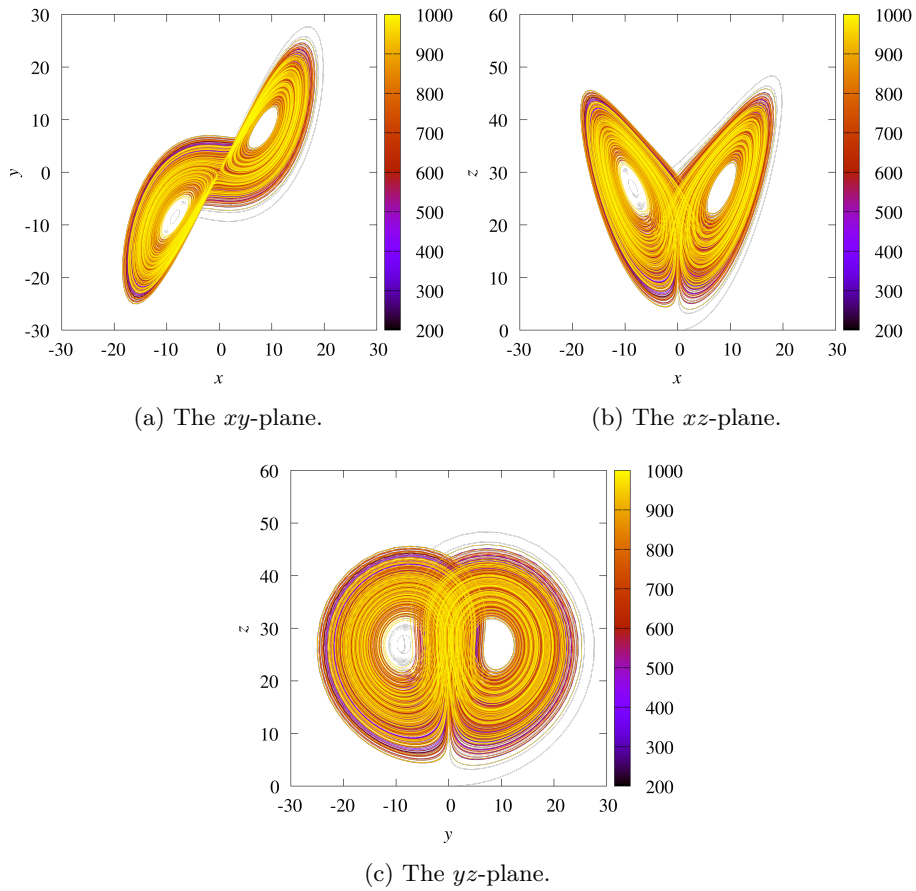


Figure 1.5: The projections of Lorenz attractor. The Lorenz attractor shown in Figure 1.4 is projected onto (a) the  $xy$ -plane, (b) the  $xz$ -plane, and (c) the  $yz$ -plane. The color scale indicates the time. The first 20000 points were omitted because they were not in the attractor.

Euclidean space:

$$y(t) = (x(t), x(t - a), x(t - 2a), \dots, x(t - (n - 1)a)), \quad (1.1.20)$$

or

$$y(t) = (x(t), x(t + a), x(t + 2a), \dots, x(t + (n - 1)a)), \quad (1.1.21)$$

where  $a$  is the time delay,  $n$  is the embedding dimension, and  $x(t)$  is the observed time series. The details of the delay-coordinates are explained in Section 2.2.

Let us see some examples of the delay-coordinates. The time series of the  $x$ -coordinate of the Lorenz attractor shown in Figure 1.4 will be mapped into a set of delay-coordinates. The delay-coordinates of three dimensions with a time delay of ten steps is a successful case. Figure 1.8 shows the reconstructed Lorenz attractor with the delay-coordinates of  $a = 10$  and  $n = 3$ . The reconstructed attractor has two holes and it is same as the attractor in the original phase space.

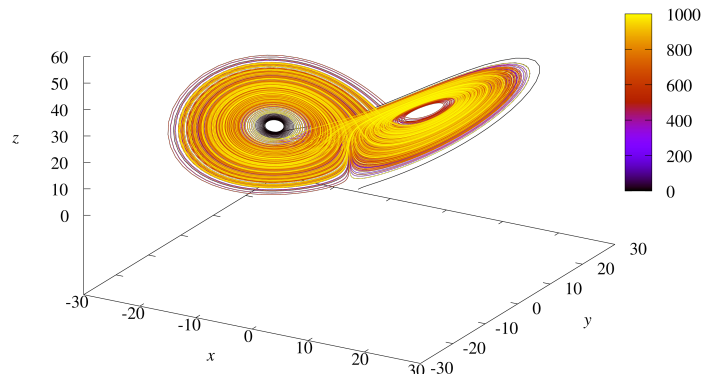


Figure 1.6: The Lorenz attractor numerically developed by the fourth order Runge-Kutta method, where the step size was set to 0.01 and the initial condition was the point  $(x, y, z) = (1, 1.00001, 0)$ . The color scale indicates the time.

An improper choice of the time delay leads to a poor reconstruction. The reconstructed Lorenz attractor mapped with the delay-coordinates of one step time delay and three embedding dimension is shown in Figure 1.9. The shape of reconstructed attractor is squeezed. Such a phenomenon is called redundancy (Casdagli, Eubank, Farmer, and Gibson, 1991). Redundancy occurs because the values of each coordinate are close to each other when the time delay is too small.

Too large time delays cause problems for chaotic attractors. Figure 1.10 shows the reconstructed Lorenz attractor mapped into the delay-coordinates of 100 steps time delay and three embedding dimension. The reconstructed attractor is highly folded and the original shape is not preserved. Such a phenomenon is called irrelevance (Casdagli et al., 1991).

These examples tell us the importance of the choice of the delay time. We are in need of methods to select the proper time delay. Many researchers have proposed such methods with different approaches. This thesis considers this problem; in order to acquire a clear recognition of the topology of the reconstructed attractor, the reconstructed attractor has to be inflated as possible as it can. Limited to periodic orbits, such as the harmonic oscillator, and recurrent orbits, such as the Lorenz attractor, it is observed in experiments that the time delay that satisfies the equation  $an = T/2$ , where  $T$  is a period or approximation, is effective.

### 1.1.3 Homology and Topological Persistence

Topology studies the properties of shapes that do not change if the shapes are deformed continuously. For example, dimension and connectedness are topological properties. The equivalence of shapes is determined by homeomorphisms. A homeomorphism is a continuous mapping which is invertible and whose inverse is continuous. I give a simple example of shapes which are not homeomorphic. Let  $X$  be a real line:  $X = \mathbb{R}$ ; let  $Y$  be a real line from which the origin is removed:  $Y = \mathbb{R} \setminus \{0\}$ . The space  $X$  has one connected component but the

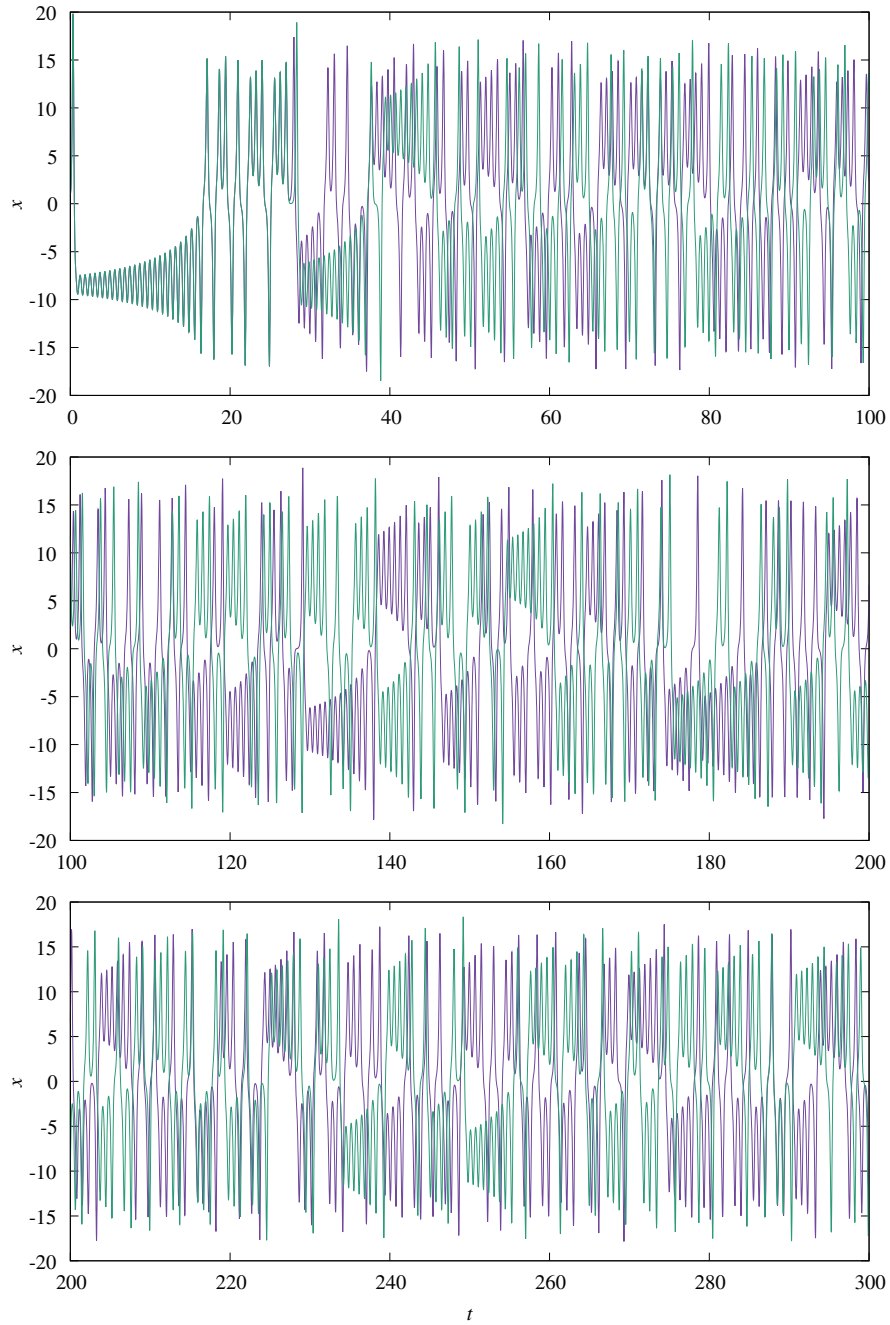


Figure 1.7: The comparison of two orbits of the Lorenz system with different initial conditions from  $t = 0$  to  $t = 300$ . The purple line is the  $x$ -coordinate of the orbit with the initial condition  $(x, y, z) = (1, 1, 0)$  and the green line is the  $x$ -coordinate of the orbit with the initial condition  $(x, y, z) = (1, 1.00001, 0)$ .

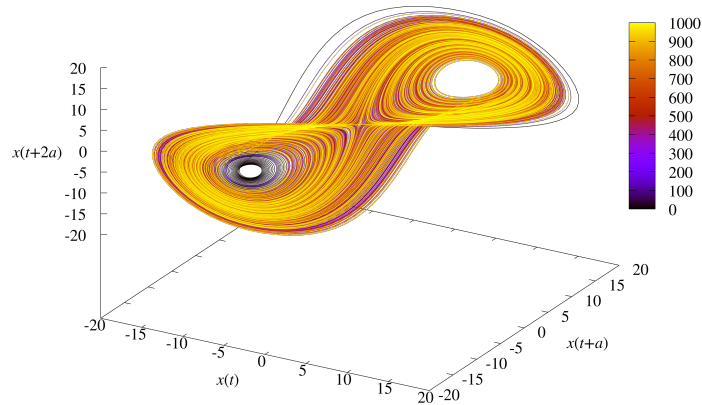


Figure 1.8: A successful case of a reconstructed Lorenz attractor: The time delay and the embedding dimension were set to  $a = 10$  and  $n = 3$ . The color scale indicates the time.

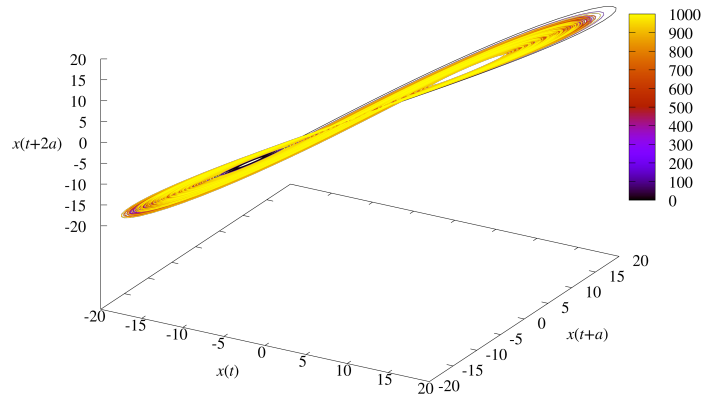


Figure 1.9: A reconstructed Lorenz attractor: The time delay and the embedding dimension were set to  $a = 1$  and  $n = 3$ . The color scale indicates the time.

space  $Y$  has two connected components. They are not homeomorphic although we have to know the properties of homeomorphisms in order to give a rigorous proof.

I give another example. Let  $X$  be a real plane:  $X = \mathbb{R}^2$ ; let  $Y$  be a real plane from which the origin is removed:  $Y = \mathbb{R}^2 \setminus \{0\}$ . In this case both  $X$  and  $Y$  have one connected components. However, they are not homeomorphic. Take a loop which encloses the origin. In the space  $X$  the loop can shrink into a point, but in  $Y$  the loop is struck in the origin.

Loops catch the holes in a shape. Holes are obstacles to the deformation of loops. We can construct a topological invariant using loops, which is called homotopy groups. The shapes with different homotopy groups are not homeomorphic, but the shapes which are not homeomorphic can have the same homotopy groups. Homotopy can be used to distinguish shapes.

Unfortunately it is difficult to compute homotopy groups in general. Homol-

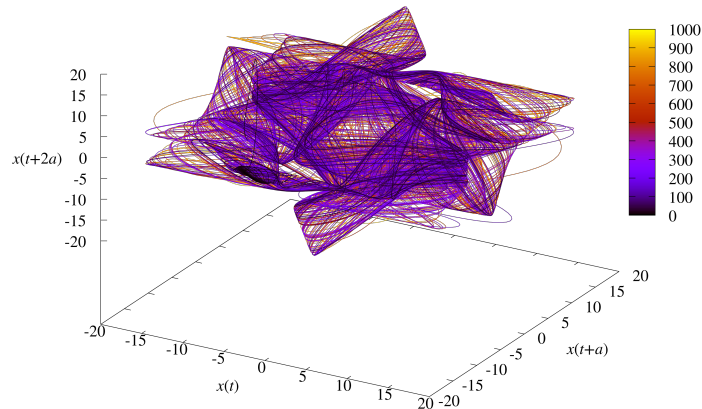


Figure 1.10: A reconstructed Lorenz attractor: The time delay and the embedding dimension were set to  $a = 100$  and  $n = 3$ . The color scale indicates the time.

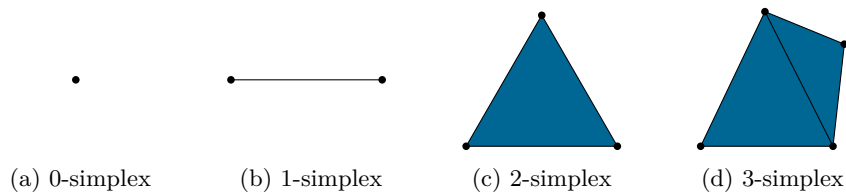


Figure 1.11: Examples of simplices.

ogy groups are easier to compute but have less information.

Homology is a topological invariant and is a sequence of algebraic objects called homology groups. Homology groups are modules, which are vector spaces whose scalars generalized to rings, associated to a simplicial complex or a topological space. Although homology groups can be defined for topological spaces, homology groups for simplicial complexes are employed in this thesis because computers can handle them.

This section gives a brief overview of homology groups. Formal definitions are given in later sections.

A simplicial complex consists of simplices. A simplex is a convex hull of its vertices. A simplex which has  $q + 1$  vertices is called a  $q$ -simplex. The dimension of a  $q$ -simplex is  $q$ . Figure 1.11 shows a 0-simplex, a 1-simplex, a 2-simplex, and a 3-simplex. A 0-simplex is a point, a 1-simplex is a line segment, a 2-simplex is a triangle, and a 3-simplex is a tetrahedron.

Simplices are glued to each other at their faces and the glued simplices are called a simplicial complex. A face of a simplex is a simplex which consists of a subset of the vertices. Figure 1.12a shows an example of a simplicial complex. However, a shape shown in Figure 1.12b is not a simplicial complex. Two triangles intersect on the region that are not faces and two line segments intersect in the middle of them.

Simplicial complexes are used to represent the topological structure of spaces in mathematics. The computation of homology groups is enabled by construct-

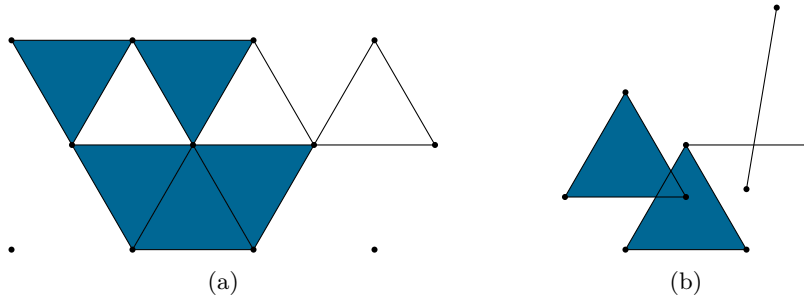


Figure 1.12: The condition of simplicial complexes: (a) A simplicial complex. (b) A shape which is not a simplicial complex.

ing a simplicial complex homeomorphic to the given space. The simplicial complex homeomorphic to a space is called the triangulation of the space. For instance, the simplicial complex with three vertices and three edges which connect the vertices is homeomorphic to a circle (Figure 1.13).

In order to compute the homology groups, modules are associated to a simplicial complex. For each dimension  $q$ , the module generated by the  $q$ -simplices in the given simplicial complex is constructed. Such module is called the  $q$ -th chain group of the simplicial complex. The  $q$ -th chain group of  $K$  is denoted as  $C_q(K)$ . Elements of the  $q$ -th chain group are called  $q$ -chains, which are formal linear combinations of  $q$ -simplices. The  $q$ -th chain group and  $(q - 1)$ -th chain group is connected with a homomorphism called the boundary operator or the boundary homomorphism. The boundary operator takes the boundary of simplices or chains.

For instance, consider a 2-simplex with the vertices  $a$ ,  $b$ , and  $c$ , say  $\sigma = \langle abc \rangle$ . The boundary of  $\sigma$  is  $\partial\sigma = \langle bc \rangle - \langle ac \rangle + \langle ab \rangle$ .

Consider the situation that we have two 2-simplices glued at an edge (Figure 1.14). The boundary of the chain  $c = \langle 012 \rangle + \langle 132 \rangle$  is calculated as follows:

$$\begin{aligned} \partial c &= \langle 12 \rangle - \langle 02 \rangle + \langle 01 \rangle \\ &\quad + \langle 32 \rangle - \langle 12 \rangle + \langle 13 \rangle \end{aligned} \tag{1.1.22}$$

$$= \langle 01 \rangle + \langle 13 \rangle + \langle 32 \rangle + \langle 20 \rangle. \tag{1.1.23}$$

The chain  $\partial c$  represents the cycle which visits the vertices 0, 1, 3, 2, and 0 in this order. The set of boundaries of chains forms a module and it is called the boundary group:

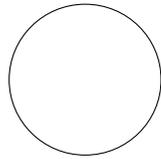
$$B_q(K) = \text{Im } \partial_{q+1} = \{b \in C_q(K) \mid \exists c, \partial_{q+1}c = b\}. \tag{1.1.24}$$

In the case of Figure 1.14, we have obtained a cycle. The boundary of this cycle (Figure 1.14b) is zero. It is known that the boundaries of cycles are always zero. Therefore cycle groups are defined as the kernel of the boundary operators:

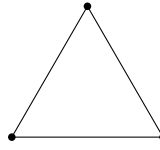
$$Z_q(K) = \text{Ker } \partial_q = \{z \in C_q(K) \mid \partial_q z = 0\}. \tag{1.1.25}$$

The  $q$ -th homology group of a simplicial complex  $K$  is defined as

$$H_q(K) = Z_q(K)/B_q(K). \tag{1.1.26}$$

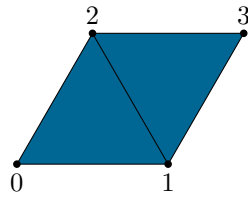


(a) A circle.

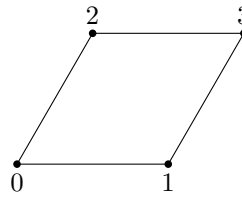


(b) A simplicial complex.

Figure 1.13: An example of triangulation. A circle (a) is homeomorphic to a simplicial complex (b).



(a)



(b)

Figure 1.14: The boundary of a simplicial complex: (a) A simplicial complex, and (b) the boundary of the simplicial complex. The numbers 0, 1, 2, and 3 are the labels of the vertices.

An element of  $H_q(K)$  is a cycle, which is a chain whose boundary is zero, but is not a boundary of other chains.

For instance, the homology groups of the simplicial complex shown in Figure 1.14b are  $H_0 = \mathbb{Z}$ ,  $H_1 = \mathbb{Z}$ , and  $H_q = 0$  for all  $q \geq 2$ .

Although simplicial complexes are made by hand in mathematics, we need methods to construct simplicial complexes from data on computers. Suppose that we have a set of points sampled from a space. Consider that a graph is constructed by connecting any two points at a distance less than a threshold. Then put  $q$ -simplices into the  $(q + 1)$ -vertices cliques of the graph. A clique of a graph is a subgraph whose all vertices are connected to each other. We obtain a simplicial complex from sampled points by this construction. However, it is difficult to choose the threshold. If the threshold is too small, the simplicial complex will be scattered; it has many connected components. If the threshold is too large, the simplicial complex will be a large ball; its holes are filled.

In order to avoid such consequences, the growing sequence of a simplicial complex, which is called filtration, is introduced. The homology groups of a simplicial complex are extended to the filtration of a simplicial complex. They are called persistent homology groups. Persistent homology groups encode the information of when cycles are born and when they vanish in the growing of a simplicial complex. The notion of how long cycles live is called topological persistence.

Let us explain topological persistence with an example of a single-valued function. The following example was made in the spirit of the examples demonstrated in the articles (Edelsbrunner and Harer, 2008) and (Vejdemo-Johansson, 2012).

Suppose that a continuous function  $f : \mathbb{R} \rightarrow \mathbb{R}$  is given. Consider the sublevel sets of the function  $f$ :

$$f^{-1}(-\infty, y] = \{x \in \mathbb{R} \mid f(x) \leq y\}, \quad (1.1.27)$$

where  $y$  is a real number. A growing sequence of the sublevel sets of the function  $f$  is obtained because for any two numbers  $y \leq y'$ , the relation  $f^{-1}(-\infty, y] \subset f^{-1}(-\infty, y']$  holds. In this case, the topological entities of the sublevel sets are connected components only since the function  $f$  has only one variable. The set of the connected components is denoted as  $\pi_0 f^{-1}(-\infty, y]$ . An example of the change of the connected components of the sublevel sets of a function is given below.

The graph of the function  $f$  is shown in Figure 1.15. The thresholds on the  $y$ -axis are taken:  $y_0 < y_1 < y_2 < y_3 < y_4 < y_5$ . The sublevel sets are calculated in the order of these thresholds.

First the sublevel set  $f^{-1}(-\infty, y_0]$  is the point that attains the minimum of the function  $f$ . The symbol  $x_0$  denotes the point. The point  $x_0$  is shown as the blue point at the level of  $y_0$  in Figure 1.15. We introduce the notation  $[x_0]$  which denotes the connected component represented by the point  $x_0$ . The sublevel set has only one connected component:  $\pi_0 f^{-1}(-\infty, y_0] = \{[x_0]\}$ .

Second the sublevel set  $f^{-1}(-\infty, y_1]$  is a segment. The segment is shown as the blue line segment at the level of  $y_1$  in Figure 1.15. The sublevel set has only one connected component that is represented by  $x_0$ . The topological information is summarized as  $\pi_0 f^{-1}(-\infty, y_1] = \{[x_0]\}$ . It is not changed from  $\pi_0 f^{-1}(-\infty, y_0]$ .

Third the sublevel set  $f^{-1}(-\infty, y_2]$  is made of a segment and a point. The segment is identified with the connected component  $[x_0]$ . It is shown as the blue segment at the level of  $y_2$  in Figure 1.15. The point, say  $x_2$ , has newly appeared. It is shown as the orange point at the level of  $y_2$  in Figure 1.15. The set of the connected components of the sublevel set is  $\pi_0 f^{-1}(-\infty, y_2] = \{[x_0], [x_2]\}$ . It is changed from  $\pi_0 f^{-1}(-\infty, y_1]$ .

Fourth the sublevel set  $f^{-1}(-\infty, y_3]$  is made of two segments. They are shown as the orange segment and the blue segment at the level of  $y_3$  in Figure 1.15. The connected components of the sublevel set are  $\pi_0 f^{-1}(-\infty, y_3] = \{[x_0], [x_2]\}$ . They are same as  $\pi_0 f^{-1}(-\infty, y_2]$ .

Fifth the sublevel set  $f^{-1}(-\infty, y_4]$  is made of only one segment. The connected component represented by  $x_2$  is merged to the connected component represented by  $x_0$ . The connected component  $[x_0]$  is shown as the blue segment at the level of  $y_4$  in Figure 1.15. When two connected components are merged, the younger one is merged into the elder one. This rule is called the elder rule. In this example, the connected component  $[x_2]$  is younger than  $[x_0]$  since  $[x_2]$  was born at  $y_2$  and  $[x_0]$  was born at  $y_0$ .

Lastly, the sublevel set  $f^{-1}(-\infty, y_5]$  is made of a segment. The segment is shown as the blue segment at the level of  $y_5$  in Figure 1.15. The connected components of the sublevel set are  $\pi_0 f^{-1}(-\infty, y_5] = \{[x_0]\}$ .

In summary, the connected component  $[x_0]$  was born at  $y_0$  and lives eternally and the connected component  $[x_2]$  was born at  $y_2$  and died at  $y_4$ .

Now the Vietoris-Rips complex is explained. The Vietoris-Rips complex is a simplicial complex constructed from a set of points in an Euclidean space. Suppose that the points are sampled from a subspace of the Euclidean space.

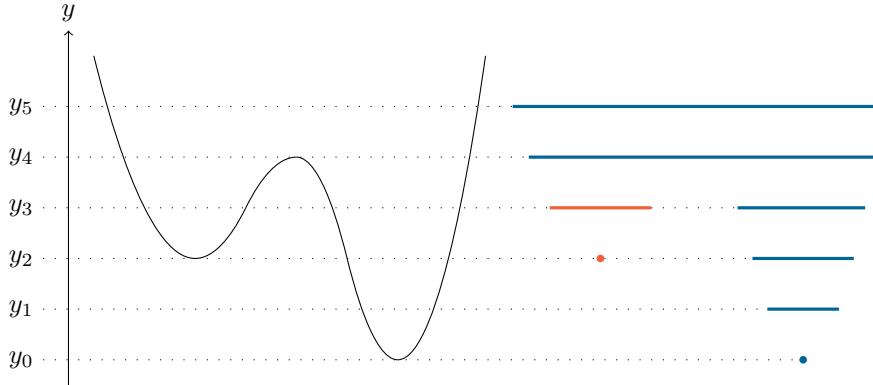


Figure 1.15: Sublevel sets of a function and topological persistence. A continuous function and the threshold values of sublevel sets (left) and the sublevel sets of the thresholds (right).

Imagine that the balls centered at the given points. The union of the balls is another subspace and we consider it as the approximation to the subspace from which the points are sampled. We have to turn it into a simplicial complex. The points are treated as the vertices of the simplicial complex. If two balls have the intersection, we add a 1-simplex whose vertices are the centers of the two balls. If any two balls of three balls have the intersection, we add a 2-simplex there. We add simplices of higher dimensions in the similar manner. The resulting simplicial complex is the Vietoris-Rips complex.

We can build the filtration of the Vietoris-Rips complex. An example is shown in Figure 1.16. Six points are sampled from a circle of radius 1. Each point is positioned at  $(\cos k\pi/3, \sin k\pi/3)$  for  $k = 0, 1, 2, 3, 4, 5$ . As the balls grow, simplices are added to the Vietoris-Rips complex.

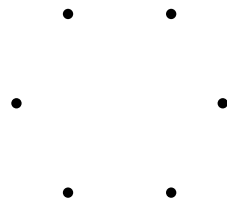
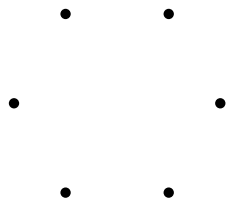
The persistent homology groups of the filtration of the Vietoris-Rips complex of this example are shown in Table 1.1. The 0-th persistent homology group consists of one homology class with an infinite lifetime and five classes which vanish at 0.5. The 1-st persistent homology group consists of one homology class which is born at 0.5 and dies at 0.866 and nine classes with a zero lifetime.

In order to help people to grasp the persistent homology groups, persistence diagrams visualize them. Persistence diagrams are scatter plots of persistent homology classes. The horizontal axis indicates the birth scale and the vertical axis indicates the death scale. The persistence diagrams of the example are shown in Figure 1.17.

Some readers may wonder how far the persistent homology groups of the Vietoris-Rips complex of the sampled points is from those of the underlying space. The following inequality is known (Chazal, de Silva, and Oudot, 2014):

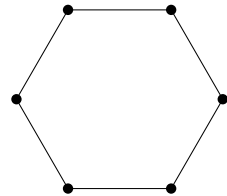
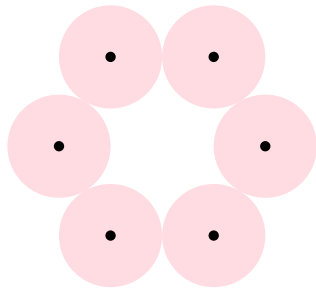
$$W_\infty(\text{Dgm}_q(\mathcal{R}(X)), \text{Dgm}_q(\mathcal{R}(Y))) \leq 2d_{\text{GH}}(X, Y), \quad (1.1.28)$$

where  $X$  and  $Y$  are metric spaces. The symbol  $\mathcal{R}(X)$  denotes the filtration of the Vietoris-Rips complex of  $X$  and  $\text{Dgm}_q$  denotes the persistence diagram of the  $q$ -th persistent homology group. The symbol  $W_\infty$  denotes the bottleneck distance between persistence diagrams and the symbol  $d_{\text{GH}}$  denotes the Gromov-Hausdorff distance between metric spaces.



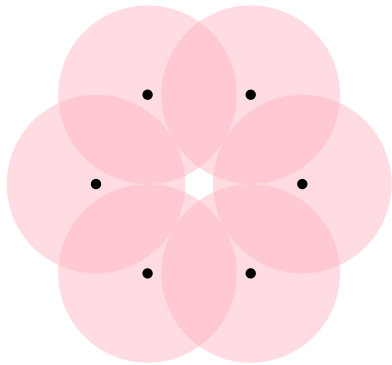
(a) The points sampled equidistantly from a circle of radius 1. They form a hexagon.

(b) The Vietoris-Rips complex that corresponds to the shape (a).

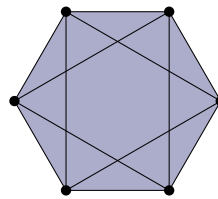


(c) The balls of radius 0.5 centered at the sampled points.

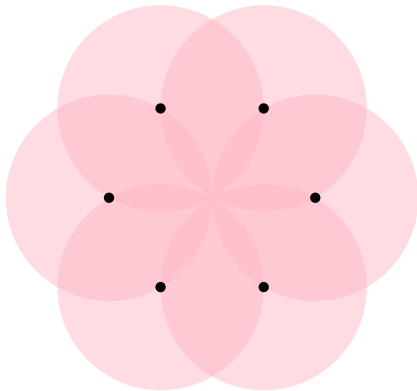
(d) The Vietoris-Rips complex that corresponds to the shape (c).



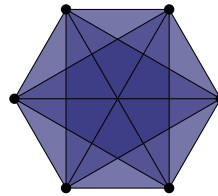
(e) The balls of radius 0.866 centered at the sampled points.



(f) The Vietoris-Rips complex that corresponds to the shape (e).



(g) The balls of radius 1.0 centered at the sampled points.



(h) The Vietoris-Rips complex that corresponds to the shape (g).

Figure 1.16: An example of the growing of the Vietoris-Rips complex. (a,c,e,g) The points and the balls. (b,d,f,h) The Vietoris-Rips complexes.

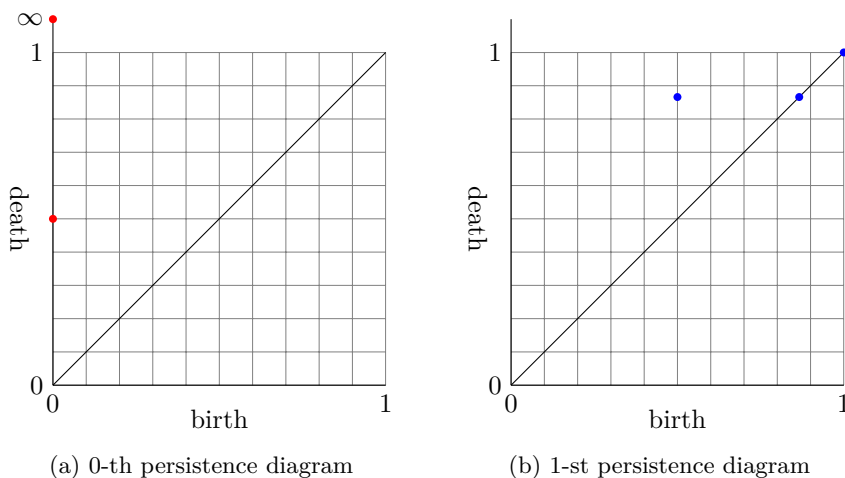


Figure 1.17: The persistence diagrams of the Vietoris-Rips complex in Figure 1.16. The horizontal axis indicates the birth scale and it ranges from 0 to 1. The vertical axis indicates the death scale; it ranges from 0 to 1 and it have an additional tick which indicates infinity. A grid is added to help people to read the values.

## 1.2 Related Work

### 1.2.1 Information Extracted from Dynamical Systems

This section provides a review of researches that extract information from the orbits of differential equations. Roughly speaking, the orbits have the information at the local, middle, and global scale. For example, the Lyapunov exponents and the fractal dimensions are the local scale information. The knots of periodic orbits are the middle scale information. The embedding manifolds are the global scale information.

At the local scale, the Lyapunov exponents can be used as features of time series data (Kantz, 1994). The Lyapunov exponent is the limit of the logarithm

Table 1.1: The persistence pairs of the Vietoris-Rips complex in Figure 1.16.

Dimension 0	Dimension 1
(0.0, $\infty$ )	(0.5, 0.866)
(0.0, 0.5)	(0.866, 0.866)
(0.0, 0.5)	(0.866, 0.866)
(0.0, 0.5)	(0.866, 0.866)
(0.0, 0.5)	(0.866, 0.866)
(0.0, 0.5)	(0.866, 0.866)
(0.0, 0.5)	(0.866, 0.866)
	(1.0, 1.0)
	(1.0, 1.0)
	(1.0, 1.0)

of the distance between an orbit and another orbit whose initial state is fluctuated from the initial state of the former orbit as the fluctuation approaches zero and the time approaches infinity. The Lyapunov exponent describes the short-time behavior of orbits. If the Lyapunov exponent is less than zero, the orbits that start from a small region converge. If the Lyapunov exponent is equal to zero, the orbits run in parallel. Otherwise the orbits diverge, which is one of the properties of chaos (Strogatz, 2014).

The fractal dimensions are used to characterize an orbit. The idea to measure the fractal dimensions is how much dimension, which is a dimension of an Euclidean space, is needed to cover a subset at a small scale. Fractal sets have non-integer dimensions. The correlation dimension (Grassberger and Procaccia, 1983) is one of a fractal dimension which is calculated in numerical methods. The correlation dimension of a set of points is the slope of the logarithm of the correlation integral. The correlation integral is the average of the numbers of points whose distance from each point is less than a threshold. It is known that chaotic attractors have a fractal dimension.

The local information such as the Lyapunov exponents, the correlation integral, and the correlation dimension is used as a descriptor of observed time series (Ali, Basharat, and Shah, 2007). The Lyapunov exponents, the correlation integral, and the correlation dimension are called the invariant features and they are employed for classification with the  $K$ -nearest neighbor method. The motion capture data and the video data of human actions were classified in the experiment of the paper (Ali et al., 2007). They achieved the accuracy of around 90%.

The knots of periodic orbits of the Lorenz attractor was investigated (Birman and Williams, 1983). A knot is a continuous oriented curve. Knots are identified through the homeomorphism preserving orientation. The first homotopy group of the complement space of a knot is called a knot group and it is a topological invariant. The representation of knot groups of the Lorenz attractor was calculated. However, this approach cannot be automated on computers.

The global information of an orbit is also useful. The topological structure of an orbit reflects the characteristics of flows, as seen in Section 1.1.1. Strictly speaking, the topology of an orbit sometimes makes no sense. Some orbits, such as an orbit of an irrational flow on 2-torus and an orbit of the Lorenz attractor, are dense in a subset of an Euclidean space. They are one dimensional curve since they are paths but they are not necessarily cycles or are not necessarily two dimensional.

For this reason, we think of the closure of the orbit. However, because we cannot compute the closure on computer, we think of the embedding manifold (Tsankov and Gilmore, 2003, 2004) of an orbit instead of the closure. The embedding manifold of an orbit is the union of the balls of a radius centered at each point of the orbit.

Before describing researches which compute the homology of embedding manifolds, I explain the work of Tsankov and Gilmore (2003, 2004). They observed the relation between the topology of the embedding manifold and the behavior of the flow of several chaotic systems like the Lorenz system. The relation between the bounding torus, which is the boundary of the embedding manifold, and the vector field of the differential equation is established by Poincaré-Hopf Index Theorem. The Euler characteristic of the bounding torus is equal to the summation of the indices of the vector field at the critical points. The Euler

characteristic  $\chi$  is related to the genus  $g$  of the bounding torus:  $\chi = 2 - 2g$ .

Tsankov and Gilmore proposed the canonical form of a dynamical system, which is obtained from the bounding torus. The canonical form is a simplified representation of the flows and the critical points of the vector field. The canonical form is a surface with the holes around the critical points. In addition, the canonical form is cut into chunks according to the direction of flows and a system of symbolic dynamics is obtained.

Because they supposed that the expression of the Lorenz system is known, the bounding torus and the canonical form has three holes: two holes at the critical points and one hole at the  $z$ -axis. Although the canonical form is strict, it requires that the critical points form holes with some width. We cannot assume such condition in observation.

The topology of embedding manifolds serves as clues to the global structure of dynamical systems. However, they may lost some critical points and different dynamical systems have the same topology of embedding manifolds.

### 1.2.2 Topology of Attractors

The attempts to compute the homology groups of an orbit date back to at least 1993. Muldoon, MacKay, Huke, and Broomhead (1993) computed the homology groups of a periodic signal and a quasiperiodic signal. The signals were obtained from a physical experiment. The signals were mapped to a delay-coordinate space. Some of points were selected to construct a simplicial complex. Similar researches were conducted after a decade (Sciamarella and Mindlin, 1991, 2001). In the works of Sciamarella and Mindlin, the homology groups of human speech data and two toy models were computed.

The researches of the paper (Muldoon et al., 1993) and the paper (Sciamarella and Mindlin, 1991, 2001) construct simplicial complexes with heuristic methods. There are no guarantees of the recovery of the topology of sampled shapes. Contrary to those, it is guaranteed that persistent homology recovers the topology of sampled shapes by the stability inequality.

The framework that combines persistent homology and delay-coordinates was proposed in 2012. Skraba, de Silva, and Vejdemo-Johansson (2012) demonstrated the computation of the persistent homology of time series data embedded into the delay-coordinate space. They did not demonstrate any application of this framework.

This framework was employed to detect a wheeze of breathing sound signals (Emrani, Gentimis, and Krim, 2014a; Emrani, Chintakunta, and Krim, 2014b). The wheeze signals were modeled as a continuous piecewise sinusoidal function whose amplitude varies. The period and phases were different for each piece. Such signals form an ellipse in the delay-coordinate space. The first persistent homology group was used to detect the wheeze signals. They judged a signal to be a wheeze signal if the longest persistence was greater than a threshold. The threshold was determined by calculating the distribution of the longest persistences of training data set.

The delay time was selected with the autocorrelation-like function (ACL). The ACL function is defined as

$$R_{xx}(t_i) = \sum_{1 \leq l \leq k} x(t_i)x(t_l), \quad (1.2.1)$$

where the function  $x(t_i)$  is the sampled signal. The delay time between the peaks of the ACL function is selected. The size of simplicial complices has already been a problem. In order to reduce the size, they used the witness complex (de Silva and Carlsson, 2004). At first they did subsampling the input points to choose the landmark (Emrani et al., 2014a), but they switched to use the density function to select for subsampling (Emrani et al., 2014b). They said that their method had accuracy higher than the methods based on time-frequency analysis or wavelet transform.

Perea and Harer (2015) made a rigorous analysis on the selection of the delay time and the embedding dimension for the framework and conducted numerical experiments. The exposition of the results of their analysis is given later. The aim of their experiment was to check that the persistent homology was efficient for detecting the periodicity of signals and was better than other methods. They defined the score of periodicity as the maximum persistence of the 1-st persistent homology group. It was compared to three methods: the JTK\_CYCLE algorithm, the Lomb-Scargle periodogram, and the total persistent homology. The JTK\_CYCLE algorithm (Hughes et al., 2010) is a period detection method based on the Jonckheere-Terpstra-Kendall test, which is a kind of statistical test. The Lomb-Scargle periodogram (Lomb, 1976; Scargle, 1982) is a periodogram obtained by fitting sinusoidal waves to non-uniformly sampled time series. The total persistence (Cohen-Steiner et al., 2010) is the summation of the persistences of the  $q$ -th persistent homology groups. In the experiment, periodic signals and non-periodic signals were classified with the methods above. They drew the graphs of the receiver operating characteristic (ROC) and calculated the values of the area under the curve (AUC). In the noisy cases, the AUC value of the framework of persistent homology and delay-coordinates were better than other methods except for trended signals.

The framework of persistent homology and delay-coordinates was applied to real-world data sets (Pereira and de Mello, 2015). The persistent homology groups were computed on lazy witness complices. In the experiment of the paper (Pereira and de Mello, 2015), the following features were calculated for each dimension: the number of holes, the maximum hole lifetime, the number of relevant holes, the average lifetime, and the sum of all lifetimes. The  $k$ -means clustering on the raw data was compared to the  $k$ -means clustering on the topological features above. The data sets had binary labels. The proposed method had better accuracy than the  $k$ -means on the raw data.

Venkataraman, Ramamurthy, and Turaga (2016b) modified the construction of the Vietoris-Rips complex for the time series data mapped into delay-coordinate spaces. They connected the  $i$ -th point and  $(i + 1)$ -th point in a delay-coordinate space for all time indices. Then they constructed the Vietoris-Rips complex. In order to compare the persistence diagrams, they used the 1-Wasserstein distance, which is a  $L_1$  version of the bottleneck distance. Their method was compared with the chaotic invariants (Ali et al., 2007) and the methods called D2 and DT2 in their previous work (Venkataraman and Turaga, 2016a). The method D2 constructs a histogram of the Euclidean distance between points randomly chosen from the delay-coordinate space. The method DT2 is a weighted version of the D2. The weight is  $\exp(-\gamma\Delta t)$  where  $\gamma$  is a given parameter and  $\Delta t$  is a difference of the sampled time of the points. The motion capture data of human actions was used for the experiment. The data had five labels and the nearest neighbor classifier was used. They reported that

the average accuracy of the D2, the DT2, and the ordinary Vietoris-Rips complex was higher than 90%, but that of the chaotic invariants was about 50%. Their proposed method achieved that the average accuracy of 96.48%, which was the highest accuracy.

Khasawneh and Munch (2016) applied the persistent homology of time series data for detecting chatter in machining processes. Chatter is a vibration of machine tools cutting materials. It is modeled as a forced damped oscillation. The maximum persistence of the 1-st persistent homology of the given time series mapped into delay-coordinates was used as an index for chatter.

Seversky, Davis, and Berger (2016) compared three features of persistence diagrams. They used the linear-size approximation of the Vietoris-Rips complex (Sheehy, 2013). The scale space kernel of persistence diagram (Reininghaus, 2015) was used as a feature. Roughly speaking, the scale space kernel is a convolution of the heat-kernel and the points in a persistence diagram. The motion capture data was classified by the kernel support vector machine. They demonstrated that the accuracy of the method was better than that of the chaotic invariants.

Umeda (2017) proposed the betti sequence for classifying time series data with convolutional neural networks. The betti number of a dimension is the number of homology classes of that dimension. The betti sequence is the betti number at some scale. It is computed from the persistent homology groups. In the experiment, a gyro sensor data set, an EEG data set, and an EMG data set were classified with several methods. The proposed method in the paper (Umeda, 2017) achieved the outstanding accuracy.

I mention other application of persistent homology to time series data. Mittal and Gupta (2017) observed the relation between the bifurcation of dynamical systems and the persistent homology of the orbit. The systems such as a logistic map, a Duffing oscillator, and a Jerk circuit were observed. However, it seems to be a preliminary result.

### 1.2.3 Speeding up the Computation of Persistent Homology

In fact, it takes long time and large memory to compute persistent homology, because simplicial complexes are large objects and the computational time of persistent homology is in the order of  $O(n^3)$  in the worst-case. There are two approaches to reduce the time and the space of the computation.

In order to speed up the computation, persistent cohomology (de Silva, Morozov, and Vejdemo-Johansson, 2011a), which is a dual of persistent homology, is better than persistent homology. The resulting persistence diagrams are same. The computation of persistent cohomology is faster than the computation of persistent homology (de Silva et al., 2011b).

The Ripser (Bauer, 2019) is the fastest implementation of persistent cohomology of the Vietoris-Rips complex. It employs several techniques to compute persistent cohomology efficiently.

The other approach is to reduce the size of simplicial complexes. The number of the simplices in the filtration of the Vietoris-Rips of dimension  $k$  is in the order of  $O(n^{k+1})$ , where  $n$  is the number of points. Because the computational time is the function of the number of the simplices, it is shortened by reducing the number of the simplices.

The Ripser (Bauer, 2019) sets the maximum threshold of the Vietoris-Rips filtration. It is set to the minimum enclosing radius of the input points. The homology group becomes trivial if the threshold is greater than the minimum enclosing radius.

A linear approximation of the Vietoris-Rips complex has been proposed by Sheehy (2013). The points that are not significant for the homology groups are ignored and the Vietoris-Rips complex is constructed from the remained points.

The reason why the size of the Vietoris-Rips complex becomes large is that points far from each other can form a simplex. In order to restrict how many points connect to each other, the alpha complex (Edelsbrunner and Harer, 2010) has been proposed. An alpha complex is constructed in the following procedure. First the Voronoi diagram of the input points is constructed. Second the union of each Voronoi cell and a ball centered at the point is taken. Then a simplex is added to the alpha complex if the vertices are connected with their neighborhood. Unfortunately, it is difficult to construct alpha complexes in the dimension higher than three due to the difficulty of constructing the Voronoi diagrams in higher dimensions.

The witness complex (de Silva and Carlsson, 2004) is a simplicial complex constructed from a subsampled points. A subset of the input data is called a landmark. The vertices of the witness complex are the points of the landmark. A simplex is added to the witness complex if there is a point to which each vertex of the simplex is the nearest among the landmark. The witness complex is an approximation of the Delaunay complex, which is the dual of the Voronoi diagram.

Garland, Bradley, and Meiss (2016) proposed the fuzzy witness complex and observed the persistent homology of the fuzzy witness complex of the Lorenz attractor and reconstructed Lorenz attractors. The fuzzy witness complex is a variation of the strong witness complex. The condition whether the simplex is added is relaxed by adding some constant to the distance from a landmark point to other points. They observed that the fuzzy witness complex recovers the topology of the Lorenz attractor with proper parameters.

#### 1.2.4 Selection of the Delay Time

We have to select the delay time and the embedding dimension when we use the delay-coordinate spaces. The selection of the delay time is only considered in this thesis.

Many researchers have proposed methods to select the delay time. The most famous method is the mutual information (Fraser and Swinney, 1986). Consider the set of the values  $x(t)$  and the set of the values of  $x(t+a)$ , where the function  $x(t)$  is a signal and the real value  $a$  is the delay time. The mutual information of the sets above is calculated with varying the delay time. We select the smallest delay time that attains the local minimum of the mutual information. This method may expand the two coordinates of the delay-coordinate space. It only considers two dimensional case.

A geometric approach to propose methods to select the delay time was popular in 1990s. The wavering product (Liebert, Pawelzik, and Shuster, 1991), the fill-factor (Buzug, Reimers, and Pfister, 1990), the integral local deformation (Buzug and Pfister, 1992), and the average displacement (Rosenstein, Collins, and de Luca, 1994) are such methods. The methods based on the min-

imal description length principle were proposed (Judd and Mees, 1998; Small and Tse, 2004). I do not expound the details of these methods.

The important research was given in the paper (Perea and Harer, 2015). Their conclusion was that the best delay time for periodic signals satisfies  $an = T/2$ , where the real value  $a$  is the delay time, the positive integer  $n$  is the embedding dimension, and the real value  $T$  is the period. In the context of the persistent homology of periodic signals, we consider the delay time that expands the hole of the loop in the delay-coordinates to be good.

The equation  $an = T/2$  was obtained by analyzing the sinusoidal wave mapped into the delay-coordinates. The shape of the sinusoidal wave mapped into the delay-coordinates is an ellipse. The lengths of its semi-major axis and semi-minor axis depend on the delay time. The ellipse is roundest, i.e. the two axes have the same length, when the delay time and the embedding dimension satisfy the equation  $an = T/2$ .

Consider the signals which can be written as the first  $N$  terms of a Fourier series. The analysis was done in the same way. Each harmonic component requires two dimensional space to form an ellipse. Therefore the embedding dimension must be equal to or greater than  $2N$ .

A loop has a hole and the width of the hole can be considered. By dilating the loop, it becomes a solid tube and the topology changes at some scale. We consider the scale where the dilating tube fills the hole of a loop as the width of the hole. The hole of a loop is numerically measured with the first persistent homology of the Vietoris-Rips filtration. The maximum persistence is used as a surrogate hole width.

### 1.3 Contribution of the Thesis

This thesis handles two problems. One problem is the selection of the delay time of the delay-coordinates for periodic and recurrent signals. The other problem is to make the computation of the persistent homology of time series data by reducing the size of the filtration.

The relation of the delay time and the width of the hole was analyzed and experimented (Chapter 3). The analysis was carried out with the assumption that the signal is periodic and has one zero-crossing in a period. It was shown that the delay time which satisfies the equation  $an = T/2$  maximizes the lower bound of the hole width. This equation is same as that of the paper (Perea and Harer, 2015) but the assumption is different.

In order to check whether such delay time maximizes the hole width, the relation of the delay time and the hole width was computed with persistent homology for several time series. It was effective for periodic signals such as sinusoidal waves and the limit cycle of the van der Pol equation. For a Japanese vowel signal, which is periodic, it was effective in the delay-coordinate space of embedding dimension higher than five.

In order to acquire an insight, it was investigated whether the delay time such that  $an = T/2$  is effective for recurrent signals such as the Rössler attractor and the Lorenz attractor. It was turned out that such delay time does not maximize the hole width but the irrelevance occurs if the delay times is larger than  $T/2n$ .

The delay times determined by the mutual information were compared with the delay times such that  $an = T/2$ . The mutual information gave us poor

results in the view of the persistent homology.

The acceleration of the computation of the persistent homology of time series was achieved by obtaining line segments approximating to a continuous time series and constructing the Vietoris-Rips complex from line segments (Chapter 4). Cubic Bézier curves are fitted to the given points and then they are divided into line segments. We can construct a Vietoris-Rips complex from line segments because their neighborhoods are convex and the intersection of the neighborhoods can be calculated with the distance between line segments. We can use existing tools of persistent homology, such as the Ripser, to construct the Vietoris-Rips complex of line segments since its construction only depends on the distance of line segments.

The experiments have shown that the proposed method reduces the computational time and space ten times smaller or more. The proposed method reduces the noise added to signals; it brings us more precise persistence diagrams under noisy observation. The computational performance and the precision of persistence diagrams were compared between the proposed method and the witness complex. The proposed method produced the results better than the witness complex.

## Chapter 2

# Mathematical Foundations

In this chapter, I give the expositions of persistent homology (Section 2.1), attractor reconstruction (Section 2.2), and Bézier curves (Section 2.3).

In Section 2.1, rigorous explanations of simplicial homology and persistent homology are given. The readers will know the reason why the size of a simplicial complex is huge through the definitions. They will know how the persistent homology groups are computed and its complexity.

In Section 2.2 introduces the delay-coordinates and Takens' theorem. Takens' theorem states that the attractors mapped into delay-coordinate spaces are diffeomorphic to the attractors in the original phase space for almost all delay times.

### 2.1 Persistent Homology for Topological Data Analysis

Topological data analysis is a method to analyze the topology of the shape of data. Topology is a field which studies the characteristic of a shape invariant under continuous deformations. Topology has several branches. Topological data analysis relies on algebraic topology especially among the branches. Algebraic topology exploits algebra to extract the information of the topology of shapes. There exist two kinds of invariants: homotopy groups and homology groups. Homotopy groups are the groups of the loops in a space. It is almost impossible to compute homotopy groups with computers. Homology groups are defined with the modules generated by the simplices in a shape. It is possible to compute homology groups with computers. Therefore topological data analysis exploits homology groups.

The homology groups used in this thesis is simplicial homology groups. The shape is represented as a simplicial complex, which consists of simplices. A simplicial complex is turned into a chain complex, an algebrization of simplicial complex. A chain complex has chain groups and boundary operators between them. A homology group is defined as the quotient of the kernel of a boundary operator divided by the image of a boundary operator.

Subsection 2.1.1 describes the notion of simplex and Subsection 2.1.2 introduces the notion of simplicial complex. Subsection 2.1.3 introduces the notion of chain complex and Subsection 2.1.4 defines the homology groups. In order

to write the descriptions in Subsection 2.1.1-2.1.4, the textbook (Tamura, 2015) was referred to.

Persistent homology (Edelsbrunner, Letcher, and Zomorodian, 2002) is one of main tools of topological data analysis. Persistent homology computes the appearance and the disappearance of the homology classes in a filtered simplicial complex. A filtered simplicial complex is a growing sequence of simplices. A persistent homology group is visualized with a persistence diagram. The bottleneck distance between persistence diagrams is defined to compare them. Subsection 2.1.5 gives the definition and the algorithm of persistent homology. Subsection 2.1.6 introduces the persistence diagram and the bottleneck distance.

Čech complex and Vietoris-Rips complex (Edelsbrunner and Harer, 2010: Chapter III) construct a simplicial complex from a set of points. Subsection 2.1.7 gives the definitions of Čech complex and Vietoris-Rips complex. The witness complex (de Silva and Carlsson, 2004) is a method to construct a simplicial complex whose simplices are less than Čech complex or Vietoris-Rips complex. Subsection 2.1.8 offers an explanation of the witness complex.

It is known that geometric complices such as the Čech complex and the Vietoris-Rips complex have the stability with respect to the Gromov-Hausdorff distance (Chazal, de Silva, and Oudot, 2014). Subsection 2.1.9 gives a short summary of the stability of complices.

### 2.1.1 Simplex

In order to introduce simplicial complices, simplices are first explained. A simplex is an element that forms a simplicial complex. A simplex has vertices and it is a convex hull of the vertices. Before the definition of simplex is given, the property that points are in general position is introduced.

**Definition 2.1.1** (points in general position). *Let  $a_0, a_1, \dots, a_m$  be  $(m+1)$  points in an  $N$ -dimensional Euclidean space, and let  $\lambda_0, \lambda_1, \dots, \lambda_m$  be  $(m+1)$  real numbers that satisfy the equation  $\lambda_0 + \lambda_1 + \dots + \lambda_m = 0$ .*

*If the logical equivalence*

$$\lambda_0 a_0 + \lambda_1 a_1 + \dots + \lambda_m a_m = 0 \Leftrightarrow \lambda_0 = \lambda_1 = \dots = \lambda_m = 0 \quad (2.1.1)$$

*holds, the points  $a_0, a_1, \dots, a_m$  are called in general position.*

When the points  $a_0, a_1, \dots, a_m$  are in general position, any vectors between two points among them are linearly independent. Fix the point  $p_0$  as the origin, and take two different points  $p_i$  and  $p_j$ . The directional vectors  $\overrightarrow{p_0 p_i}$  and  $\overrightarrow{p_0 p_j}$  are written as  $p_i - p_0$  and  $p_j - p_0$  respectively. Let  $\mu_i$  and  $\mu_j$  be real numbers and assume the equation  $\mu_i(p_i - p_0) = \mu_j(p_j - p_0)$  hold. This equation can be written as  $(\mu_i - \mu_j)p_0 - \mu_i p_i + \mu_j p_j = 0$ . Then  $0 \cdot p_k$  for  $k = 1, 2, \dots, m$  but  $i$  and  $j$  are added to this equation. We obtain an equation  $(\mu_i - \mu_j)p_0 - \mu_i p_i + \mu_j p_j + \sum_k 0 \cdot p_k = 0$ . Since the points  $p_0, p_1, \dots, p_m$  are in general position, the real numbers satisfy that  $\mu_i - \mu_j = \mu_i = \mu_j = 0$ . Thus the vectors  $\overrightarrow{p_0 p_i}$  and  $\overrightarrow{p_0 p_j}$  cannot be linearly dependent.

In order to introduce the concepts related to simplices, a lemma on points in general position is given.

**Lemma 2.1.2.** *Let  $a_0, a_1, \dots, a_m$  be points in general position. The  $(q+1)$  points  $a_{i_0}, a_{i_1}, \dots, a_{i_q}$  are arbitrarily chosen from the points  $a_0, a_1, \dots, a_m$ . These  $(q+1)$  points  $a_{i_0}, a_{i_1}, \dots, a_{i_q}$  are also in general position.*

*Proof.* Let  $\mu_0, \mu_1, \dots, \mu_q$  be real numbers that satisfy  $\mu_0 + \mu_1 + \dots + \mu_q = 0$ . First, we consider the case that the equation  $\mu_0 a_{i_0} + \mu_1 a_{i_1} + \dots + \mu_q a_{i_q} = 0$  holds. Let  $\lambda_{i_j} = \mu_j$  for each index  $j$  and  $\lambda_k = 0$  for the index  $k$  other than  $j$ . The equation above can be written as

$$\sum_{j=0}^q \lambda_{i_j} a_{i_j} + \sum_{k \neq i_j} \lambda_k a_k = \sum_{i=0}^m \lambda_i a_i = 0. \quad (2.1.2)$$

Since the points  $a_0, a_1, \dots, a_m$  are in general position, this equation implies that the equations  $\lambda_0 = \lambda_1 = \dots = \lambda_m = 0$  hold. Thus we obtain  $\mu_0 = \mu_1 = \dots = \mu_q = 0$ .

Conversely, if the equations  $\mu_0 = \mu_1 = \dots = \mu_q = 0$  hold, it is clear that the equation  $\mu_0 a_{i_0} + \mu_1 a_{i_1} + \dots + \mu_q a_{i_q} = 0$  holds. Therefore the points  $a_{i_0}, a_{i_1}, \dots, a_{i_q}$  are in general position.  $\square$

Now we can define a simplex in an Euclidean space.

**Definition 2.1.3** (simplex). *A  $q$ -simplex in an Euclidean space is a set defined as*

$$|a_0 a_1 \cdots a_q| = \{ \lambda_0 a_0 + \lambda_1 a_1 + \dots + \lambda_q a_q \mid \lambda_0 + \lambda_1 + \dots + \lambda_q = 1, \lambda_i \geq 0 \}, \quad (2.1.3)$$

where  $a_0, a_1, \dots, a_q$  are points in general position.

The notions on simplices are introduced. The symbols like  $\sigma$  or  $\tau$  denote a simplex. To express the dimension of a simplex, let  $\sigma^q$  denote a  $q$ -simplex. The dimension of a  $q$ -simplex is denoted as  $\dim |a_0 a_1 \cdots a_q|$  or  $\dim \sigma$ .

A simplex has its faces. A face of a simplex is a simplex made up of a subset of the vertices of the simplex. The definition is given below:

**Definition 2.1.4** (face of simplex). *For a  $q$ -simplex  $\sigma = |a_0 a_1 \cdots a_q|$ , choose  $r$  vertices among the vertices of the simplex:  $a_{i_0}, a_{i_1}, \dots, a_{i_r}$ .*

*The  $r$ -simplex*

$$\tau = |a_{i_0} a_{i_1} \cdots a_{i_r}| \quad (2.1.4)$$

*is called an  $r$ -face of the simplex  $\sigma$ . A symbol  $\tau \prec \sigma$  or  $\sigma \succ \tau$  denotes the relation that  $\tau$  is a face of  $\sigma$ .*

The faces of a simplex is well-defined because of Lemma 2.1.2.

The difference of the dimension of a simplex  $\sigma$  and the dimension of a face  $\tau$  is called the codimension of  $\tau$ . The codimension of the face  $\tau$  is defined as  $\dim \sigma - \dim \tau$ .

**Lemma 2.1.5.** *The number of the faces of a  $q$ -simplex is*

$$2^{q+1} - 1 \quad (2.1.5)$$

*Proof.* The number of the  $r$ -faces of the  $q$ -simplex is equal to the number of  $(r+1)$ -combinations from the  $(q+1)$  vertices. The number of the faces of all dimensions is the summation of that of each dimension. It is calculated as

$$\sum_{r=0}^q \binom{q+1}{r+1} = 2^{q+1} - 1. \quad (2.1.6)$$

$\square$

I show some examples of simplices and faces.

**Example 2.1.6** (0, 1, 2, and 3-simplex). *A 0-simplex is a point because it has only one vertex. More precisely, a 0-simplex is the set defined as*

$$|a_0| = \{\lambda_0 a_0 \mid \lambda_0 = 1, \lambda_0 \geq 0\} = \{a_0\}. \quad (2.1.7)$$

*This set consists of only one point  $a_0$ .*

*A 1-simplex is a line segment. By definition, a 1-simplex is the set written as*

$$|a_0 a_1| = \{\lambda_0 a_0 + \lambda_1 a_1 \mid \lambda_0 + \lambda_1 = 1, \lambda_0 \geq 0, \lambda_1 \geq 0\} \quad (2.1.8)$$

$$= \{(1 - \lambda_1)a_0 + \lambda_1 a_1 \mid 0 \leq \lambda_1 \leq 1\}. \quad (2.1.9)$$

*This means that it is a line segment that starts from the point  $a_0$  and ends at the point  $a_1$ .*

*A 2-simplex is a triangle. It is written as*

$$|a_0 a_1 a_2| = \{\lambda_0 a_0 + \lambda_1 a_1 + \lambda_2 a_2 \mid \lambda_0 + \lambda_1 + \lambda_2 = 1, \lambda_i \geq 0\} \quad (2.1.10)$$

$$= \{a_0 + \lambda_1 \overrightarrow{a_0 a_1} + \lambda_2 \overrightarrow{a_0 a_2} \mid \lambda_1 \geq 0, \lambda_2 \geq 0, 0 \leq \lambda_1 + \lambda_2 \leq 1\}. \quad (2.1.11)$$

*It means that the simplex is a triangle with vertices  $a_0$ ,  $a_1$ , and  $a_2$ .*

*A 3-simplex is a tetrahedron. It is expressed as*

$$|a_0 a_1 a_2 a_3| = \{\lambda_0 a_0 + \lambda_1 a_1 + \lambda_2 a_2 + \lambda_3 a_3 \mid \lambda_0 + \lambda_1 + \lambda_2 + \lambda_3 = 1, \lambda_i \geq 0\} \quad (2.1.12)$$

$$= \{a_0 + \lambda_1 \overrightarrow{a_0 a_1} + \lambda_2 \overrightarrow{a_0 a_2} + \lambda_3 \overrightarrow{a_0 a_3} \mid \lambda_i \geq 0, 0 \leq \lambda_1 + \lambda_2 + \lambda_3 \leq 1\}. \quad (2.1.13)$$

*It means that the simplex is a tetrahedron with vertices  $a_0$ ,  $a_1$ ,  $a_2$ , and  $a_3$ .*

**Example 2.1.7** (faces). *What the faces of a simplex are is explained through examples of 0, 1, 2, and 3-simplex.*

*For a 0-simplex, there is only one face, the 0-simplex itself. The simplex itself is its face because it satisfies the condition given in Definition 2.1.4.*

*A 1-simplex has three faces. Let  $|a_0 a_1|$  be a 1-simplex. The 1-simplex itself is its face. Moreover, the 0-simplices  $|a_0|$  and  $|a_1|$  are faces of  $|a_0 a_1|$ . Therefore, the set of the faces of  $|a_0 a_1|$  is  $\{|a_0|, |a_1|, |a_0 a_1|\}$ .*

*A 2-simplex  $|a_0 a_1 a_2|$  has seven faces. The faces of dimension 0 are  $|a_0|$ ,  $|a_1|$ , and  $|a_2|$ . The faces of dimension 1 are  $|a_1 a_2|$ ,  $|a_0 a_2|$ , and  $|a_0 a_1|$ . The face of dimension 2 is  $|a_0 a_1 a_2|$ , which is the simplex itself.*

*A 3-simplex  $|a_0 a_1 a_2 a_3|$  has fifteen faces. The set of the faces is*

$$\begin{aligned} & \{|a_0|, |a_1|, |a_2|, |a_3|, |a_0 a_1|, |a_0 a_2|, |a_0 a_3|, |a_1 a_2|, |a_1 a_3|, |a_2 a_3|, \\ & |a_0 a_1 a_2|, |a_0 a_1 a_3|, |a_0 a_2 a_3|, |a_1 a_2 a_3|, |a_0 a_1 a_2 a_3|\}. \end{aligned} \quad (2.1.14)$$

## 2.1.2 Simplicial Complex

A simplicial complex is a shape assembled from simplices. The simplices in a simplicial complex are glued at their faces to each other. A simplicial complex is turned into a chain complex and the homology groups are computed from the chain complex.

**Definition 2.1.8** (simplicial complex). *Let  $K$  be a set of simplices in an Euclidean space. The set  $K$  is called a simplicial complex if and only if it satisfies the following conditions:*

1.  $\forall \sigma \in K, \forall \tau \prec \sigma, \tau \in K$ .
2.  $\forall \sigma \in K, \forall \tau \in K, \sigma \cap \tau \neq \emptyset \implies \sigma \cap \tau \prec \sigma \wedge \sigma \cap \tau \prec \tau$ .

The first condition in Definition 2.1.8 means that all the faces of each simplex of a simplicial complex  $K$  belong to  $K$ . The second condition means that if any two simplices have a non-empty intersection, the intersection must be a face of both simplices.

The 0-simplices in a simplicial complex are called vertices. The dimension of simplicial complex is denoted as  $\dim K$  and it is defined as:

$$\dim K = \max_{\sigma \in K} \dim \sigma. \quad (2.1.15)$$

A subset of a simplicial complex becomes a simplicial complex if it satisfies the conditions of Definition 2.1.8. Such a subset is called a subcomplex. Subcomplex is an important notion to compute the persistent homology groups.

**Definition 2.1.9** (subcomplex). *Let  $K$  be a simplicial complex and let  $L$  be a subset of  $K$ . The subset  $L$  is called a subcomplex of  $K$  if and only if it satisfies the following condition:*

1.  $\forall \sigma \in L, \forall \tau \prec \sigma, \tau \in L$ .

Let  $L \subset K$  denote the relation that  $L$  is a subcomplex of  $K$ .

If a subset  $L$  of a simplicial complex  $K$  satisfies the condition of Definition 2.1.9, it also satisfies the conditions of Definition 2.1.8 with respect to  $L$ , which means that the subset  $L$  is also a simplicial complex. It is trivial that the first condition of Definition 2.1.8 is satisfied with respect to  $L$ . The second condition is satisfied because the simplices  $L$  also belong to  $K$  and the faces belong to  $L$ . Thus a subcomplex of a simplicial complex is a simplicial complex.

The skeletons are the special cases of subcomplexes. The definition of the skeleton is shown below.

**Definition 2.1.10** (skeleton). *Let  $K$  be a simplicial complex. A subcomplex of  $K$  defined as*

$$K^{(q)} = \{\sigma \mid \sigma \in K, \dim \sigma \leq q\} \quad (2.1.16)$$

*is called the  $q$ -skeleton of  $K$ .*

The  $q$ -skeleton of a simplicial complex  $K$  is a subcomplex which consists of the simplices of dimension equal to  $q$  or less than  $q$ . It is clear that skeletons are subcomplexes by definition.

I show an example of a simplicial complex.

**Example 2.1.11** (2-skeleton of 3-simplex). *Let  $K$  be a simplicial complex whose simplices are the faces of a simplex  $|0123|$ . The numbers 0, 1, 2, and 3 denote the vertices. The 2-skeleton  $K^{(2)}$  is a subcomplex made up of the 0-simplices, 1-simplices, and 2-simplices of  $K$ .*

The 0-simplices of  $K$  are  $|0|$ ,  $|1|$ ,  $|2|$ , and  $|3|$ . There are six 1-simplices of  $K$ :  $|01|$ ,  $|02|$ ,  $|03|$ ,  $|12|$ ,  $|13|$ , and  $|23|$ . The 2-skeleton have four 3-simplices:  $|012|$ ,  $|013|$ ,  $|023|$ , and  $|123|$ . Therefore the 2-skeleton  $K^{(2)}$  is

$$K^{(2)} = \{|0|, |1|, |2|, |3|, |01|, |02|, |03|, |12|, |13|, |23|, |012|, |013|, |023|, |123|\}. \quad (2.1.17)$$

In order to define persistent homology groups, it is needed to define simplicial mappings. A simplicial mapping is a mapping between two simplicial complexes which preserves the structure of simplicial complexes.

**Definition 2.1.12** (simplicial mapping). *Let  $K$  and  $K'$  be simplicial complexes and let  $\hat{K}$  and  $\hat{K}'$  be the sets of the vertices of  $K$  and  $K'$  respectively. Consider a mapping  $\varphi : \hat{K} \rightarrow \hat{K}'$ . The mapping  $\varphi$  is called a simplicial mapping if and only if for each simplex  $\sigma = |a_{i_0} \cdots a_{i_q}|$  in  $K$ , the simplicial complex  $K'$  has a simplex with the vertices  $\{\varphi(a_{i_0}), \dots, \varphi(a_{i_q})\}$ . The notation  $\varphi : K \rightarrow K'$  denotes a simplicial mapping.*

A simplex mapped with a simplicial mapping may have dimension smaller than the original simplex because the mapping may map two different vertices to the same vertex.

For a simplicial complex  $K$ , the identity mapping  $\text{id}_{\hat{K}} : \hat{K} \rightarrow \hat{K}$ , which is a mapping between sets, induces a simplicial mapping  $\text{id}_K : K \rightarrow K$ , because each vertex of  $K$  is mapped to itself and each simplex is mapped to the simplex itself.

Let  $K$ ,  $K'$ , and  $K''$  be simplicial complexes and  $\varphi : K \rightarrow K'$  and  $\varphi' : K' \rightarrow K''$  be simplicial mappings. The composition  $\varphi' \circ \varphi : K \rightarrow K''$  is also a simplicial mapping. Take a simplex  $\sigma$  from the simplicial complex  $K$ . There is a simplex  $\varphi(\sigma)$  in  $K'$  since the mapping  $\varphi$  is a simplicial mapping. Then there is a simplex  $\varphi'(\varphi(\sigma))$ , which is a simplex mapped from  $\varphi(\sigma)$  with the simplicial mapping  $\varphi'$ . Therefore the composition  $\varphi' \circ \varphi$  is a simplicial mapping.

Let  $K$  be a simplicial complex and let  $L$  be a subcomplex of  $K$ . The inclusion mapping from the set of the vertices  $L$  to that of  $K$ , which  $\iota : \hat{L} \rightarrow \hat{K}$  denotes, induces a simplicial mapping  $\iota : L \rightarrow K$ . It is trivial that  $\iota$  is simplicial because every simplex in  $L$  belongs to the simplicial complex  $K$ .

### 2.1.3 Chain Complex

The orientation on a simplex is introduced to define chain complexes. The simplices defined in Section 2.1.1 are not oriented. The order of the vertices does not affect the identity of a simplex without an orientation. There are two orientations of a simplex. These orientations are made correspond to the signs: the positive and the negative. This correspondence enables us to use the coefficients of simplices and to introduce the algebra of simplices.

An orientation of a simplex is defined with the substitutions of the vertices.

**Definition 2.1.13** (substitution). *Let  $N$  be a set which consists of the integers from 1 to  $n$ . A bijection  $\sigma : N \rightarrow N$  is called a substitution of  $N$ . A substitution  $\sigma$  is denoted as*

$$\begin{pmatrix} 1 & 2 & \cdots & n \\ s_1 & s_2 & \cdots & s_n \end{pmatrix}, \quad (2.1.18)$$

where  $s_i = \sigma(i)$  for  $i = 1, 2, \dots, n$ .

A substitution which changes only two numbers is called a transposition.

**Definition 2.1.14** (transposition). *A transposition  $(p\ q)$  is a substitution defined as follows:*

$$(p\ q)(i) = \begin{cases} q & \text{if } i = p, \\ p & \text{if } i = q, \\ i & \text{otherwise.} \end{cases} \quad (2.1.19)$$

A substitution can be decomposed to a composition of transpositions. The sign of a substitution is defined with the number of the transpositions.

**Definition 2.1.15** (sign of substitution). *A substitution  $\sigma$  is called even when the number of the transpositions whose composition is  $\sigma$  is even. It is called odd when that number is odd.*

*The sign of the substitution  $\sigma$  is defined as follows:*

$$\epsilon(\sigma) = \begin{cases} +1 & \text{if } \sigma \text{ is even,} \\ -1 & \text{if } \sigma \text{ is odd.} \end{cases} \quad (2.1.20)$$

The orientation of a simplex is defined with the sign of the substitution of the vertices.

**Definition 2.1.16** (orientation of a simplex). *Let  $\sigma$  be a  $q$ -simplex. The vertices of  $\sigma$  are  $a_0, a_1, \dots, a_q$ . Consider the sequences made up of those vertices. Let  $(a_{i_0}, a_{i_1}, \dots, a_{i_q})$  and  $(a_{j_0}, a_{j_1}, \dots, a_{j_q})$  be sequences of the vertices.*

*An equivalent relation  $(a_{i_0}, a_{i_1}, \dots, a_{i_q}) \sim (a_{j_0}, a_{j_1}, \dots, a_{j_q})$  is defined as follows:*

$$(a_{i_0}, a_{i_1}, \dots, a_{i_q}) \sim (a_{j_0}, a_{j_1}, \dots, a_{j_q}) \Leftrightarrow \epsilon \left( \begin{pmatrix} 0 & 1 & \cdots & q \\ a_{i_0} & a_{i_1} & \cdots & a_{i_q} \end{pmatrix} \right) = \epsilon \left( \begin{pmatrix} 0 & 1 & \cdots & q \\ a_{j_0} & a_{j_1} & \cdots & a_{j_q} \end{pmatrix} \right), \quad (2.1.21)$$

where

$$\begin{pmatrix} 0 & 1 & \cdots & q \\ a_{i_0} & a_{i_1} & \cdots & a_{i_q} \end{pmatrix} \quad (2.1.22)$$

and

$$\begin{pmatrix} 0 & 1 & \cdots & q \\ a_{j_0} & a_{j_1} & \cdots & a_{j_q} \end{pmatrix} \quad (2.1.23)$$

are substitutions.

*There are two equivalent classes, which are called orientations of a simplex.*

The symbol  $\langle a_0 a_1 \cdots a_q \rangle$  denotes an oriented simplex. The minus sign denotes a simplex with the other orientation. For example,  $-\langle a_0 a_1 \cdots a_q \rangle$  denotes the simplex with the other orientation of a simplex  $\langle a_0 a_1 \cdots a_q \rangle$ .

**Example 2.1.17** (orientation of a simplex). *Let  $|01|$  be a 1-simplex. It has two orientations:  $\langle 01 \rangle$  and  $\langle 10 \rangle = -\langle 01 \rangle$ . The former is interpreted as a line segment from 0 to 1 and the latter is interpreted as a line segment from 1 to 0.*

*Let  $|012|$  be a 2-simplex. The permutations of the vertices are 012, 021, 102, 120, 201, and 210.*

The permutation 012 is the identity and the substitution is composed of zero transpositions. Thus 012 has the positive sign.

The permutation 021 is made by transposing 1 and 2 in 012. Thus 021 has the negative sign.

The permutation 102 is obtained by applying a transposition (0 1) to 012. Thus 021 has the negative sign.

The permutation 120 is the result of a composition of transpositions (0 1) and (1 2). Thus 120 has the positive sign.

The permutation 201 is the result of transpositions (0 1) · (0 2). Thus 201 has the positive sign.

The permutation 210 is obtained through the following steps. First 0 and 1 are transposed; we get 102. Second 0 and 2 are transposed; we get 120. Third 1 and 2 are transposed; we get 210. Thus 210 has the negative sign.

Therefore the oriented simplices are written as follows:

$$\begin{aligned}\langle 012 \rangle &= \langle 120 \rangle = \langle 201 \rangle, \\ \langle 021 \rangle &= \langle 102 \rangle = \langle 210 \rangle, \\ \langle 012 \rangle &= -\langle 021 \rangle.\end{aligned}\tag{2.1.24}$$

A chain complex is an algebraic object made from a simplicial complex. In fact a chain complex can be made from a complex other than simplicial complex, but I mention only how to make a chain complex from a simplicial complex. A chain complex consists of chain groups and boundary operators. A chain group is a module generated by simplices in a simplicial complex of some dimension. A boundary operator is a homomorphism which computes the boundary of simplices. A boundary operator connects a chain group of a certain dimension to the chain group of the smaller dimension.

**Definition 2.1.18** (*q*-th chain group). Let  $K$  be a simplicial complex and let  $\sigma_1^q, \sigma_2^q, \dots, \sigma_u^q$  be  $q$ -simplices in  $K$ . We choose orientations of the  $q$ -simplices:  $\langle \sigma_1^q \rangle, \langle \sigma_2^q \rangle, \dots, \langle \sigma_u^q \rangle$ .

An  $R$ -free module generated by the oriented  $q$ -simplices, which

$$C_q(K) = \left\{ c = \sum_{i=1}^u \gamma_i \langle \sigma_i^q \rangle \mid \gamma_i \in R \ (i = 1, \dots, u) \right\}\tag{2.1.25}$$

denotes, is called a  $q$ -chain group of  $K$ , where  $R$  is a ring.

An element of  $C_q(K)$  is called a  $q$ -chain. The addition of two  $q$ -chains  $c = \sum_{i=1}^u \gamma_i \langle \sigma_i^q \rangle$  and  $c' = \sum_{i=1}^u \gamma'_i \langle \sigma_i^q \rangle$  is defined as follows:

$$c + c' = \sum_{i=1}^u (\gamma_i + \gamma'_i) \langle \sigma_i^q \rangle.\tag{2.1.26}$$

For an oriented simplex  $\langle \sigma^q \rangle$ , a simplex with the other orientation  $-\langle \sigma^q \rangle$  is identified with  $(-1)\langle \sigma^q \rangle \in C_q(K)$ .

**Definition 2.1.19** (chain group). The chain group of a simplicial complex  $K$  is defined as follows:

$$C(K) = \{C_q(K)\}_{q \in \mathbb{Z}},\tag{2.1.27}$$

where  $C_q(K)$  is the  $q$ -th chain group of  $K$  for  $0 \leq q \leq \dim K$  and  $C_q(K) = 0$  for the other indices.

To complete the definition of chain complexes, the boundary operators have to be introduced.

**Definition 2.1.20** (boundary operator). *First the boundary of an oriented  $q$ -simplex  $\sigma^q = \langle a_0 a_1 \cdots a_q \rangle$  is defined as follows:*

$$\partial_q \sigma^q = \sum_{i=0}^q (-1)^i \langle a_0 \cdots \hat{a}_i \cdots a_q \rangle. \quad (2.1.28)$$

The symbol  $\hat{\phantom{a}}$  means that the vertex with  $\hat{\phantom{a}}$  is eliminated. The boundary of a 0-simplex is defined as  $\partial_0 \langle a \rangle = 0$ .

Then the operator  $\partial_q$  is linearly extended to a  $q$ -chain  $c = \sum_{j=1}^u \gamma_j \langle \sigma_j^q \rangle$ :

$$\partial_q c = \sum_{j=1}^u \gamma_j \partial_q \langle \sigma_j^q \rangle. \quad (2.1.29)$$

This homomorphism  $\partial_q : C_q(K) \rightarrow C_{q-1}(K)$  is called a boundary operator.

Next an important property of boundary operators is shown. This property is used later to define the homology groups.

**Proposition 2.1.21** (boundary operator). *For all  $q$ ,  $\partial_q \circ \partial_{q+1} = 0$  holds.*

*Proof.*

$$\partial_q \circ \partial_{q+1} \langle \sigma^{q+1} \rangle = \sum_{i=0}^{q+1} (-1)^i \partial_q \langle a_0 \cdots \hat{a}_i \cdots a_{q+1} \rangle \quad (2.1.30)$$

$$= \sum_{i=0}^{q+1} (-1)^i \left( \sum_{j=0}^{i-1} (-1)^j \langle a_0 \cdots \hat{a}_j \cdots \hat{a}_i \cdots a_{q+1} \rangle + \sum_{j=i+1}^{q+1} (-1)^{j-1} \langle a_0 \cdots \hat{a}_i \cdots \hat{a}_j \cdots a_{q+1} \rangle \right) \quad (2.1.31)$$

$$= \sum_{j < i} (-1)^{i+j} \langle a_0 \cdots \hat{a}_j \cdots \hat{a}_i \cdots a_{q+1} \rangle + \sum_{j > i} (-1)^{i+j-1} \langle a_0 \cdots \hat{a}_i \cdots \hat{a}_j \cdots a_{q+1} \rangle \quad (2.1.32)$$

$$= 0. \quad (2.1.33)$$

□

Before introducing chain complexes, some examples of boundary operators are given.

**Example 2.1.22** (the boundary of 1-simplex). *Let  $\sigma$  be a 1-simplex:  $\sigma = \langle a_0 a_1 \rangle$ . Its boundary is*

$$\partial_1 \sigma = \langle a_1 \rangle - \langle a_0 \rangle. \quad (2.1.34)$$

*The boundary of  $\partial_1 \sigma$  is*

$$\partial_0 \partial_1 \sigma = \partial_0 \langle a_1 \rangle - \partial_0 \langle a_0 \rangle = 0 - 0 = 0. \quad (2.1.35)$$

**Example 2.1.23** (the boundary of 2-simplex). Let  $\sigma$  be a 2-simplex:  $\sigma = \langle a_0 a_1 a_2 \rangle$ . Its boundary is

$$\partial_2 \sigma = \langle a_1 a_2 \rangle - \langle a_0 a_2 \rangle + \langle a_0 a_1 \rangle. \quad (2.1.36)$$

The boundary of  $\partial_2 \sigma$  is

$$\partial_1 \partial_2 \sigma = \partial_1 \langle a_1 a_2 \rangle - \partial_1 \langle a_0 a_2 \rangle + \partial_1 \langle a_0 a_1 \rangle \quad (2.1.37)$$

$$= (\langle a_2 \rangle - \langle a_1 \rangle) - (\langle a_2 \rangle - \langle a_0 \rangle) + (\langle a_1 \rangle - \langle a_0 \rangle) \quad (2.1.38)$$

$$= 0. \quad (2.1.39)$$

**Example 2.1.24** (the boundary of 3-simplex). Let  $\sigma$  be a 3-simplex:  $\sigma = \langle a_0 a_1 a_2 a_3 \rangle$ . Its boundary is

$$\partial_3 \sigma = \langle a_1 a_2 a_3 \rangle - \langle a_0 a_2 a_3 \rangle + \langle a_0 a_1 a_3 \rangle - \langle a_0 a_1 a_2 \rangle. \quad (2.1.40)$$

The boundary of  $\partial_3 \sigma$  is

$$\partial_2 \partial_3 \sigma = \partial_2 \langle a_1 a_2 a_3 \rangle - \partial_2 \langle a_0 a_2 a_3 \rangle + \partial_2 \langle a_0 a_1 a_3 \rangle - \partial_2 \langle a_0 a_1 a_2 \rangle \quad (2.1.41)$$

$$= (\langle a_2 a_3 \rangle - \langle a_1 a_3 \rangle + \langle a_1 a_2 \rangle) - (\langle a_2 a_3 \rangle - \langle a_0 a_3 \rangle + \langle a_0 a_2 \rangle) \quad (2.1.42)$$

$$+ (\langle a_1 a_3 \rangle - \langle a_0 a_3 \rangle + \langle a_0 a_1 \rangle) - (\langle a_1 a_2 \rangle - \langle a_0 a_2 \rangle + \langle a_0 a_1 \rangle) \quad (2.1.43)$$

$$= 0.$$

**Definition 2.1.25** (chain complex). The pair of the chain groups of a simplicial complex  $K$

$$C_*(K) = \{C_q(K)\}_{q \in \mathbb{Z}} \quad (2.1.44)$$

and the boundary operators

$$\partial_* = \{\partial_q : C_q(K) \rightarrow C_{q-1}(K) \mid \partial_q \partial_{q+1} = 0\}_{q \in \mathbb{Z}} \quad (2.1.45)$$

is called the chain complex of  $K$ .

The notion that corresponds to simplicial mappings is introduced, which is called the chain homomorphism.

**Definition 2.1.26** (chain homomorphism). Let  $K$  and  $K'$  be simplicial complexes and let  $(C_*(K), \partial_*)$  and  $(C_*(K'), \partial'_*)$  be their chain complexes respectively. Consider the homomorphisms  $h_q : C_q(K) \rightarrow C_q(K')$  for all  $q$ . The homomorphisms  $\{h_q\}_{q \in \mathbb{Z}}$  is called a chain homomorphism if and only if they satisfy the following equations for all  $q$ :

$$h_{q-1} \circ \partial_q = \partial'_q \circ h_q. \quad (2.1.46)$$

The identity mapping  $\text{id}_{C_q(K)} : C_q(K) \rightarrow C_q(K)$  is a chain homomorphism. This fact is trivial. The composition of two chain homomorphisms is a chain homomorphism. It is proved later. For a simplicial complex  $K$  and its subcomplex  $L$ , a chain homomorphism  $\iota_{\neq q} : C_q(L) \rightarrow C_q(K)$  is induced from the inclusion mapping  $\iota : L \hookrightarrow K$ . It is proved by introducing a chain homomorphism induced from a simplicial mapping.

**Proposition 2.1.27** (composition of chain homomorphisms). Let  $K$ ,  $K'$  and  $K''$  be simplicial complexes. Two chain homomorphisms  $h_q : C_q(K) \rightarrow C_q(K')$  and  $g_q : C_q(K') \rightarrow C_q(K'')$  are given. The composition  $g_q \circ h_q : C_q(K) \rightarrow C_q(K'')$  is a chain homomorphism.

*Proof.* Let  $\partial_q : C_q(K) \rightarrow C_{q-1}(K)$ ,  $\partial'_q : C_q(K') \rightarrow C_{q-1}(K')$  and  $\partial''_q : C_q(K'') \rightarrow C_{q-1}(K'')$  denote the boundary operators. The equation  $(g_{q-1} \circ h_{q-1}) \circ \partial_q = \partial''_q \circ (g_q \circ h_q)$  is shown below:

$$(g_{q-1} \circ h_{q-1}) \circ \partial_q = g_{q-1} \circ (h_{q-1} \circ \partial_q) \quad (2.1.47)$$

$$= g_{q-1} \circ (\partial'_q \circ h_q) \quad (2.1.48)$$

$$= (g_{q-1} \circ \partial'_q) \circ h_q \quad (2.1.49)$$

$$= (\partial''_q \circ g_q) \circ h_q \quad (2.1.50)$$

$$= \partial''_q \circ (g_q \circ h_q). \quad (2.1.51)$$

□

**Proposition 2.1.28** (chain homomorphism induced from simplicial mapping). *Let  $K$  and  $K'$  be simplicial complices and let  $\varphi : K \rightarrow K'$  be a simplicial mapping. For a  $q$ -simplex  $\langle \sigma^q \rangle = \langle a_0 a_1 \cdots a_q \rangle$ , a mapping  $\varphi_{\#q} \langle a_0 a_1 \cdots a_q \rangle$  is defined as follows:*

$$\varphi_{\#q}(\langle a_0 a_1 \cdots a_q \rangle) = \begin{cases} \langle \varphi(a_0) \varphi(a_1) \cdots \varphi(a_q) \rangle, & \text{if } \varphi(a_0), \dots, \varphi(a_q) \text{ are differ-} \\ & \text{ent from each other,} \\ 0 & \text{otherwise.} \end{cases} \quad (2.1.52)$$

For a  $q$ -chain  $c = \sum_i \gamma_i \langle \sigma_i \rangle$ , the mapping  $\varphi_{\#q}$  is linearly extended as

$$\varphi_{\#q}(c) = \sum_i \gamma_i \varphi_{\#q}(\langle \sigma_i \rangle), \quad (2.1.53)$$

then  $\varphi_{\#q} : C_q(K) \rightarrow C_q(K')$  becomes a chain homomorphism.

*Proof.* Consider the case where  $\varphi(a_0), \varphi(a_1), \dots, \varphi(a_q)$  are different from each other. Prove Equation (2.1.46) with respect to  $\varphi_{\#q}$ :

$$\partial'_q(\varphi_{\#q} \langle a_0 a_1 \cdots a_q \rangle) = \partial'_q \langle \varphi(a_0) \varphi(a_1) \cdots \varphi(a_q) \rangle \quad (2.1.54)$$

$$= \sum_{i=0}^q (-1)^i \langle \varphi(a_0) \cdots \varphi(\hat{a}_i) \cdots \varphi(a_q) \rangle \quad (2.1.55)$$

$$= \varphi_{\#q-1}(\partial_q \langle a_0 \cdots a_q \rangle). \quad (2.1.56)$$

Therefore  $\varphi_{\#q-1} \circ \partial_q = \partial'_q \circ \varphi_{\#q}$  holds.

Consider the case where there are the same vertices among  $\varphi(a_0), \dots, \varphi(a_q)$ . Let  $\varphi(a_j) = \varphi(a_k)$  for two indices  $j < k$ . The equation

$$\partial'_q(\varphi_{\#q} \langle a_0 \cdots a_q \rangle) = \partial'_q(0) = 0 \quad (2.1.57)$$

holds.

Then we obtain the equation

$$\varphi_{\#q-1}(\partial_q \langle a_0 a_1 \cdots a_q \rangle) = \varphi_{\#q-1} \left( \sum_{i=0}^q (-1)^i \langle a_0 \cdots \hat{a}_i \cdots a_q \rangle \right) \quad (2.1.58)$$

$$= (-1)^j \varphi_{\#q-1} \langle a_0 \cdots \hat{a}_j \cdots a_q \rangle + (-1)^k \varphi_{\#q-1} \langle a_0 \cdots \hat{a}_k \cdots a_q \rangle \quad (2.1.59)$$

$$= (-1)^j \langle \varphi(a_0) \cdots \varphi(a_{j-1}) \varphi(a_{j+1}) \cdots \varphi(a_q) \rangle + (-1)^k \langle \varphi(a_0) \cdots \varphi(a_{k-1}) \varphi(a_{k+1}) \cdots \varphi(a_q) \rangle. \quad (2.1.60)$$

Arrange the vertices of the first term:

$$\langle \varphi(a_0) \cdots \varphi(a_{j-1}) \varphi(a_{j+1}) \cdots \varphi(a_{k-1}) \varphi(a_k) \varphi(a_{k+1}) \cdots \varphi(a_q) \rangle \quad (2.1.61)$$

Move the  $\varphi(a_k)$  left by  $k - j + 1$ :

$$(-1)^{k-j+1} \langle \varphi(a_0) \cdots \varphi(a_{j-1}) \varphi(a_k) \varphi(a_{j+1}) \cdots \varphi(a_{k-1}) \varphi(a_{k+1}) \cdots \varphi(a_q) \rangle. \quad (2.1.62)$$

Because  $\varphi(a_k) = \varphi(a_j)$ , the equation

$$\varphi_{\#q-1} \langle a_0 \cdots \hat{a}_j \cdots a_q \rangle = (-1)^{k-j+1} \varphi_{\#q-1} \langle a_0 \cdots \hat{a}_k \cdots a_q \rangle \quad (2.1.63)$$

holds and we obtain

$$(-1)^j \varphi_{\#q-1} \langle a_0 \cdots \hat{a}_j \cdots a_q \rangle + (-1)^k \varphi_{\#q-1} \langle a_0 \cdots \hat{a}_k \cdots a_q \rangle = 0. \quad (2.1.64)$$

Therefore we obtain  $\varphi_{\#q-1} \circ \partial_q = \partial'_q \circ \varphi_{\#q}$  and  $\varphi_{\#q}$  is a chain homomorphism.  $\square$

#### 2.1.4 Homology Group

Homology groups are introduced by using the concepts on chain complexes. The boundary operators give us the boundary groups and the cycle groups. A boundary group is an ensemble of the boundaries of chains and a cycle group is an ensemble of the chains whose boundary is zero. A cycle, which is a member of a cycle group, represents a hole in a shape. Although we can detect the holes in a shape by enumerating the cycles at first glance, we must exclude the cycles that are the boundaries of the higher dimensional chains; thus a cycle group is divided by the boundary group of the same dimension, and the quotient group is called the homology group.

**Definition 2.1.29** (boundary group). *The  $q$ -th boundary group of a simplicial complex  $K$  is defined as follows:*

$$B_q(K) = \text{Im } \partial_{q+1} = \{b \mid \exists c' \in C_{q+1}(K), b = \partial_{q+1} c'\}. \quad (2.1.65)$$

An element of  $B_q(K)$  is called a  $q$ -boundary.

**Definition 2.1.30** (cycle group). *The  $q$ -th cycle group of a simplicial complex  $K$  is defined as follows:*

$$Z_q(K) = \text{Ker } \partial_q = \{c \mid c \in C_q(K), \partial_q c = 0\}. \quad (2.1.66)$$

An element of  $Z_q(K)$  is called a  $q$ -cycle.

A boundary group  $B_q(K)$  is a submodule of a cycle group  $Z_q(K)$ . It is proved with the property of the boundary operators.

**Proposition 2.1.31.** *The relation  $B_q(K) \subset Z_q(K)$  holds for all  $q$ .*

*Proof.* Take a  $q$ -boundary  $b \in B_q(K)$ . By definition, there is a  $(q+1)$ -chain  $c \in C_{q+1}(K)$  which satisfies  $b = \partial_{q+1} c$ . Taking the boundary of  $b$ , we obtain the equation

$$\partial_q b = \partial_q \partial_{q+1} c = 0. \quad (2.1.67)$$

This equation means that  $b \in Z_q(K)$ , and therefore,  $B_q(K) \subset Z_q(K)$  holds.  $\square$

This proposition justifies computing the quotient group of a cycle group divided by a boundary group.

**Definition 2.1.32** (homology group). *The  $q$ -th homology group of a simplicial complex is defined as follows:*

$$H_q(K) = Z_q(K)/B_q(K). \quad (2.1.68)$$

The direct sum

$$H_*(K) = \bigoplus_{q \in \mathbb{Z}} H_q(K) \quad (2.1.69)$$

is called the homology group of  $K$ .

An element of  $q$ -th homology group is denoted as  $[z_q]$  or  $z_q + B_q(K)$ , where  $z_q$  is a  $q$ -cycle. An element  $[z_q]$  is called a homology class.

Similar to chain complexes, there are mappings between homology groups induced from chain homomorphisms.

**Definition 2.1.33** (induced homomorphism). *Let  $K$  and  $K'$  be simplicial complexes and let  $\{h_q\} : \{C_q(K)\} \rightarrow \{C_q(K')\}$  be a chain homomorphism. Define a mapping from  $H_q(K)$  to  $H_q(K')$  by making a homology class  $[z] = z + B_q(K)$  correspond to  $[h_q(z)] = h_q(z) + B_q(K')$ . The mapping is denoted as*

$$(h_q)_*[z] = [h_q(z)]. \quad (2.1.70)$$

The mapping  $(h_q)_* : H_q(K) \rightarrow H_q(K')$  is called the induced homomorphism.

**Lemma 2.1.34.** *The induced mapping of homology groups is well-defined.*

*Proof.* First it is proved that the mapped cycle belongs to a cycle group and the mapped boundary belongs to a boundary group. Second it is proved that the mapped homology class does not depend on the choice of the representative cycle.

Take a cycle  $z \in Z_q(K)$  and map it with the chain homomorphism  $h_q$ . We obtain  $h_q(z)$ . The boundary of  $h_q(z)$  satisfies the equation

$$\partial'_q h_q(z) = h_{q-1} \partial_q z = h_{q-1}(0) = 0 \quad (2.1.71)$$

because of the commutativity of chain homomorphisms.

Take a boundary  $b \in B_q(K)$  and there is a chain  $c \in C_{q+1}(K)$  which satisfies  $b = \partial_{q+1} c$ . The image of  $b$  satisfies the equation

$$h_q(b) = h_q \partial_{q+1} c = \partial'_q (h_{q+1}(c)) \quad (2.1.72)$$

and thus  $h_q(b) \in B_q(K')$  holds.

Let  $z$  and  $z'$  be  $q$ -cycles homologous to each other. The relation

$$z - z' \in B_q(K) \quad (2.1.73)$$

holds. Apply the mapping  $h_q$  to the relation above:

$$h_q(z - z') \in h_q(B_q(K)). \quad (2.1.74)$$

The left-hand side of Equation (2.1.74) is  $h_q(z) - h_q(z')$  and the right-hand side satisfies the relation  $h_q(B_q(K)) \subset B_q(K')$ . We have the relation

$$h_q(z) - h_q(z') \in B_q(K'). \quad (2.1.75)$$

The homology classes satisfy that

$$(h_q)_*[z] - (h_q)_*[z'] = [h_q(z)] - [h_q(z')] \quad (2.1.76)$$

$$= (h_q(z) + B_q(K')) - (h_q(z') + B_q(K')) \quad (2.1.77)$$

$$= h_q(z) - h_q(z') + B_q(K') \quad (2.1.78)$$

$$= 0 + B_q(K'), \quad (2.1.79)$$

and thus  $(h_q)_*[z]$  is homologous to  $(h_q)_*[z']$ . Therefore the induced homomorphism is well-defined.  $\square$

The homology group of a simplicial complex is computed with the images and the kernels of the boundary operators. The images and the kernels are computed by manipulating the matrices representing the boundary operators. I give no examples of homology groups because the computation of persistent homology groups gives homology groups. I give examples of persistent homology groups later.

### 2.1.5 Persistent Homology

Persistent homology groups are defined on a filtered simplicial complex. A filtered simplicial complex is a simplicial complex whose simplices are sorted in an order, and a filtered simplicial complex becomes an increasing sequence of subcomplexes. A subset which consists of simplices from the start to some index of a filtered simplicial complex becomes a subcomplex of the filtered simplicial complex. The filtration, an ordered sequence of subcomplexes, gives the notion of topological persistence. Topological persistence means how long a topological entity lives through the change of a shape.

**Definition 2.1.35** (filter of simplicial complex). *Let  $K = \{\sigma_i\}_{i=1}^n$  be a simplicial complex. A total order of the simplices is given; for any two simplices  $\sigma$  and  $\tau$  in  $K$ , there is an inequality  $\sigma \leq \tau$  or  $\sigma \geq \tau$ . For all simplices  $\sigma$ , if the set*

$$\sigma^- = \{\tau \mid \tau \in K, \tau \leq \sigma\} \quad (2.1.80)$$

*is a subcomplex of  $K$ , such a total order is called a filter of simplicial complex.*

A filter gives a filtered simplicial complex or a filtration of a simplicial complex.

**Definition 2.1.36** (filtration). *A filter of a simplicial complex  $K = \{\sigma_i\}_{i=1}^n$  is given:*

$$\sigma_1 \leq \sigma_2 \leq \cdots \leq \sigma_n. \quad (2.1.81)$$

*Let  $K_i$  be the  $i$ -th subcomplex  $\sigma_i^-$ . The increasing sequence*

$$K_1 \subset K_2 \subset \cdots \subset K_n = K \quad (2.1.82)$$

*is called a filtration of  $K$ .*

There are inclusions between the subcomplexes in a filtration. The induced homomorphisms of the inclusions give us the definition of persistent homology.

**Definition 2.1.37** (persistent homology group). *A filtration of a simplicial complex is given:*

$$K_1 \subset K_2 \subset \cdots \subset K_n. \quad (2.1.83)$$

Let  $\iota^{l,l+p}$  denote the inclusion mapping from  $K_l$  to  $K_{l+p}$ . There is the induced homomorphism  $\iota_*^{l,l+p} : H_*(K_l) \rightarrow H_*(K_{l+p})$ . The induced homomorphism of the  $q$ -th homology group is denoted as  $\iota_{*q}^{l,l+p} : H_q(K_l) \rightarrow H_q(K_{l+p})$ . The  $q$ -th persistent homology group of  $K_l$  with persistence  $p$  is defined as follows:

$$H_q^{l,p}(K) = \text{Im } \iota_{*q}^{l,l+p} = Z_q(K_l) / (B_q(K_{l+p}) \cap Z_q(K_l)). \quad (2.1.84)$$

It is needed to explain the well-definedness of the definition above. An element of  $\text{Im } \iota_{*q}^{l,l+p}$  is identified with the equivalence relation  $z - z' \in B_q(K_{l+p})$  for  $z, z' \in Z_q(K_l)$ . Because the relation  $z - z' \in Z_q(K_l)$  also holds, the relation  $z - z' \in B_q(K_{l+p}) \cap Z_q(K_l)$  holds. Thus the intersection  $B_q(K_{l+p}) \cap Z_q(K_l)$  is a subset of  $Z_q(K_l)$  and the persistent homology is well-defined.

Now introduced is an algorithm to compute the persistent homology of a filtered simplicial complex. The algorithm, proposed by Cohen-Steiner, Edelsbrunner, and Morozov (2006), is called the matrix reduction and the persistence pairing. Below, the coefficient ring of chain complexes is fixed to  $\mathbb{Z}/2\mathbb{Z}$ .

The algorithm requires a matrix representing the boundary operator.

**Definition 2.1.38** (boundary matrix). *Let  $m$  be the dimension of a filtered simplicial complex  $K$ . The non-zero chain groups are  $C_0(K), C_1(K), \dots, C_m(K)$ . The simplices of  $K$  are sorted in the following order:*

$$\langle \sigma_1 \rangle, \langle \sigma_2 \rangle, \dots, \langle \sigma_n \rangle. \quad (2.1.85)$$

Let  $\mathcal{C}$  denote the linear space whose basis is the simplices in the order above. The isomorphism

$$\mathcal{C} \simeq C_0(K) \oplus C_1(K) \oplus \cdots \oplus C_m(K) \quad (2.1.86)$$

holds, because the basis  $\mathcal{C}$  is the rearranged set of the bases of  $C_0(K), C_1(K), \dots, C_m(K)$ . The direct sum of the boundary operators is defined as

$$\partial = \partial_0 \oplus \partial_1 \oplus \cdots \oplus \partial_m. \quad (2.1.87)$$

The representation of  $\partial$  with respect to  $\mathcal{C}$  is called the boundary matrix of  $K$ . It is denoted as  $D$ . The elements of the boundary matrix is

$$D_{i,j} = \begin{cases} 1 & \text{if } \sigma_i \text{ is a face of } \sigma_j \text{ of codimension 1,} \\ 0 & \text{otherwise.} \end{cases} \quad (2.1.88)$$

The matrix reduction algorithm (Cohen-Steiner, Edelsbrunner, and Morozov, 2006; Edelsbrunner and Harer, 2010: pp. 152-153) reveals the image and

the kernel of a boundary matrix. It is a variation of the gaussian elimination, but it only uses column-wise addition.

---

**Algorithm 1:** Matrix reduction

---

**Data:** a boundary matrix  $D$ .  
**Result:** a reduced matrix  $R$ .

```

1 begin
2    $R \leftarrow D$ ;
3   for  $j = 1, \dots, n$  do
4     while  $\exists j' < j$  s.t.  $\text{low}_R(j') = \text{low}_R(j)$  do
5        $\lfloor$  Add the  $j'$ -th column to the  $j$ -th column;

```

---

The notation  $\text{low}_R(j)$  means that the index of the lowest 1 element of the  $j$ -th column of the matrix  $R$ , in other words, the maximum index of the element whose value is 1. The term "lowest" means that the element whose value is 1 is positioned at the lowest position in the view that the  $j$ -th column is written in the form of a horizontal vector. If the  $j$ -th column is a zero vector, the  $\text{low}_R(j)$  is none.

**Definition 2.1.39.** Let  $A$  be a matrix whose elements are 0 or 1. The function  $\text{low}_A$  is defined as

$$\text{low}_A(j) = \max \{i \mid A_{i,j} = 1\} \quad (2.1.89)$$

if the set  $\{i \mid A_{i,j} = 1\}$  is not empty. The function  $\text{low}_A$  is defined as none otherwise.

**Example 2.1.40.** The matrix  $A$  is given as follows:

$$A = \begin{pmatrix} 1 & 0 & 1 & 0 \\ 1 & 0 & 1 & 1 \\ 0 & 0 & 0 & 1 \\ 0 & 0 & 1 & 0 \end{pmatrix}. \quad (2.1.90)$$

It has four columns. The values of  $\text{low}_A$  for each column are shown below:

$$\text{low}_A(1) = 2, \quad (2.1.91)$$

$$\text{low}_A(2) = \text{None}, \quad (2.1.92)$$

$$\text{low}_A(3) = 4, \quad (2.1.93)$$

$$\text{low}_A(4) = 3. \quad (2.1.94)$$

If the matrix computed with Algorithm 1 satisfies the equations  $\text{low}_R(j) \neq \text{low}_R(j')$  for any two non-zero columns  $j \neq j'$ , the matrix  $R$  is called reduced and the  $\text{low}_R$  is called a pairing function.

The matrix  $D$  is decomposed as  $D = RU$  where  $U$  is an invertible upper triangular matrix. The matrix  $U$  is invertible because it is a composition of elementary operations.

The zero columns of the matrix  $R$  are paired to the non-zero columns with the persistence pairing algorithm (Cohen-Steiner, Edelsbrunner, and Morozov,

---

**Algorithm 2:** Persistence pairing

---

**Data:** a reduced matrix  $R$ .

**Result:** persistence pairs of each dimension.

```

1 for  $j = 1, \dots, n$  do
2   if the  $j$ -th column is a zero vector then
3     if  $\exists k$  s.t.  $\text{low}_R(k) = j$  then
4        $\lfloor$  Add a persistence pair  $(j, k)$  of dimension  $\dim \sigma_j$ ;
5        $\lfloor$  Add a persistence pair  $(j, \infty)$  of dimension  $\dim \sigma_j$ ;

```

---

A persistence pair whose lifetime is finite is called an inessential homology class and a persistence pair whose lifetime is infinite is called an essential homology class.

The matrix reduction algorithm only uses the operation of adding the  $j'$ -th column to the  $j$ -th column ( $j' < j$ ), which is one of the elementary transformations of matrix. This operation changes the basis of the linear space  $\mathcal{C}$ . Let  $\langle c_1, c_2, \dots, c_n \rangle$  denote the basis of  $\mathcal{C}$ . The operation updates the  $j$ -th chain of the basis to  $c_j + c_{j'}$ . The linear space  $\mathcal{C}$  is the domain of the boundary operator  $\partial$ . The operation changes a chain whose boundary is to be taken. On the other hand, the basis of the codomain is not touched. Thus a column of the matrix represents the simplices that makes the boundary of a chain. The lowest 1 index of a column means the time when the boundary of a chain completes emerging. If a column is a zero vector, it means that the chain is a cycle.

The matrix reduction algorithm reduces the index when the boundary of each chain is born. Some columns become zero, which means that they are cycles. Others become non-zero vectors, which means that they are boundaries. The persistence pairing algorithm pairs the cycles and the boundaries according to the birth indices. The  $j$ -th column borns at the index  $j$ . This column must be paired to the column whose lowest 1 index is  $j$ . The column paired to the  $j$ -th column represents a boundary. This boundary shares the same simplex  $\sigma_j$  with the cycle represented by the  $j$ -th column. Thus they are same and the cycle dies at the index of the paired column  $k$ . If there is no pairable column, the cycle does not vanish.

Some properties of the algorithm are introduced. I explain the birth indices of the chains of the basis, the worst-case time complexity, and the number of non-zero columns of the reduced matrix. The analysis of the worst-case time complexity is originally found in (Edelsbrunner and Harer, 2010: pp.157-158). Moreover, a proof of the uniqueness of the pairing function that proved by Cohen-Steiner, Edelsbrunner, and Morozov (2006) is given.

**Proposition 2.1.41.** *The basis  $\langle c_1, c_2, \dots, c_n \rangle$  of the linear space  $\mathcal{C}$  is given. The chain  $c_j$  is born at the index  $j$ .*

*Proof.* Assume that the iterations on the 1-st column to the  $(j - 1)$ -th column have been done and the statement of the proposition holds. When the operations on the  $j$ -th column have been finished, some of the chains  $c_1, \dots, c_{j-1}$  are added to  $\sigma_j$ . The chains  $c_1, \dots, c_{j-1}$  are born before the index  $j$  and the chain  $c_j$  is born at the index  $j$  since it includes  $\sigma_j$ . Hence the chain  $c_j$  is born just at the index  $j$ .  $\square$

**Proposition 2.1.42.** *The matrix reduction algorithm stops in finite steps and its worst-case time complexity is  $O(n^3)$ .*

*Proof.* Consider the case that there is an index  $j'$  which satisfies the equation  $\text{low}_R(j') = \text{low}_R(j)$  for the index  $j$  that is greater than  $j'$ . The  $j'$ -th column being added to the column  $j$ , the  $\text{low}_R(j)$  decreases or becomes none. If the  $j$ -th column becomes a zero vector, the operation on the column  $j$  are finished. Otherwise the operations are repeated at most  $n$  times because the  $\text{low}_R(j)$  ranges from 1 to  $n$ . The operations are applied to  $n$  columns and thus the algorithm stops in finite steps.

Assume that the addition of columns takes  $n$  times additions of integers. For each column, the number of the column additions is at most  $n$ . Since there are  $n$  columns, the number of additions is at most  $n^3$ .  $\square$

The following two propositions give an explanation how the matrix reduction algorithm reveals the rank of a boundary matrix.

**Proposition 2.1.43.** *Suppose that the matrix reduction algorithm has finished till the  $(j - 1)$ -th column. Let  $\sigma_j$  be a simplex which is newly added to the basis of  $\mathcal{C}$ . The operations on the  $j$ -th column give us a chain  $c_j$ . The logical equivalence*

$$\{\partial c_1, \partial c_2, \dots, \partial c_{j-1}, \partial \sigma_j\} \text{ is linearly dependent} \Leftrightarrow \partial c_j = 0 \quad (2.1.95)$$

holds.

*Proof.* First the implication

$$\{\partial c_1, \partial c_2, \dots, \partial c_{j-1}, \partial \sigma_j\} \text{ is linearly dependent} \Rightarrow \partial c_j = 0 \quad (2.1.96)$$

is proved. From the assumption, the equation

$$\partial \sigma_j = \gamma_1 \partial c_1 + \dots + \gamma_{j-1} \partial c_{j-1} \quad (\gamma_k \in \mathbb{Z}/2\mathbb{Z}) \quad (2.1.97)$$

holds. The letters  $k_1, \dots, k_l$  denote the indices that the coefficient is 1. The equation is written as

$$\partial \sigma_j = \partial c_{k_1} + \dots + \partial c_{k_l}. \quad (2.1.98)$$

Because  $\text{low}(\partial c_{k_1}), \dots, \text{low}(\partial c_{k_l})$  are different from each other, the equation

$$\text{low}(\partial \sigma_j) = \max \{\text{low}(\partial c_{k_1}), \dots, \text{low}(\partial c_{k_l})\} \quad (2.1.99)$$

holds. The column that has the maximum  $\text{low}(\cdot)$  among  $\partial c_{k_1}, \dots, \partial c_{k_l}$  is selected, which  $\partial c_{k_a}$  denotes. The chain  $c_{k_a}$  is added to  $\sigma_j$ . Thus we obtain

$$\partial(\sigma_j + c_{k_a}) = \partial c_{k'_1} + \dots + \partial c_{k'_{l-1}}. \quad (2.1.100)$$

By repeating this operation, all the terms in the right-hand side of Equation (2.1.98) are moved to the left-hand side and let  $c_j$  denote the resulting chain, which satisfies that  $\partial c_j = 0$ .

Second the implication

$$\{\partial c_1, \partial c_2, \dots, \partial c_{j-1}, \partial \sigma_j\} \text{ is linearly dependent} \Leftarrow \partial c_j = 0 \quad (2.1.101)$$

is proved.

The chain  $c_j$  is written as

$$c_j = \eta_1 \sigma_1 + \cdots + \eta_j \sigma_j \quad (2.1.102)$$

with the initial basis of  $\mathcal{C}$ . The equation  $\partial c_j = 0$  gives us the equation

$$\partial c_j = \eta_1 \partial \sigma_1 + \cdots + \eta_j \partial \sigma_j = 0. \quad (2.1.103)$$

The simplex  $\sigma_j$  must be included in the chain  $c_j$ , hence  $\eta_j = 1$ . By adding  $\partial \sigma_j$  to the both sides of the equation above, we obtain the equation

$$\partial \sigma_j = \eta_1 \partial \sigma_1 + \cdots + \eta_{j-1} \partial \sigma_{j-1}. \quad (2.1.104)$$

Changing the basis suitably, we obtain the equation

$$\partial \sigma_j = \gamma_1 \partial c_1 + \cdots + \gamma_{j-1} \partial c_{j-1} \quad (2.1.105)$$

and it means that  $\partial c_1, \partial c_2, \dots, \partial c_{j-1}$  and  $\partial \sigma_j$  are linearly dependent.  $\square$

**Proposition 2.1.44.** *The number of non-zero columns of the reduced matrix is equal to  $\dim \text{Im } \partial$ .*

*Proof.* The boundary operator  $\partial$  is restricted to the basis  $\langle c_1, \dots, c_j \rangle$ , which  $\partial|_j$  denotes.  $R^{(j)}$  denotes the matrix reduced till the  $j$ -th column.

When  $j = 1$ , the matrix  $R^{(1)}$  consists of only one column and  $\partial \sigma_1 = 0$  since the first simplex  $\sigma_1$  must be a 0-simplex. Thus the number of non-zero columns of  $R^{(1)}$  is zero. On the other hand, the equation  $\dim \text{Im } \partial|_1 = 0$  holds because  $\sigma_1$  is a cycle.

Consider the case that the operations on the columns are done till the  $(j-1)$ -th column. Let  $r_j = \dim \text{Im } \partial|_j$  and the  $r_j$  satisfies that  $r_j = r_{j-1}$  or  $r_j = r_{j-1} + 1$ .

When  $r_j = r_{j-1}$ , for the simplex  $\sigma_j$  newly added to the basis, the boundary  $\partial \sigma_j$  is linearly dependent to  $\partial c_1, \dots, \partial c_{j-1}$ . Because of Proposition 2.1.43, the chain  $c_j$  satisfies  $\partial c_j = 0$ . Thus the number of non-zero columns of  $R^{(j)}$  does not change from that of  $R^{(j-1)}$ . Conversely, if the chain  $c_j$  satisfies  $\partial c_j = 0$ , the boundary  $\partial \sigma_j$  is linearly dependent to  $\partial c_1, \dots, \partial c_{j-1}$  and thus  $r_j$  is equal to  $r_{j-1}$ .

When  $r_j = r_{j-1} + 1$ , the boundary  $\sigma_j$  is linearly independent to  $\partial c_1, \dots, \partial c_{j-1}$ . The boundary  $\partial c_j$  does not become zero. Therefore the number of non-zero columns of  $R^{(j)}$  is incremented by one from that of  $R^{(j-1)}$  and vice versa.

By the mathematical induction, the statement holds.  $\square$

The uniqueness of the pairing function, which has been proved by Cohen-Steiner et al. (2006), is shown below. The proof is based on their work. Before giving the proposition, a quantity of a reduced matrix is introduced (Cohen-Steiner et al., 2006; Edelsbrunner and Harer, 2010: p. 154).

**Definition 2.1.45.** *Let  $A$  be an  $n$ -by- $n$  matrix. Let  $A_i^j$  be the submatrix of  $A$  composed of the  $i$ -th row to the  $n$ -th row and the 1-st column to the  $j$ -th column. The quantity  $r_A(i, j)$  is defined as follows:*

$$r_A(i, j) = \text{rank } A_i^j - \text{rank } A_{i+1}^j + \text{rank } A_{i+1}^{j-1} - \text{rank } A_i^{j-1}. \quad (2.1.106)$$

For any  $i$  and  $j$ ,  $\text{rank } A_i^j$  does not change when a column of  $A$  is added from left to right. This operation does not add a vector which is not contained in  $A_i^j$ . Thus the quantity  $r_A(i, j)$  is invariant under this operation. The following proposition ensures the uniqueness of the pairing function (Cohen-Steiner et al., 2006; Edelsbrunner and Harer, 2010: p. 154).

**Proposition 2.1.46** (pairing uniqueness). *A boundary matrix  $D$  is decomposed as  $D = RU$ , where  $R$  is a reduced matrix and  $U$  is an invertible upper triangle matrix. The logical equivalence*

$$\text{low}_R(j) = i \Leftrightarrow r_D(i, j) = 1 \quad (2.1.107)$$

*holds. Especially the pairing function does not depend on the  $RU$  decomposition.*

*Proof.* It is sufficient to prove the statement on the matrix  $R$  because the equation  $r_D(i, j) = r_R(i, j)$  holds.

First prove the implication

$$\text{low}_R(j) = i \Rightarrow r_D(i, j) = 1. \quad (2.1.108)$$

Assume that  $\text{low}_R(j) = i$ . The non-zero columns of the submatrix  $R_i^j$  are linearly independent. The last column of  $R_i^j$  is non-zero because of the assumption. Thus the equation  $\text{rank } R_i^j - \text{rank } R_i^{j-1} = 1$  holds. Removing the first row of  $R_i^j$ , we obtain a submatrix whose  $j$ -th column is zero since  $\text{low}_R(j) = i$ . Thus the equation  $\text{rank } R_{i+1}^j - \text{rank } R_{i+1}^{j-1} = 0$  holds. Therefore we obtain the equation

$$r_R(i, j) = (\text{rank } R_i^j - \text{rank } R_i^{j-1}) - (\text{rank } R_{i+1}^j - \text{rank } R_{i+1}^{j-1}) = 1 - 0 = 1. \quad (2.1.109)$$

Second prove the contraposition

$$\text{low}_R(j) \neq i \implies r_R(i, j) \neq 1. \quad (2.1.110)$$

in order to prove  $r_R(i, j) = 1 \implies \text{low}_R(j) = i$ . It is sufficient to prove the equation  $r_R(i, j) = 0$  because the difference of the ranks of the submatrices that defines the quantity  $r_R(i, j)$  is at most one.

If  $\text{low}_R(j) < i$ , the last columns of  $R_i^j$  and  $R_{i+1}^j$  are zero and we obtain the equations  $\text{rank } R_i^j = \text{rank } R_i^{j-1}$  and  $\text{rank } R_{i+1}^j = \text{rank } R_{i+1}^{j-1}$ . Thus the equation  $r_R(i, j) = 0$  holds.

If  $\text{low}_R(j) > i$ , the last columns of  $R_i^j$  and  $R_{i+1}^j$  are non-zero and we obtain the equations  $\text{rank } R_i^j = \text{rank } R_i^{j-1} + 1$  and  $\text{rank } R_{i+1}^j = \text{rank } R_{i+1}^{j-1} + 1$ . Thus the equation  $r_R(i, j) = 0$ .

Therefore the first statement was proved.

Suppose that a boundary matrix  $D$  is decomposed in two ways:  $D = R_1U_1$  and  $D = R_2U_2$ . Since the matrix  $U_1$  is invertible we obtain  $R_1 = R_2U_2U_1^{-1}$ . Because the matrix  $U_2U_1^{-1}$  means the composition of the operations that add a column from left to right, the equation  $r_{R_1}(i, j) = r_{R_2}(i, j)$  holds. Therefore the pairing function  $\text{low}_R$  does not depend on the decomposition of boundary matrix.  $\square$

I give an example of the computation of persistent homology groups.

**Example 2.1.47** (2-skeleton of 3-simplex). *Make a filtration of the 2-skeleton of a 3-simplex in the following order:*

$$\langle 0 \rangle, \langle 1 \rangle, \langle 2 \rangle, \langle 3 \rangle, \langle 01 \rangle, \langle 12 \rangle, \langle 02 \rangle, \langle 03 \rangle, \langle 23 \rangle, \langle 13 \rangle, \langle 012 \rangle, \langle 023 \rangle, \langle 013 \rangle, \langle 123 \rangle. \quad (2.1.111)$$

*The boundary matrix is as follows:*

$$\left( \begin{array}{cccc|cccc|cccc} 0 & 0 & 0 & 0 & 1 & 0 & 1 & 1 & 0 & 0 & 0 & 0 & 0 & 0 \\ 0 & 0 & 0 & 0 & 1 & 1 & 0 & 0 & 0 & 1 & 0 & 0 & 0 & 0 \\ 0 & 0 & 0 & 0 & 0 & 1 & 1 & 0 & 1 & 0 & 0 & 0 & 0 & 0 \\ 0 & 0 & 0 & 0 & 0 & 0 & 0 & 1 & 1 & 1 & 0 & 0 & 0 & 0 \\ 0 & 0 & 0 & 0 & 0 & 0 & 0 & 0 & 0 & 0 & 1 & 0 & 1 & 0 \\ 0 & 0 & 0 & 0 & 0 & 0 & 0 & 0 & 0 & 0 & 1 & 0 & 0 & 1 \\ 0 & 0 & 0 & 0 & 0 & 0 & 0 & 0 & 0 & 0 & 1 & 1 & 0 & 0 \\ 0 & 0 & 0 & 0 & 0 & 0 & 0 & 0 & 0 & 0 & 0 & 1 & 1 & 0 \\ 0 & 0 & 0 & 0 & 0 & 0 & 0 & 0 & 0 & 0 & 0 & 1 & 0 & 1 \\ 0 & 0 & 0 & 0 & 0 & 0 & 0 & 0 & 0 & 0 & 0 & 0 & 1 & 1 \\ 0 & 0 & 0 & 0 & 0 & 0 & 0 & 0 & 0 & 0 & 0 & 0 & 0 & 0 \\ 0 & 0 & 0 & 0 & 0 & 0 & 0 & 0 & 0 & 0 & 0 & 0 & 0 & 0 \\ 0 & 0 & 0 & 0 & 0 & 0 & 0 & 0 & 0 & 0 & 0 & 0 & 0 & 0 \end{array} \right) \quad (2.1.112)$$

*Apply the matrix reduction algorithm to this boundary matrix. There are 14 columns.*

**Column 1-4**

*The 1-st column to the 4-th column are zero columns. Thus they are cycles and no reduction is applied.*

**Column 5**

*The value of the  $\text{low}(5)$  is 2. There is no column whose  $\text{low}(\cdot)$  is 2 before the 5-th column. Thus no reduction is applied.*

**Column 6**

*The value of the  $\text{low}(6)$  is 3. There is no columns whose  $\text{low}(\cdot)$  is 3 before the 6-th column. Thus no reduction is applied.*

**Column 7**

The value of the  $\text{low}(7)$  is 3. The 6-th column has the same value. Thus the 6-th column is added to the 7-th column:

$$\left( \begin{array}{cccc|cccc|cccc} 0 & 0 & 0 & 0 & 1 & 0 & 1 & 1 & 0 & 0 & 0 & 0 & 0 & 0 & 0 \\ 0 & 0 & 0 & 0 & 1 & 1 & 1 & 0 & 0 & 1 & 0 & 0 & 0 & 0 & 0 \\ 0 & 0 & 0 & 0 & 0 & 1 & 0 & 0 & 1 & 0 & 0 & 0 & 0 & 0 & 0 \\ 0 & 0 & 0 & 0 & 0 & 0 & 0 & 1 & 1 & 1 & 0 & 0 & 0 & 0 & 0 \\ 0 & 0 & 0 & 0 & 0 & 0 & 0 & 0 & 0 & 0 & 1 & 0 & 1 & 0 & 0 \\ 0 & 0 & 0 & 0 & 0 & 0 & 0 & 0 & 0 & 0 & 1 & 0 & 0 & 1 & 0 \\ 0 & 0 & 0 & 0 & 0 & 0 & 0 & 0 & 0 & 0 & 1 & 1 & 0 & 0 & 0 \\ 0 & 0 & 0 & 0 & 0 & 0 & 0 & 0 & 0 & 0 & 0 & 1 & 1 & 0 & 0 \\ 0 & 0 & 0 & 0 & 0 & 0 & 0 & 0 & 0 & 0 & 0 & 1 & 0 & 1 & 0 \\ 0 & 0 & 0 & 0 & 0 & 0 & 0 & 0 & 0 & 0 & 0 & 0 & 1 & 1 & 0 \\ 0 & 0 & 0 & 0 & 0 & 0 & 0 & 0 & 0 & 0 & 0 & 0 & 0 & 1 & 1 \\ 0 & 0 & 0 & 0 & 0 & 0 & 0 & 0 & 0 & 0 & 0 & 0 & 0 & 0 & 0 \\ 0 & 0 & 0 & 0 & 0 & 0 & 0 & 0 & 0 & 0 & 0 & 0 & 0 & 0 & 0 \\ 0 & 0 & 0 & 0 & 0 & 0 & 0 & 0 & 0 & 0 & 0 & 0 & 0 & 0 & 0 \end{array} \right). \quad (2.1.113)$$

The value of the  $\text{low}(7)$  has changed into 2. The 5-th column has the same value. Thus the 5-th column is added to the 7-th column:

$$\left( \begin{array}{cccc|cccc|cccc} 0 & 0 & 0 & 0 & 1 & 0 & 0 & 1 & 0 & 0 & 0 & 0 & 0 & 0 & 0 \\ 0 & 0 & 0 & 0 & 1 & 1 & 0 & 0 & 0 & 1 & 0 & 0 & 0 & 0 & 0 \\ 0 & 0 & 0 & 0 & 0 & 1 & 0 & 0 & 1 & 0 & 0 & 0 & 0 & 0 & 0 \\ 0 & 0 & 0 & 0 & 0 & 0 & 0 & 1 & 1 & 1 & 0 & 0 & 0 & 0 & 0 \\ 0 & 0 & 0 & 0 & 0 & 0 & 0 & 0 & 0 & 0 & 1 & 0 & 1 & 0 & 0 \\ 0 & 0 & 0 & 0 & 0 & 0 & 0 & 0 & 0 & 0 & 1 & 0 & 0 & 1 & 0 \\ 0 & 0 & 0 & 0 & 0 & 0 & 0 & 0 & 0 & 0 & 1 & 1 & 0 & 0 & 0 \\ 0 & 0 & 0 & 0 & 0 & 0 & 0 & 0 & 0 & 0 & 0 & 1 & 1 & 0 & 0 \\ 0 & 0 & 0 & 0 & 0 & 0 & 0 & 0 & 0 & 0 & 0 & 1 & 0 & 1 & 0 \\ 0 & 0 & 0 & 0 & 0 & 0 & 0 & 0 & 0 & 0 & 0 & 1 & 0 & 1 & 0 \\ 0 & 0 & 0 & 0 & 0 & 0 & 0 & 0 & 0 & 0 & 0 & 0 & 1 & 1 & 0 \\ 0 & 0 & 0 & 0 & 0 & 0 & 0 & 0 & 0 & 0 & 0 & 0 & 0 & 1 & 1 \\ 0 & 0 & 0 & 0 & 0 & 0 & 0 & 0 & 0 & 0 & 0 & 0 & 0 & 0 & 0 \\ 0 & 0 & 0 & 0 & 0 & 0 & 0 & 0 & 0 & 0 & 0 & 0 & 0 & 0 & 0 \\ 0 & 0 & 0 & 0 & 0 & 0 & 0 & 0 & 0 & 0 & 0 & 0 & 0 & 0 & 0 \end{array} \right). \quad (2.1.114)$$

The 7-th column has become zero. Therefore it is a cycle and is represented as  $\langle 01 \rangle + \langle 12 \rangle + \langle 20 \rangle$ .

**Column 8**

The value of  $\text{low}(8)$  is 4. It is unique before the 8-th column. Thus no reduction is applied.



$$\left( \begin{array}{cccc|cccc|cccc} 0 & 0 & 0 & 0 & 1 & 0 & 0 & 1 & 0 & 0 & 0 & 0 & 0 & 0 \\ 0 & 0 & 0 & 0 & 1 & 1 & 0 & 0 & 0 & 1 & 0 & 0 & 0 & 0 \\ 0 & 0 & 0 & 0 & 0 & 1 & 0 & 0 & 0 & 0 & 0 & 0 & 0 & 0 \\ 0 & 0 & 0 & 0 & 0 & 0 & 0 & 1 & 0 & 1 & 0 & 0 & 0 & 0 \\ 0 & 0 & 0 & 0 & 0 & 0 & 0 & 0 & 0 & 0 & 1 & 0 & 1 & 0 \\ 0 & 0 & 0 & 0 & 0 & 0 & 0 & 0 & 0 & 0 & 1 & 0 & 0 & 1 \\ 0 & 0 & 0 & 0 & 0 & 0 & 0 & 0 & 0 & 0 & 1 & 1 & 0 & 0 \\ 0 & 0 & 0 & 0 & 0 & 0 & 0 & 0 & 0 & 0 & 0 & 1 & 1 & 0 \\ 0 & 0 & 0 & 0 & 0 & 0 & 0 & 0 & 0 & 0 & 0 & 1 & 0 & 1 \\ 0 & 0 & 0 & 0 & 0 & 0 & 0 & 0 & 0 & 0 & 0 & 0 & 1 & 1 \\ 0 & 0 & 0 & 0 & 0 & 0 & 0 & 0 & 0 & 0 & 0 & 0 & 0 & 0 \\ 0 & 0 & 0 & 0 & 0 & 0 & 0 & 0 & 0 & 0 & 0 & 0 & 0 & 0 \\ 0 & 0 & 0 & 0 & 0 & 0 & 0 & 0 & 0 & 0 & 0 & 0 & 0 & 0 \end{array} \right). \quad (2.1.117)$$

The 9-th column has become zero. Therefore it is a cycle and is represented as  $\langle 01 \rangle + \langle 12 \rangle + \langle 03 \rangle + \langle 32 \rangle$ .

#### Column 10

The value of  $\text{low}(10)$  is 4. The 8-th column has the same value. Thus the 8-th column is added to the 10-th column:

$$\left( \begin{array}{cccc|cccc|cccc} 0 & 0 & 0 & 0 & 1 & 0 & 0 & 1 & 0 & 1 & 0 & 0 & 0 & 0 \\ 0 & 0 & 0 & 0 & 1 & 1 & 0 & 0 & 0 & 1 & 0 & 0 & 0 & 0 \\ 0 & 0 & 0 & 0 & 0 & 1 & 0 & 0 & 0 & 0 & 0 & 0 & 0 & 0 \\ 0 & 0 & 0 & 0 & 0 & 0 & 0 & 1 & 0 & 0 & 0 & 0 & 0 & 0 \\ 0 & 0 & 0 & 0 & 0 & 0 & 0 & 0 & 0 & 0 & 1 & 0 & 1 & 0 \\ 0 & 0 & 0 & 0 & 0 & 0 & 0 & 0 & 0 & 0 & 1 & 0 & 0 & 1 \\ 0 & 0 & 0 & 0 & 0 & 0 & 0 & 0 & 0 & 0 & 1 & 1 & 0 & 0 \\ 0 & 0 & 0 & 0 & 0 & 0 & 0 & 0 & 0 & 0 & 0 & 1 & 1 & 0 \\ 0 & 0 & 0 & 0 & 0 & 0 & 0 & 0 & 0 & 0 & 0 & 1 & 0 & 1 \\ 0 & 0 & 0 & 0 & 0 & 0 & 0 & 0 & 0 & 0 & 0 & 0 & 1 & 1 \\ 0 & 0 & 0 & 0 & 0 & 0 & 0 & 0 & 0 & 0 & 0 & 0 & 0 & 0 \\ 0 & 0 & 0 & 0 & 0 & 0 & 0 & 0 & 0 & 0 & 0 & 0 & 0 & 0 \\ 0 & 0 & 0 & 0 & 0 & 0 & 0 & 0 & 0 & 0 & 0 & 0 & 0 & 0 \\ 0 & 0 & 0 & 0 & 0 & 0 & 0 & 0 & 0 & 0 & 0 & 0 & 0 & 0 \end{array} \right). \quad (2.1.118)$$

The value of  $\text{low}(10)$  has changed into 2. The 5-th column has the same

value. Thus the 5-th column is added to the 10-th column:

$$\left( \begin{array}{cccc|cccc|cccc} 0 & 0 & 0 & 0 & 1 & 0 & 0 & 1 & 0 & 0 & 0 & 0 & 0 & 0 & 0 & 0 \\ 0 & 0 & 0 & 0 & 1 & 1 & 0 & 0 & 0 & 0 & 0 & 0 & 0 & 0 & 0 & 0 \\ 0 & 0 & 0 & 0 & 0 & 1 & 0 & 0 & 0 & 0 & 0 & 0 & 0 & 0 & 0 & 0 \\ 0 & 0 & 0 & 0 & 0 & 0 & 0 & 1 & 0 & 0 & 0 & 0 & 0 & 0 & 0 & 0 \\ 0 & 0 & 0 & 0 & 0 & 0 & 0 & 0 & 0 & 0 & 1 & 0 & 1 & 0 & 0 & 0 \\ 0 & 0 & 0 & 0 & 0 & 0 & 0 & 0 & 0 & 0 & 1 & 0 & 0 & 1 & 0 & 0 \\ 0 & 0 & 0 & 0 & 0 & 0 & 0 & 0 & 0 & 0 & 1 & 1 & 0 & 0 & 0 & 0 \\ 0 & 0 & 0 & 0 & 0 & 0 & 0 & 0 & 0 & 0 & 0 & 1 & 1 & 0 & 0 & 0 \\ 0 & 0 & 0 & 0 & 0 & 0 & 0 & 0 & 0 & 0 & 0 & 1 & 0 & 1 & 0 & 0 \\ 0 & 0 & 0 & 0 & 0 & 0 & 0 & 0 & 0 & 0 & 0 & 0 & 1 & 1 & 0 & 0 \\ 0 & 0 & 0 & 0 & 0 & 0 & 0 & 0 & 0 & 0 & 0 & 0 & 0 & 1 & 1 & 0 \\ 0 & 0 & 0 & 0 & 0 & 0 & 0 & 0 & 0 & 0 & 0 & 0 & 0 & 0 & 0 & 0 \\ 0 & 0 & 0 & 0 & 0 & 0 & 0 & 0 & 0 & 0 & 0 & 0 & 0 & 0 & 0 & 0 \\ 0 & 0 & 0 & 0 & 0 & 0 & 0 & 0 & 0 & 0 & 0 & 0 & 0 & 0 & 0 & 0 \end{array} \right). \quad (2.1.119)$$

The 10-th column has become zero. Therefore it is a cycle and is represented as  $\langle 01 \rangle + \langle 03 \rangle + \langle 13 \rangle$ .

#### Column 11-13

The 11-th column to the 13-th column have their own unique lowest 1 index. Thus no reduction is applied to these columns.

#### Column 14

The value of  $\text{low}(14)$  is 10. The 13-th column has the same value. Thus the 13-th column is added to the 14-th column:

$$\left( \begin{array}{cccc|cccc|cccc} 0 & 0 & 0 & 0 & 1 & 0 & 0 & 1 & 0 & 0 & 0 & 0 & 0 & 0 & 0 & 0 \\ 0 & 0 & 0 & 0 & 1 & 1 & 0 & 0 & 0 & 0 & 0 & 0 & 0 & 0 & 0 & 0 \\ 0 & 0 & 0 & 0 & 0 & 1 & 0 & 0 & 0 & 0 & 0 & 0 & 0 & 0 & 0 & 0 \\ 0 & 0 & 0 & 0 & 0 & 0 & 0 & 1 & 0 & 0 & 0 & 0 & 0 & 0 & 0 & 0 \\ 0 & 0 & 0 & 0 & 0 & 0 & 0 & 0 & 0 & 0 & 1 & 0 & 1 & 1 & 0 & 0 \\ 0 & 0 & 0 & 0 & 0 & 0 & 0 & 0 & 0 & 0 & 1 & 0 & 0 & 1 & 0 & 0 \\ 0 & 0 & 0 & 0 & 0 & 0 & 0 & 0 & 0 & 0 & 1 & 1 & 0 & 0 & 0 & 0 \\ 0 & 0 & 0 & 0 & 0 & 0 & 0 & 0 & 0 & 0 & 0 & 1 & 1 & 1 & 0 & 0 \\ 0 & 0 & 0 & 0 & 0 & 0 & 0 & 0 & 0 & 0 & 0 & 1 & 0 & 1 & 0 & 0 \\ 0 & 0 & 0 & 0 & 0 & 0 & 0 & 0 & 0 & 0 & 0 & 0 & 1 & 0 & 0 & 0 \\ 0 & 0 & 0 & 0 & 0 & 0 & 0 & 0 & 0 & 0 & 0 & 0 & 0 & 1 & 0 & 0 \\ 0 & 0 & 0 & 0 & 0 & 0 & 0 & 0 & 0 & 0 & 0 & 0 & 0 & 0 & 0 & 0 \\ 0 & 0 & 0 & 0 & 0 & 0 & 0 & 0 & 0 & 0 & 0 & 0 & 0 & 0 & 0 & 0 \\ 0 & 0 & 0 & 0 & 0 & 0 & 0 & 0 & 0 & 0 & 0 & 0 & 0 & 0 & 0 & 0 \end{array} \right). \quad (2.1.120)$$

The value of  $\text{low}(14)$  has changed into 9. The 12-th column has the same value. Thus the 12-th column is added to the 14-th column:

$$\left( \begin{array}{cccc|cccc|cccc} 0 & 0 & 0 & 0 & 1 & 0 & 0 & 1 & 0 & 0 & 0 & 0 & 0 & 0 \\ 0 & 0 & 0 & 0 & 1 & 1 & 0 & 0 & 0 & 0 & 0 & 0 & 0 & 0 \\ 0 & 0 & 0 & 0 & 0 & 1 & 0 & 0 & 0 & 0 & 0 & 0 & 0 & 0 \\ 0 & 0 & 0 & 0 & 0 & 0 & 0 & 1 & 0 & 0 & 0 & 0 & 0 & 0 \\ 0 & 0 & 0 & 0 & 0 & 0 & 0 & 0 & 0 & 0 & 1 & 0 & 1 & 1 \\ 0 & 0 & 0 & 0 & 0 & 0 & 0 & 0 & 0 & 0 & 1 & 0 & 0 & 1 \\ 0 & 0 & 0 & 0 & 0 & 0 & 0 & 0 & 0 & 0 & 1 & 1 & 0 & 1 \\ 0 & 0 & 0 & 0 & 0 & 0 & 0 & 0 & 0 & 0 & 0 & 1 & 1 & 0 \\ 0 & 0 & 0 & 0 & 0 & 0 & 0 & 0 & 0 & 0 & 0 & 1 & 0 & 0 \\ 0 & 0 & 0 & 0 & 0 & 0 & 0 & 0 & 0 & 0 & 0 & 0 & 1 & 0 \\ 0 & 0 & 0 & 0 & 0 & 0 & 0 & 0 & 0 & 0 & 0 & 0 & 0 & 0 \\ 0 & 0 & 0 & 0 & 0 & 0 & 0 & 0 & 0 & 0 & 0 & 0 & 0 & 0 \\ 0 & 0 & 0 & 0 & 0 & 0 & 0 & 0 & 0 & 0 & 0 & 0 & 0 & 0 \end{array} \right). \quad (2.1.121)$$

The value of  $\text{low}(14)$  has changed into 7. The 11-th column has the same value. Thus the 11-th column is added to the 14-th column:

$$\left( \begin{array}{cccc|cccc|cccc} 0 & 0 & 0 & 0 & 1 & 0 & 0 & 1 & 0 & 0 & 0 & 0 & 0 & 0 \\ 0 & 0 & 0 & 0 & 1 & 1 & 0 & 0 & 0 & 0 & 0 & 0 & 0 & 0 \\ 0 & 0 & 0 & 0 & 0 & 1 & 0 & 0 & 0 & 0 & 0 & 0 & 0 & 0 \\ 0 & 0 & 0 & 0 & 0 & 0 & 0 & 1 & 0 & 0 & 0 & 0 & 0 & 0 \\ 0 & 0 & 0 & 0 & 0 & 0 & 0 & 0 & 0 & 0 & 1 & 0 & 1 & 0 \\ 0 & 0 & 0 & 0 & 0 & 0 & 0 & 0 & 0 & 0 & 1 & 0 & 0 & 0 \\ 0 & 0 & 0 & 0 & 0 & 0 & 0 & 0 & 0 & 0 & 1 & 1 & 0 & 0 \\ 0 & 0 & 0 & 0 & 0 & 0 & 0 & 0 & 0 & 0 & 0 & 1 & 1 & 0 \\ 0 & 0 & 0 & 0 & 0 & 0 & 0 & 0 & 0 & 0 & 0 & 1 & 0 & 0 \\ 0 & 0 & 0 & 0 & 0 & 0 & 0 & 0 & 0 & 0 & 0 & 0 & 1 & 0 \\ 0 & 0 & 0 & 0 & 0 & 0 & 0 & 0 & 0 & 0 & 0 & 0 & 0 & 0 \\ 0 & 0 & 0 & 0 & 0 & 0 & 0 & 0 & 0 & 0 & 0 & 0 & 0 & 0 \\ 0 & 0 & 0 & 0 & 0 & 0 & 0 & 0 & 0 & 0 & 0 & 0 & 0 & 0 \\ 0 & 0 & 0 & 0 & 0 & 0 & 0 & 0 & 0 & 0 & 0 & 0 & 0 & 0 \end{array} \right). \quad (2.1.122)$$

The 14-th column has become zero. Therefore it is a cycle and is represented by  $\langle 012 \rangle + \langle 032 \rangle + \langle 013 \rangle + \langle 123 \rangle$ .

The matrix reduction has been done. It is the time to execute the persistence pairing algorithm. The cycles are column 1, 2, 3, 4, 7, 9, 10, and 14.

### Column 1

The 1-st column represents an essential cycle because there is no column with  $\text{low}(k) = 1$ . We obtain a pair  $(1, \infty)$  of dimension 0.

### Column 2

The 5-th column has the value  $\text{low}(5) = 2$ . We obtain a 0-dimensional persistence pair  $(2, 5)$ .

### Column 3

The 6-th column has the value  $\text{low}(6) = 3$ . We obtain a 0-dimensional persistence pair  $(3, 6)$ .

**Column 4**

The 8-th column has the value  $\text{low}(8) = 4$ . We obtain a 0-dimensional persistence pair  $(4, 8)$ .

**Column 7**

The 11-th column has the value  $\text{low}(11) = 7$ . We obtain a 1-dimensional persistence pair  $(7, 11)$ .

**Column 9**

The 12-th column has the value  $\text{low}(12) = 9$ . We obtain a 1-dimensional persistence pair  $(9, 12)$ .

**Column 10**

The 13-th column has the value  $\text{low}(13) = 10$ . We obtain a 1-dimensional persistence pair  $(10, 13)$ .

**Column 14**

There is no column with  $\text{low}(k) = 14$ . It is an essential cycle. We obtain a 2-dimensional persistence pair  $(14, \infty)$ .

In summary, the persistence pairs are shown in the table below:

Table 2.1: Persistence pairs in Example 2.1.47

Dimension 0	Dimension 1	Dimension 2
$(1, \infty)$	$(7, 11)$	$(14, \infty)$
$(2, 5)$	$(9, 12)$	
$(3, 6)$	$(10, 13)$	
$(4, 8)$		

### 2.1.6 Persistence Diagram

The persistence diagram visualizes persistence homology groups. It is a plane with the vertical axis of birth scale and the horizontal axis of death scale. A generator of a persistent homology group is plotted as a point on a persistence diagram. The generators plotted near to the diagonal line have short persistences and those plotted far from the diagonal line have long persistences.

**Definition 2.1.48** (persistence diagram). *Let  $PH_q(K)$  be the  $q$ -th persistence homology group of a simplicial complex  $K$ . Let  $\text{Dgm}_q(K)$  denote the persistence diagram of  $PH_q(K)$ . For each generator of  $PH_q(K)$  with the persistence  $(b, d)$ , the diagram  $\text{Dgm}_q(K)$  has a point at  $(b, d)$ . If there are  $m$  generators with the same persistence, the corresponding point of  $\text{Dgm}_q(K)$  has the multiplicity  $m$ . The diagram  $\text{Dgm}_q(K)$  also has the points on the diagonal line with infinite multiplicity.*

A distance between persistence diagrams can be defined and it enables us to compare persistence diagrams. Although several distances have been proposed, only the bottleneck distance is introduced.

**Definition 2.1.49** (bottleneck distance). *Let  $X$  and  $Y$  be persistence diagrams. The bottleneck distance between  $X$  and  $Y$  is defined as follows:*

$$W_\infty(X, Y) = \inf_{\eta: X \rightarrow Y} \sup_{x \in X} \|x - \eta(x)\|_\infty, \quad (2.1.123)$$

where  $\eta$  is a bijection and  $\|(b, d)\|_\infty = \max\{b, d\}$ .

The computation of a bottleneck distance is treated as a matching problem of bipartite graph (Edelsbrunner and Harer, 2010: p.191). Let  $X_0$  and  $Y_0$  be the set of the off-diagonal points of  $X$  and  $Y$  respectively. Let  $u'$  denote the orthogonal projection to the diagonal line of a point  $u = (b, d)$ . Let  $X'_0 = \{u' \mid u \in X_0\}$  and  $Y'_0 = \{v' \mid v \in Y_0\}$ . Define the sets of vertices  $U = X_0 \cup X'_0$  and  $V = Y_0 \cup Y'_0$ . We have a weighted bipartite graph

$$G = (U \sqcup V, U \times V, c), \quad (2.1.124)$$

where the weight function  $c$  is defined as

$$c(u, v) = \begin{cases} \|u - v\|_\infty & \text{if } u \in X_0 \text{ or } v \in Y_0, \\ 0 & \text{otherwise.} \end{cases} \quad (2.1.125)$$

Efrat, Itai, and Katz (2001) observed the following fact. Let  $G[r]$  be a subgraph of  $G$  whose edge has weight at most  $r$ . The bottleneck distance is the least value of  $r$  that  $G[r]$  has a perfect matching. This problem is solved with the combination of the Hopcroft-Karp algorithm (Hopcroft and Karp, 1973) and the binary search.

### 2.1.7 Čech Complex and Vietoris-Rips Complex

In order to analyze the shape of data, the shape must be constructed from the given data. The situation that the data to be analyzed is given as a set of points in an Euclidean space is considered. There are several methods of constructing a simplicial complex from a point cloud. The Čech complex and the Vietoris-Rips complex are such methods and they are popular in the field of topological data analysis. The Čech complex is constructed from the balls centered at the given points. The Vietoris-Rips complex is an approximation of the Čech complex and the conditions to construct a complex are relaxed.

First I introduce the nerve of a cover and related notions. Second I introduce the Čech complex by using the nerve of a cover. Finally the Vietoris-Rips complex is introduced as a relaxation of the Čech complex.

**Definition 2.1.50** (open cover). *Let  $X$  be a subspace of an Euclidean space. A set of open sets  $\mathcal{U} = \{U_\alpha\}_\alpha$  is called a cover of  $X$  if and only if it satisfies that*

$$X = \bigcup_{\alpha} U_\alpha. \quad (2.1.126)$$

**Definition 2.1.51** (nerve of a cover). *Let  $X$  be a subspace of an Euclidean space and let  $\mathcal{U} = \{U_\alpha\}_\alpha$  be an open cover of  $X$ . The nerve of the cover  $\mathcal{U}$  is a simplicial complex defined as follows:*

$$\mathcal{N}(\mathcal{U}) = \{|\alpha_0\alpha_1\cdots\alpha_q| \mid U_{\alpha_0} \cap U_{\alpha_1} \cap \cdots \cap U_{\alpha_q} \neq \emptyset\}. \quad (2.1.127)$$

Consider the computation of the topology of a space from the nerve of its cover. A nerve does not necessarily reflect the topology of the given space. The nerve theorem guarantees the homotopy equivalence between the nerve and the space.

**Definition 2.1.52** (good cover). *An open cover  $\mathcal{U} = \{U_\alpha\}$  is called a good cover if and only if any non-empty intersection of open sets  $U_{\alpha_0} \cap U_{\alpha_1} \cap \cdots \cap U_{\alpha_p}$  is contractible.*

**Theorem 2.1.53** (nerve theorem). *Let  $X$  be a subspace of an Euclidean space and let  $\mathcal{U}$  be an open cover of  $X$ . If the cover  $\mathcal{U}$  is a good cover then the space  $X$  and the nerve  $\mathcal{N}(\mathcal{U})$  are homotopy equivalent.*

The proof of Theorem 2.1.53 for topological space is found in the book of Hatcher (Hatcher, 2015: Corollary 4G.3). The original proof of Theorem 2.1.53 was given in (Borsuk, 1948) for a subspace of an Euclidean space.

**Lemma 2.1.54.** *Let  $\mathcal{U} = \{U_\alpha\}$  be an open cover of a subspace of an Euclidean space. If all the open sets of  $\mathcal{U}$  is convex then the open cover  $\mathcal{U}$  is a good cover.*

*Proof.* The intersection of convex sets is convex and a convex set is contractible. Hence the cover  $\mathcal{U}$  is a good cover.  $\square$

A Čech complex is a nerve of a cover where the space is the union of the balls centered at the given points and the cover is the set of the balls.

**Definition 2.1.55** (Čech complex). *Let  $S = \{x_i\}_{i=1}^n$  be a set of points in an Euclidean space. The Čech complex of  $S$  with threshold  $r$  is defined as follows:*

$$\mathcal{C}_r(S) = \{i_0i_1\cdots i_q \mid B_r(x_{i_0}) \cap B_r(x_{i_1}) \cap \cdots \cap B_r(x_{i_q}) \neq \emptyset\}, \quad (2.1.128)$$

where  $B_r(x)$  is a ball of radius  $r$  centered at  $x$ .

Since the balls are convex, the cover  $\mathcal{U} = \{B_r(x_i)\}_{i=1}^n$  is a good cover. Hence the Čech complex  $\mathcal{C}_r(S)$  and the space  $X = \bigcup_{i=1}^n B_r(x_i)$  are homotopy equivalent. The computation of the homology groups of the Čech complex produces the homology groups of the union of the balls.

It is obvious that the filtration of the Čech complex can be constructed because the relation  $\mathcal{C}_{r_1}(S) \subset \mathcal{C}_{r_2}(S)$  holds for  $r_1 \leq r_2$ .

The condition of the Čech complex to make a simplex is difficult to compute since it is required to detect the intersection of more than two balls. The Vietoris-Rips complex is introduced to avoid this difficulty.

**Definition 2.1.56** (Vietoris-Rips complex). *Let  $S = \{x_i\}_{i=1}^n$  be a set of points in an Euclidean space. The Vietoris-Rips complex of  $S$  with threshold  $r$  is defined as*

$$\mathcal{R}_r(S) = \{i_0i_1\cdots i_q \mid \forall k, \forall l, k \neq l, B_r(x_{i_k}) \cap B_r(x_{i_l}) \neq \emptyset\}, \quad (2.1.129)$$

where  $B_r(x)$  is a ball of radius  $r$  centered at  $x$ .

It is easy to test whether two balls have the intersection because it can be checked by comparing the distance between the centers with the two times of  $r$ .

In the same way as the Čech complex, the filtration of the Vietoris-Rips complex can be constructed because the relation  $\mathcal{R}_{r_1}(S) \subset \mathcal{R}_{r_2}(S)$  holds for  $r_1 \leq r_2$ .

The threshold  $r$  is often set to infinity when the filtration is constructed. The Vietoris-Rips complex with infinity threshold  $\mathcal{R}_\infty(S)$  becomes a simplicial complex that consists of all the faces of an  $(n-1)$ -simplex. The filtered Vietoris-Rips complex of  $\mathcal{R}_\infty(S)$  is obtained by sorting the simplices in the ascending order of the values defined below:

$$f(\sigma) = \begin{cases} 0 & \text{if } \dim \sigma = 0, \\ d(u, v) & \text{if } \sigma = |uv|, \\ \max_{\tau \prec \sigma} f(\tau) & \text{otherwise,} \end{cases} \quad (2.1.130)$$

where  $d(u, v)$  denotes the Euclidean distance between  $u$  and  $v$ .

The number of the simplices in  $\mathcal{R}_\infty(S)$  is  $2^n - 1$  because of Lemma 2.1.5. This number is incredibly large. In order to reduce the number of the simplices, the dimension of the complex is restricted in practice. For example, consider that the dimension of  $\mathcal{R}_\infty(S)$  is restricted to a maximum of two. In other words, we consider the 2-skeleton of  $\mathcal{R}_\infty(S)$ . The number of the simplices is

$$\sum_{k=1}^3 \binom{n}{k} = \frac{1}{6}n^3 + \frac{5}{6}n, \quad (2.1.131)$$

where  $n$  is the cardinality of  $S$ .

### 2.1.8 Witness Complex

We have seen that a Vietoris-Rips complex may have a tremendously huge number of simplices. It results in intolerably long computational time of the persistent homology. It is natural that faster methods to construct a simplicial complex from a point cloud are desired. The witness complex, proposed by de Silva and Carlsson (2004), is such a method. A witness complex approximates a simplicial complex constructed from a point cloud. A subset called landmark points is used for approximation. The definition of the witness complex is given below.

**Definition 2.1.57** (strict witness complex). *Let  $S = \{x_i\}_{i=1}^n$  be a set of points in an Euclidean space and let  $L = \{l_j\}_{j=1}^m$  be a subset of  $S$ . The strict witness complex of  $S$ , which  $W_\infty(S)$  denotes, is defined as follows: A  $p$ -simplex  $|a_0 a_1 \cdots a_p|$  belongs to  $W_\infty(S)$  if and only if there exists a point  $x \in S$  such that the equation  $d(a_q, x) = \min_{1 \leq i \leq n} d(a_q, x_i)$  holds for all  $1 \leq q \leq p$  and  $a_q \in L$ .*

It is tedious to test the condition whether a simplex belongs to the strict witness complex. The lazy version of the witness complex is proposed by de Silva and Carlsson (2004). It is an analogue of the Vietoris-Rips complex.

**Definition 2.1.58** (lazy witness complex). *Let  $S$  be a point cloud and let  $L$  be landmark points defined in the same manner of Definition 2.1.57. The lazy witness complex  $W_1(S)$  is defined as follows: A  $p$ -simplex  $|a_0 a_1 \cdots a_p|$  belongs to*

$W_1(S)$  if and only if there exists a point  $x \in S$  such that the equations  $d(a, x) = \min_{1 \leq i \leq n} d(a, x_i)$  and  $d(b, x) = \min_{1 \leq i \leq n} d(b, x_i)$  for all  $a, b \in \{a_0, a_1, \dots, a_p\}$  such that  $a \neq b$ .

The methods to choose the landmarks recommended (de Silva and Carlsson, 2004) are the random selection and the maximin selection. The maximin selection has the following procedure. Choose a point  $l_1 \in S$  at random. Suppose that  $(i - 1)$  points  $l_1, l_2, \dots, l_{i-1}$  have been chosen. Take the point  $l_i \in S \setminus \{l_1, l_2, \dots, l_{i-1}\}$  such that maximizes the function

$$x \mapsto \min_{1 \leq j \leq i-1} d(x, l_j). \quad (2.1.132)$$

The points chosen by the procedure above are landmark points:  $L = \{l_i\}_{i=1}^m$ .

### 2.1.9 Stability

It is known that the persistent homology groups of the complices introduced above are stable with respect to the Gromov-Hausdorff distance (Chazal, de Silva, and Oudot, 2014). In order to introduce the result of (Chazal et al., 2014), several notions are introduced in this section.

The definition of the Gromov-Hausdorff distance requires the notion of multivalued mappings. A multivalued mapping from the set  $X$  to the set  $Y$ , say  $C : X \rightrightarrows Y$ , is a subset of  $X \times Y$  and the image of  $C$  under the canonical projection  $\pi_X : X \times Y \rightarrow X$  is equal to the set  $X$ , that is  $\pi_X(C) = X$ . A multivalued mapping  $C : X \rightrightarrows Y$  is called a correspondence if the image of  $C$  under the canonical projection  $\pi_Y : X \times Y \rightarrow Y$  is equal to the set  $Y$ , that is  $\pi_Y(C) = Y$ .

For metric spaces  $(X, d_X)$  and  $(Y, d_Y)$ , the distortion of a correspondence  $C : X \rightrightarrows Y$  is defined as

$$\text{dis}(C) = \sup\{|d_X(x, x') - d_Y(y, y')| \mid (x, y), (x', y') \in C\}. \quad (2.1.133)$$

**Definition 2.1.59** (Gromov-Hausdorff distance). *The Gromov-Hausdorff distance between metric spaces  $(X, d_X)$  and  $(Y, d_Y)$  is defined as*

$$d_{\text{GH}}(X, Y) = \frac{1}{2} \inf\{\text{dis}(C) \mid C : X \rightrightarrows Y\}, \quad (2.1.134)$$

where  $C$  is a correspondence.

The inequalities between the bottleneck distance and the Gromov-Hausdorff distance are proved in (Chazal et al., 2014). The metric spaces are restricted to totally bounded metric spaces. The metric space  $(X, d_X)$  is totally bounded if it has a finite  $\epsilon$ -sample for all  $\epsilon > 0$ . For a positive real value  $\epsilon > 0$ , a finite  $\epsilon$ -sample of the metric space  $(X, d_X)$  is a subset  $F \subset X$  such that for any  $x \in X$  there exists an element  $f \in F$  which satisfies  $d_X(x, f) < \epsilon$ . For example, bounded subsets of an Euclidean space are totally bounded.

**Theorem 2.1.60** (Chazal, de Silva, and Oudot (2014)). *Let  $X$  and  $Y$  be totally bounded metric spaces. Then*

$$W_\infty(\text{Dgm}_q(\mathcal{R}(X)), \text{Dgm}_q \mathcal{R}(Y)) \leq 2d_{\text{GH}}(X, Y), \quad (2.1.135)$$

$$W_\infty(\text{Dgm}_q(\mathcal{C}(X)), \text{Dgm}_q \mathcal{C}(Y)) \leq 2d_{\text{GH}}(X, Y), \quad (2.1.136)$$

where  $\mathcal{R}(\cdot)$  is a filtration of the Vietoris-Rips complex and  $\mathcal{C}(\cdot)$  is a filtration of the Čech complex; and  $\text{Dgm}_q$  denotes the  $q$ -th persistence diagram.

## 2.2 Attractor Reconstruction and Takens' Theorem

My first study focuses on attractor reconstruction, which reconstructs a trajectory of a dynamical system from observed data. The delay-coordinate mapping (Takens, 1981) is used to reconstruct the attractor.

**Definition 2.2.1** (delay-coordinate mapping). *The observed data  $x(t)$ , which is a function of time, is given. Let  $a$  be a positive real number and  $n$  be a positive integer. The mapping*

$$\phi(x(t)) = (x(t), x(t-a), \dots, x(t-(n-1)a)) \quad (2.2.1)$$

*is called a backward delay-coordinate mapping. The mapping*

$$\phi(x(t)) = (x(t), x(t+a), \dots, x(t+(n-1)a)) \quad (2.2.2)$$

*is called a forward delay-coordinate mapping. For convenience, both delay-coordinate mappings are called a delay-coordinate mapping. The number  $a$  is called the delay time and the integer  $n$  is called the embedding dimension.*

Takens' theorem (Takens, 1981) guarantees that the reconstructed attractor is diffeomorphic to the original attractor under a certain situation.

**Theorem 2.2.2** (Takens). *Let  $\xi : \mathbb{R} \rightarrow M$  be a trajectory of a dynamical system on a manifold  $M$  of dimension  $m$ . Let  $h : M \rightarrow \mathbb{R}$  be a continuous function. The mapping obtained by letting  $x = h \circ \xi$  in Definition 2.2.1, which is*

$$\Phi(\xi(t)) = \phi(h \circ \xi(t)) : M \rightarrow \mathbb{R}^n \quad (2.2.3)$$

*is an embedding in generic if  $n > 2m$ .*

The choice of the delay time is important to obtain the reconstructed attractor. For example, suppose that the trajectory  $\xi(t)$  is periodic with a period  $T$ . The mapping  $\Phi$  is not embedding when the delay time is a multiple of  $T$  because all the points of  $\Phi(\xi(t))$  falls on the diagonal set.

Several criteria have been proposed to select the delay time. The brief reviews of the mutual information and the method of Perea and Harer are given. The following paragraphs in this section are based on the paper (Tsuji and Aihara, 2019a).

Fraser and Swinney (1986) proposed the method that uses the mutual information to determine the optimal delay. The first minimum of the mutual information between  $x(t)$  and  $x(t+a)$  is chosen when  $a$  increases from 0. Then,  $x(t)$  and  $x(t+a)$  are the most independent with respect to  $a$ . Such  $x(t)$  and  $x(t+a)$  are well distinguishable and expand the shape of the reconstructed attractor. Choosing a minimum of the mutual information avoids redundancy. The first minimum is selected to avoid irrelevance.

The mutual information between  $x(t)$  and  $x(t+a)$  is defined as follows. Let  $S$  be the set of the values of  $x(t)$ , and  $Q$  be the set of the values of  $x(t+a)$ . Then, the product of  $S$  and  $Q$  is defined as the set of pairs  $(x(t), x(t+a))$ . The probability distribution of  $S$ ,  $Q$ , and  $(S, Q)$  is denoted by  $P_S$ ,  $P_Q$ , and  $P_{SQ}$ , respectively. Then, the mutual information of  $S$  and  $Q$  is defined as

$$I(S; Q) = \int P_{SQ}(s, q) \log \left( \frac{P_{SQ}(s, q)}{P_S(s)P_Q(q)} \right) dsdq. \quad (2.2.4)$$

Perea and Harer (2015) analyzed the behavior of the circles embedded in the delay-coordinate space. Their aim was to detect periodic signals from time series data. They assumed that the periodic signals can be expanded into Fourier series. Before analyzing such periodic signals they mapped a circle into the delay-coordinate space for simplicity.

They found that the embedded circle is roundest when the delay satisfies  $an = T/2$ . The embedded circle becomes an ellipse in the delay-coordinate space. In their study, “roundest” implies that the major axis and the minor axis of the ellipse have the same length.

It should be noted that when the embedded circle is “roundest”, it has the maximum width.

The mutual information method does not appear to be suitable for expanding reconstructed attractors. It does not directly imply the expansion of the reconstructed space although the values of  $x(t)$  and  $x(t + a)$  may not be correlated.

The problem is that the delay determined by mutual information does not depend on the embedding dimension. Essentially, this method is suitable only for the case where the embedding dimension is two, because it only calculates the mutual information between  $x(t)$  and  $x(t + a)$ .

Some readers may wonder if the mutual information is extended to three or more random variables. The extensions can be defined (McGill, 1954; Baudot et al., 2019), but they will not be practical. In order to calculate mutual information, we need to estimate joint probabilities from samples. Because the number of the samples is small, it is difficult to estimate joint probabilities. Careful treatment for the estimation is required to calculate mutual information with a sufficient precision. Fraser and Swinney (1986) adopted varying the size of bins for estimating the mutual information of two random variables. The estimation of mutual information of three or more variables will be more difficult.

The criterion suggested by Perea and Harer can be used only for signals of a certain class. It is restricted to periodic signals that can be expanded in Fourier series. The simplest example of such signals is a sine wave. It is not known whether this criterion can be applied to arbitrary periodic or chaotically periodic signals.

## 2.3 Bézier Curve and Its Fitting

In the second work of my research, Bézier curves are used to approximate continuous curves. A Bézier curve of degree  $r$  is a polynomial of degree  $r$ . It is a superposition of the Bernstein polynomials and their coefficients are called control points. The control points are in an Euclidean space and the Bézier curve are in the Euclidean space. The shape of a Bézier curve is determined by the control points.

I adopted Bézier curves to extend the method proposed in Chapter 4. It is easy to change the model complexity by increasing or decreasing the degree. It is also easy to design a method to connect Bézier curves smoothly because the derivative of a Bézier curve is also a Bézier curve.

The control points of a Bézier curve are often given by hand in several areas such as computer graphics. In my work, however, a Bézier curve is fitted to sampled points and the control points have to be calculated with an optimization

method. The least squares method is adopted to fit a Bézier curve. Several researchers have proposed the methods to fit a Bézier curve (Shao and Zhou, 1996; Pastva, 1998), but I derived the normal equation by myself.

First the Bernstein polynomials and Bézier curves are introduced.

**Definition 2.3.1** (bernstein polynomials). *The Bernstein polynomials of degree  $r$  are defined as*

$$b_{q,r}(t) = \binom{r}{q} t^q (1-t)^{r-q} \quad (2.3.1)$$

for  $q = 0, \dots, r$ , where  $t$  is a real number and  $\binom{r}{q}$  denotes the binomial coefficient.

**Definition 2.3.2** (Bézier curve). *A Bézier curve of degree  $r$  is defined as*

$$\boldsymbol{\beta}(t) = \sum_{q=0}^r b_{q,r}(t) \mathbf{p}_q \quad (2.3.2)$$

for  $0 \leq t \leq 1$ , where  $\mathbf{p}_0, \dots, \mathbf{p}_r \in \mathbb{R}^d$  are the control points and  $d$  is the dimension of an Euclidean space.

It is clear that a Bézier curve starts from  $\boldsymbol{\beta}(0) = \mathbf{p}_0$  and ends at  $\boldsymbol{\beta}(1) = \mathbf{p}_r$ . Second the loss function is defined for the least squares method.

**Definition 2.3.3** (loss function). *The loss function of a Bézier curve of degree  $r$  is defined as*

$$L(\mathbf{p}_0, \mathbf{p}_1, \dots, \mathbf{p}_r) = \frac{1}{2} \sum_{i=1}^n \|\boldsymbol{\beta}(t_i) - \mathbf{x}_i\|^2, \quad (2.3.3)$$

where  $\{(t_i, \mathbf{x}_i) \mid t_i \in [0, 1], \mathbf{x}_i \in \mathbb{R}^d\}_{i=1}^n$  is a training data.

For simplicity, the loss function is separated into each component of the coordinates. Let  $v^{(k)}$  denote the  $k$ -th component of a vector  $\mathbf{v}$ . In this notation, the vector  $\mathbf{p}_q$  is written as

$$\mathbf{p}_q = \begin{pmatrix} p_q^{(1)} \\ \vdots \\ p_q^{(d)} \end{pmatrix}$$

and the vector  $\mathbf{x}_i$  is written as

$$\mathbf{x}_i = \begin{pmatrix} x_i^{(1)} \\ \vdots \\ x_i^{(d)} \end{pmatrix}.$$

Because

$$\boldsymbol{\beta}(t_i) - \mathbf{x}_i = \begin{pmatrix} \sum_{q=0}^r b_{q,r}(t_i) p_q^{(1)} - x_i^{(1)} \\ \vdots \\ \sum_{q=0}^r b_{q,r}(t_i) p_q^{(d)} - x_i^{(d)} \end{pmatrix}, \quad (2.3.4)$$

the loss function is developed as follows:

$$L(\mathbf{p}_1, \dots, \mathbf{p}_r) = \frac{1}{2} \sum_{i=1}^n \left\| \sum_{q=0}^r b_{q,r}(t_i) \mathbf{p}_q - \mathbf{x}_i \right\|^2 \quad (2.3.5)$$

$$= \frac{1}{2} \sum_{i=1}^n \sum_{k=1}^d \left( \sum_{q=0}^r b_{q,r}(t_i) p_q^{(k)} - x_i^{(k)} \right)^2. \quad (2.3.6)$$

By letting  $L^{(k)} = \frac{1}{2} \sum_{i=1}^n \left( \sum_{q=0}^r b_{q,r}(t_i) p_q^{(k)} - x_i^{(k)} \right)^2$ , we obtain the equation

$$L = \sum_{k=1}^d L^{(k)}. \quad (2.3.7)$$

To calculate the derivative of  $L^{(k)}$ , the component-wise loss function is written with vectors and a matrix. Define an  $(r+1)$ -by- $n$  matrix

$$B_r(\mathbf{t}) = \begin{pmatrix} b_{0,r}(t_1) & \cdots & b_{r,r}(t_1) \\ \vdots & \ddots & \vdots \\ b_{0,r}(t_n) & \cdots & b_{r,r}(t_n) \end{pmatrix}, \quad (2.3.8)$$

where  $\mathbf{t} = (t_1, \dots, t_n)^\top$ , and define an  $(r+1)$ -vector and an  $n$ -vector

$$\mathbf{p}^{(k)} = \begin{pmatrix} p_0^{(k)} \\ \vdots \\ p_r^{(k)} \end{pmatrix}, \quad \mathbf{x}^{(k)} = \begin{pmatrix} x_1^{(k)} \\ \vdots \\ x_n^{(k)} \end{pmatrix} \quad (2.3.9)$$

respectively.

Hence  $L^{(k)}$  can be written as

$$L^{(k)} = \frac{1}{2} \left\| B_r(\mathbf{t}) \mathbf{p}^{(k)} - \mathbf{x}^{(k)} \right\|^2. \quad (2.3.10)$$

Since  $L^{(k)}$  is the function of  $\mathbf{p}^{(k)}$ , the derivative is

$$\frac{\partial L^{(k)}}{\partial \mathbf{p}^{(k)}} = B_r(\mathbf{t})^\top B_r(\mathbf{t}) \mathbf{p}^{(k)} - B_r(\mathbf{t})^\top \mathbf{x}^{(k)}. \quad (2.3.11)$$

By solving the equation  $\partial L^{(k)} / \partial \mathbf{p}^{(k)} = 0$  for each  $k$ , the control points of the fitted Bézier curve are obtained.

## Chapter 3

# Attractor Reconstruction and Persistent Homology

It is interesting to compute the homology of an orbit of a dynamical system. A dynamical system may produce orbits whose shapes are different from each other depending on the parameters. Different systems also produce orbits of different shapes. Chaotic systems such as the Lorenz system have an orbit which stays in a certain set. Such orbit is called an attractor. A chaotic attractor has a strange shape. Those attractors drove me to compute their homology.

Those attractors are obtained by numerical integration; we are not able to compute their homology groups by hand, and therefore we have to rely on a numerical method of the computation of the homology groups. Persistent homology is a method to compute the homology groups of a shape sampled in a discrete manner. Persistent homology can compute the homology of the attractors developed by numerical integration since the data that we obtain is sampled in discrete time.

It is needed to find an application of the computation of the homology of attractors; it was fortune that several researchers have already invented the applications; such applications compute the persistent homology of time series data mapped into the delay-coordinates and then use the persistent homology as feature data of machine learning algorithm. Emrani, Gentimis, and Krim (2014a); Emrani, Chintakunta, and Krim (2014b) proposed a periodicity detection method using delay-coordinates and persistent homology. Perea and Harer (2015) analyzed the relation between the time delay and the period of the signal. Pereira and de Mello (2015) proposed a time series clustering method using persistent homology. Garland, Bradley, and Meiss (2016) observed the persistent homology of the witness complex of the reconstructed Lorenz attractor. Venkataraman, Ramamurthy, and Turaga (2016b) compared the method of delay-coordinates and persistent homology with non-topological methods. Seversky, Davis, and Berger (2016) experimented on the time series clustering method using delay-coordinates and persistent homology for several data sets and they compared three metrics of persistence diagrams: the scale space kernel, the bottleneck distance, and the Wasserstein distance. Umeda (2017) proposed the Betti sequence, which is a descriptor of persistence homology, to use the convolutional neural networks.

As explained in Section 2.2, the delay-coordinates maps the observed time series into a higher dimensional Euclidean space. The first component of the delay-coordinates is a value of the observed data at some time. The second component is that at the time shifted before. The shift of the time is called the delay time. The components after the second is put in the same manner.

The choice of the delay time is important to reconstruct the orbit or the trajectory of a dynamical system. An unsuitable choice of the delay time causes redundancy or irrelevance (Casdagli, Eubank, Farmer, and Gibson, 1991). Redundancy is the phenomenon that a trajectory mapped into the delay-coordinates concentrates around the diagonal set. All the trajectory suffer from redundancy if the delay time is overly small. An overly small delay time makes the values of the components of the delay-coordinates near to each other. Irrelevance is the phenomenon that a reconstructed chaotic attractor has a shape more complicate than the original shape. It occurs when the delay time is overly large.

Desirable is a delay time which does not cause both redundancy and irrelevance. I regard that the minimum delay that maximize the hole width of a reconstructed trajectory as optimal. The trajectories with periodicity or chaotic periodicity are considered. The optimal delay avoids redundancy since the hole of the trajectory is widened and it avoids irrelevance since the smallest of the such delays is chosen. The proposed index for choosing the delay time is named the most significant death value, which is abbreviated to MSDV. It is based on the persistent homology of the trajectory mapped into the delay-coordinates.

Section 3.1 gives the explanation of the proposed criterion and its brief analysis. Section 3.2 describes the materials and the procedure of the experiments. Section 3.3 shows the results of the experiments. Section 3.4 discuss the results of the experiments. Chapter 5 draws a conclusion.

The contents presented in Section 3.1, Section 3.2, Section 3.3, Section 3.4, and Chapter 5 are excerpted from (Tsuji and Aihara, 2019a), which appeared in the journal *Nonlinear Theory and Its Applications*, volume 10, number 1, pages 74-89. The paragraphs and the figures below in this chapter is reused from (Tsuji and Aihara, 2019a) under the permission of the Institute of Electronics, Information and Communication Engineers.

### 3.1 Proposed Criterion

Perea and Harer (2015) combined delay-coordinates and persistent homology in order to recognize the given time series as periodic as summarized below. They introduced the maximum persistence as an index of periodicity. It is defined as

$$\text{mp}(A) = \max_{x \in \text{PH}_1(A)} \text{pers}(x), \quad (3.1.1)$$

where  $A$  is the reconstructed attractor and  $\text{pers}(x)$  is the persistence of the homology generator  $x$ .

They supposed that the time series data can be written as

$$x(t) = \cos(Lt), \quad (3.1.2)$$

and embedded this into the delay coordinate space of dimension  $n$  with the delay  $a$ . They obtained an ellipse in the delay coordinate space. They investigated

when the delay makes the ellipse “rounder”. The semi-major axis and the semi-minor axis of this ellipse can be calculated by hand. The thought was that the longer the semi-minor axis the rounder the ellipse. They found that the delay that makes the ellipse “rounder” is given by

$$a = \frac{1}{n} \frac{2\pi}{L}. \quad (3.1.3)$$

Moreover, they investigated the delay coordinate embedding when the time series data can be written as

$$x(t) = \sum_{k=0}^N (a_k \cos kt + b_k \sin kt). \quad (3.1.4)$$

It means that the time series data are represented by the partial sum of the Fourier series. They analyzed the condition on the dimension of embedding and they obtained the following inequality:

$$n > 2N. \quad (3.1.5)$$

There are concerns on the analysis of Perea and Harer. How large  $N$  should we choose? Furthermore, the optimal delay is different for each higher harmonics. This can be an obstacle for choosing the delay.

Let us see the frequency spectrum of some real data. Figure 3.1a shows the signal of the Japanese vowel /a/ and Figure 3.1b shows the FFT spectrum of the Japanese vowel /a/. Even if we count the number of prominent harmonics we should set  $N = 30$ .

Figure 3.2b shows that the FFT spectrum of the limit cycle of van der Pol equations, whose signal is shown in Figure 3.2a, has a lot of higher harmonics. Such data require large  $N$  and it makes us to face the difficulty to choose the optimal delay because there are many harmonics. If we take the peaks whose amplitude is higher than  $-40$  dB, that is 1% of the maximum amplitude,  $N$  has to be set to 20. It is much larger than the delay time actually needed to reconstruct the limit cycle. Another analysis of delay coordinate embedding for this problem is given later.

In addition, the maximum persistence is slightly smaller than the width of the hole because the birth time of the homology generator is not zero since the points in the data are apart from each other. Let us propose another index to measure the periodicity of a signal from the point of view of the hole width. The most significant death value  $\text{MSDV}(A)$  is defined as the death value of  $a$ , where  $a \in PH_1(A)$  and  $\text{pers}(a) = \max_{c \in PH_1(A)} \text{pers}(c)$ .

We evaluate the width of the hole of the reconstructed attractor under some assumptions, without Fourier series. Consider a function  $x : \mathbb{R} \rightarrow \mathbb{R}$ . Let  $x(t)$  denote the value of  $x$  at  $t$ . We assume that the function  $x$  is continuous and has the period of  $T$ . Without loss of generality, we can assume that  $x(0) = x(T) = 0$ . We also assume that  $x(T/2) = 0$  holds and  $x(t) > 0$  for  $0 < t < T/2$  and  $x(t) < 0$  for  $T/2 < t < T$  hold.

We consider the following set:

$$A = \{x(t) \mid t \in I, I \subset \mathbb{R}\}, \quad (3.1.6)$$

where  $I$  is an interval. We embed this set into the delay coordinate space of dimension  $n$  with delay  $a$ . Let  $y_a(t)$  be the vectors of the embedded set of  $A$ :

$$y_a(t) = (x(t), x(t+a), \dots, x(t+(n-1)a)). \quad (3.1.7)$$

Let  $\tilde{A}$  be the set of  $y_a(t)$ :  $\tilde{A} = \{y_a(t) \mid t \in I\}$ . The set  $\tilde{A}$  becomes a closed curve because the function  $x$  is periodic if we choose the length of  $I$  that is sufficiently larger than the value of  $T$ .

Let  $w_a(\tilde{A})$  denote the hole width of  $\tilde{A}$ . Intuitively, as follows the minimum of the distance between the origin and the point  $y_a(t)$  is smaller than the hole width:

$$\min_t \|y_a(t)\| \leq w_a(\tilde{A}). \quad (3.1.8)$$

Let  $\xi$  be a trigonometric function with the period of  $T$ :

$$\xi(t) = C \sin\left(\frac{2\pi}{T}t\right), \quad (3.1.9)$$

where  $C$  is the constant that satisfies  $|\xi(t)| \leq |x(t)|$  for all  $t$ . We embed  $\xi(t)$  into the delay-coordinate space:

$$\eta_a(t) = (\xi(t), \xi(t+a), \dots, \xi(t+(n-1)a)). \quad (3.1.10)$$

Then we obtain the following inequalities:

$$\min_t \|\eta_a(t)\| \leq \min_t \|y_a(t)\| \leq w_a(\tilde{A}). \quad (3.1.11)$$

Furthermore, we calculate the first term of the equation above and get the following inequalities:

$$C \left( \frac{n}{2} - \frac{1}{2} \sqrt{\frac{1 - \cos(4an\pi/T)}{1 - \cos(4a\pi/T)}} \right) \leq \min_t \|y_a(t)\| \leq w_a(\tilde{A}). \quad (3.1.12)$$

Although we cannot know whether  $w_a(\tilde{A})$  attains the maximum when  $\eta_a(t)$  attains the maximum with varying the value of  $a$ , at least the value of  $w_a(\tilde{A})$  may be sufficient large and it is larger than  $\max_a \min_t \|\eta_a(t)\|$ . The first term of Equation 3.1.12 attains the maximum when  $a = \frac{1}{n} \frac{T}{2}$  holds and then we get the following inequalities:

$$C \frac{n}{2} \leq \min_t \|y_a(t)\| \leq w_a(\tilde{A}). \quad (3.1.13)$$

Further we consider whether we can apply the analysis above to several time series data. We can apply the analysis to the van der Pol system because we can see that the data in Figure 3.2a satisfies the assumption. Figure 3.3a shows the  $x$ -coordinate of the Rössler attractor. Though the signal is not strictly periodic, we are interested in whether our analysis works in this case. Figure 3.4a shows the  $x$ -coordinate of the Lorenz attractor. The Lorenz attractor has two holes and each hole corresponds to the positive value and negative value of Figure 3.4a respectively. Although the Lorenz attractor is not strictly periodic but has two holes, our analysis may be able to roughly applied to each hole. But we cannot choose the period of the signal from the spectrum the Lorenz attractor shown in Figure 3.4b. Thus, instead of the spectrum, we use the median intervals of crossing some positive and negative values. Here we choosed 7.5 and -7.5 respectively.

## 3.2 Methods

Numerical experiments were conducted to test the proposed criterion. Then, the results were compared with those obtained by the mutual information method and the criterion of Perea and Harer.

### 3.2.1 Materials

The harmonic oscillator, the van der Pol system, the Rössler system, and the speech signal of a Japanese vowel /a/ were used in the experiment. The definitions of these systems as well as the reason for their choice will now be provided.

The harmonic oscillator was chosen for investigating the relation between the proposed criterion and the criterion of Perea and Harer. The harmonic oscillator is defined as

$$\begin{cases} \dot{x} = y, \\ \dot{y} = -x, \end{cases} \quad (3.2.1)$$

where the period of the solution is 628 steps.

The van der Pol system (Strogatz, 2014: p.200) was chosen as an example of a periodic signal with high harmonics that can be expressed by Fourier series. The van der Pol system is defined as

$$\begin{cases} \dot{x} = y, \\ \dot{y} = \mu(1 - x^2)y - x, \end{cases} \quad (3.2.2)$$

where  $\mu = 10$ , and the period of the solution is 1908 steps.

The Rössler system (Rössler, 1976) was chosen as an example of a chaotically periodic signal. The Rössler system is defined as

$$\begin{cases} \dot{x} = -y - z, \\ \dot{y} = x + ay, \\ \dot{z} = b + z(x - c), \end{cases} \quad (3.2.3)$$

where  $a = 0.2$ ,  $b = 0.2$ , and  $c = 5.7$ . The solution converges to a strange attractor. The inverse of the strongest frequency of the FFT spectrum was used as the characteristic period, as the trajectory of the Rössler attractor has no strict period; however, it is nearly periodic. The characteristic period is 625 steps.

The Lorenz system (Lorenz, 1963) was chosen as another example of a chaotically periodic signal. The Lorenz system is defined as

$$\begin{cases} \dot{x} = s(y - z), \\ \dot{y} = x(r - z) - y, \\ \dot{z} = xy - bz, \end{cases} \quad (3.2.4)$$

where  $r = 28$ ,  $s = 10$ , and  $c = 8/3$ . The solution converges to a strange attractor. The median of the interval that the  $x$ -coordinate value crosses 7.5 and that that value crosses -7.5 was used as the half of the characteristic period. The characteristic period is 58 steps.

The speech signal was chosen to test the application of the proposed criterion to a real world signal. The signal for the Japanese vowel /a/, spoken by a female speaker, was used. The data were obtained from the Vowel Database:

Five Japanese Vowels of Males, Females, and Children Along with Relevant Physical Data (JVPD) (Ohyama, Deguchi, and Kasuya, 2011). This database is maintained by the Speech Resources Consortium of the National Institute for Informatics. The signal for Japanese vowel /a/ is shown in Figure 3.1a, and its FFT spectrum is shown in Figure 3.1b. The period of the signal is 170 steps.

The solution of each dynamical system was calculated by the fourth order Runge-Kutta method with step size 0.01. It was evolved for sufficiently large time. The first 1000 samples of the solutions were dropped because the solutions that are not in the attractor should be discarded.

The first projection map, that is the map taking the first coordinate of the signal, was used as an observation function. The resulting time series data were used as input to the experiment.

### 3.2.2 Procedure

Each input time series data were first embedded into a delay-coordinate space to obtain a reconstructed attractor. The dimension of the delay-coordinate spaces ranged from 2 to 10. The delay time varied from one step to the step that was equal to half the period of the input signal. The first 5000 points of each attractor were used.

Subsequently, the first persistent homology of each reconstructed attractor was computed. The Ripser (Bauer, 2019) software application was used for computation. The computer that was used had four Intel Xeon E5-4640 CPUs (2.40GHz, 8 cores) and 1TB RAM. The computation time for one attractor ranged from a few seconds to a day.

Finally, the graph of the most significant death value versus the delay was plotted for each embedding dimension of each reconstructed attractor. The most significant death value was extracted from the first persistent homology of each reconstructed attractor. The delay time was normalized by the period or the characteristic period.

## 3.3 Results

This section presents the results of the numerical experiments.

Figure 3.5 shows the most significant death values of the harmonic oscillator. The first peaks are achieved at  $a = \frac{1}{n} \frac{T}{2}$ . This result coincides with the prediction of Perea and Harer.

Figure 3.6 shows the most significant death values of the limit cycle of the van der Pol system with parameter  $\mu = 10$ . It is clear that the first peaks are achieved at  $a = \frac{1}{n} \frac{T}{2}$  except for the case of embedding dimension three, where the point around  $a = \frac{1}{3} \frac{T}{2}$  is flattened; however, this point can be considered the maximum.

Figure 3.7 shows the most significant death values of the Rössler attractor. The ravine in the graphs is realized at a point slightly smaller than  $1/2$ . At the points  $a = \frac{1}{n} \frac{T}{2}$ , the graphs exhibit saddle points instead of peaks. The graphs increase after the point  $a = \frac{1}{n} \frac{T}{2}$ .

Figure 3.8 shows the most significant death values of the Lorenz attractor. There is no ravine such as in the case of the Rössler attractor. At the points  $a = \frac{1}{n} \frac{T}{2}$ , each value of the graphs is near to the first peak.

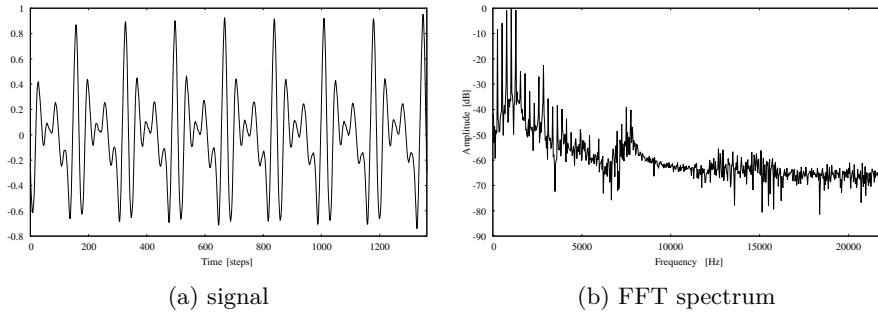


Figure 3.1: The signal and its FFT spectrum of the Japanese vowel /a/.

Figure 3.9 shows the most significant death values of the Japanese vowel /a/. The graphs have several ravines between  $a/T = 0$  and  $a/T = 0.5$ . The points where  $a = \frac{1}{n} \frac{T}{2}$  do not correspond to peaks. In fact, they fall near the minimum in the case  $n = 3$ .

### 3.4 Discussion

The relationship between the proposed criterion and that of Perea and Harer is herein discussed in light of the experimental results.

#### 3.4.1 Dynamical Systems

The most significant death value yields results that coincide with those of Perea and Harer for the harmonic oscillator. Figure 3.5 clearly shows that the first peaks are attained at  $a = \frac{1}{n} \frac{T}{2}$ . This fact implies that the word “roundest” in Perea and Harer’s study is equivalent to the maximum of the width of a circle.

The criterion suggested by Perea and Harer is appropriate for the limit cycle of the van der Pol system. This system is an example of a nonlinear periodic signal. As the period of zero-crossing points is half the period of the limit cycle, the given signal can be made to correspond to a sine wave with the period of the given signal. The absolute value of this sine wave is bounded by that of the given signal.

The reconstructed attractor does not always recover its original shape when the delay time maximizes the most significant death value. Figure 3.10 shows a reconstructed trajectory of the harmonic oscillator embedded in the delay-coordinate space with delay equal to 63 and embedding dimension equal to five, which makes the equation  $a = \frac{1}{n} \frac{T}{2}$  hold. This reconstructed trajectory recovers its original shape. By contrast, Figure 3.11 shows a reconstructed limit cycle of the van der Pol system embedded in the delay-coordinate space with delay equal to 191 and embedding dimension equal to five, which makes the equation  $a = \frac{1}{n} \frac{T}{2}$  hold. This reconstructed trajectory does not recover its original shape. We have to explain why the reconstructed trajectory of the harmonic oscillator recovers its original shape but that of the limit cycle of the van der Pol system does not. The harmonic oscillator is a special case. It can recover its original

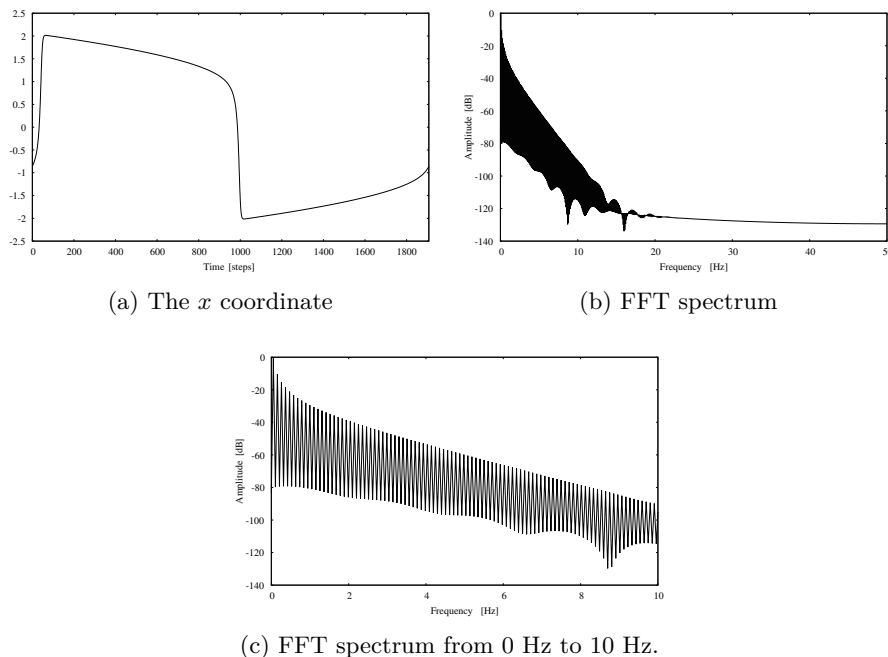


Figure 3.2: The  $x$ -coordinate and its FFT spectrum of the limit cycle of the van der Pol equation ( $\mu = 10$ ).

shape because the reconstructed ellipse that has the widest hole width is the circle.

For the Rössler attractor, it should be considered whether to use or not the criterion  $a = \frac{1}{n} \frac{T}{2}$ . In the results, the first peak of the graphs turns into a saddle. The maximum of the most significant death value is attained for larger delay time. Considering irrelevance, excessively large delay time results in unsatisfactory reconstruction. The reconstructed attractors are checked for irrelevance.

Two figures are examined to compare the delay satisfying the criterion with the delay attaining the maximum. Figure 3.12 shows a plot of the reconstructed Rössler attractor with embedding dimension equal to five and delay equal to 62. This delay time satisfies the equation  $a = \frac{1}{n} \frac{T}{2}$ . Figure 3.13 shows a plot of the reconstructed Rössler attractor with embedding dimension equal to five and delay equal to 198. This delay time attains the maximum of the graph shown in Figure 3.7. It can be seen that Figure 3.12 shows the reconstructed attractor whose shape resembles that of the original attractor. The trajectory of the reconstructed attractor shown in Figure 3.13 is considerably tangled. Thus, it can be concluded that the delay satisfying the criterion  $a = \frac{1}{n} \frac{T}{2}$  is preferable to the larger delay. This is natural because the aim was to maximize the hole width, and the original shape cannot be obtained from the observed signals. The reason why the MSDV of the Rössler attractor became large when the delay was large may be the irrelevance. The irrelevance deformed the reconstructed attractor and the hole width may be enlarged.

For the Lorenz attractor, the criterion  $a = \frac{1}{n} \frac{T}{2}$  is almostly appropriate. The

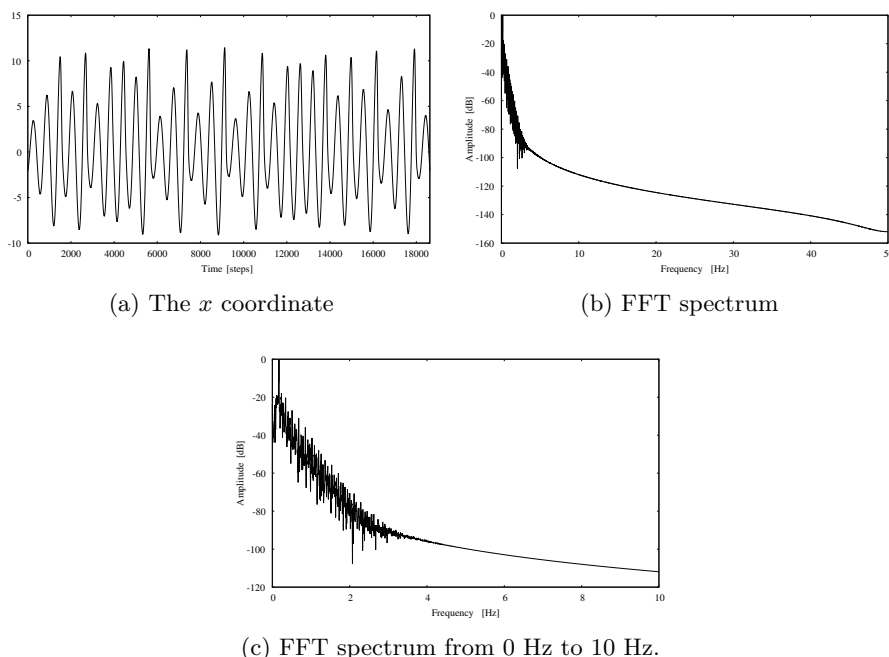


Figure 3.3: The  $x$ -coordinate and its FFT spectrum of the Rössler attractor.

most significant values where the criterion holds are slightly smaller than the peaks in Figure 3.8. This may be because the crossing intervals vary around the characteristic period. Moreover, the MSDVs get greater where the delay has greater values, except the  $n = 2$  case. We check what happens in the case of larger delays. Figure 3.16 shows a plot of the reconstructed Lorenz attractor with embedding dimension equal to five and delay equal to 6. This delay time satisfies the equation  $a = \frac{1}{n} \frac{T}{2}$ . Figure 3.17 shows the reconstructed attractor where the delay attains the maximum of the MSDV of the  $n = 5$  case. The graph of the MSDV is shown in Figure 3.8 and this delay is 22. The shape shown in Figure 3.16 resembles the original attractor, but the reconstructed attractor shown in Figure 3.17 is extremely deformed. Thus, it can be concluded that the delay satisfying the criterion  $a = \frac{1}{n} \frac{T}{2}$  is also preferable. In the case of the Lorenz attractor, the third hole appears when the delay is large. This is seen in Figure 3.17. This third hole makes the MSDV higher. This may be caused because the number of the sampled points is small. The third hole will be filled up with the infinite length of samples.

### 3.4.2 Japanese Vowel /a/

The graph of the most significant death values of the signal for the Japanese vowel /a/ has several ravines, as shown in Figure 3.9. This is due to the fact that the human voice resonates in the mouth and the speech signal has higher harmonics. The eighth harmonic contributes to the first ravine in the graph. As the speech signal has several harmonics, it is difficult to determine a single period  $T$  for the criterion of Perea and Harer. By contrast, the most significant

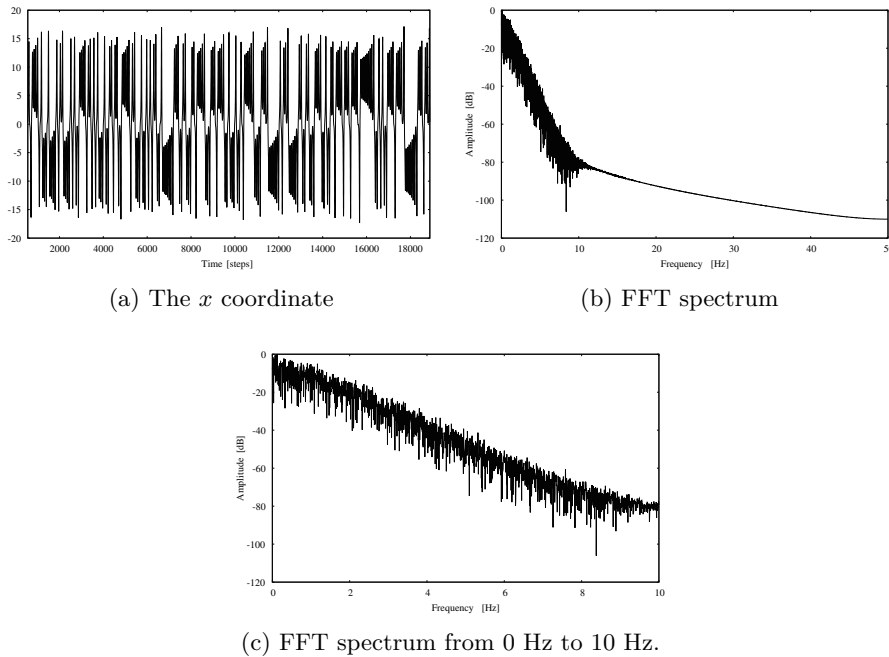


Figure 3.4: The  $x$ -coordinate and its FFT spectrum of the Lorenz attractor.

death value can determine the delay time.

An example of reconstruction is shown in Figure 3.18, and its persistence diagram is shown in Figure 3.19. The embedding dimension is 10 and the delay is 12. This delay attains the maximum of the most significant death value in Figure 3.9. It cannot be determined whether the reconstruction is satisfactory or not because the original is unknown. The persistence diagram suggests that the reconstructed attractor has one large hole.

### 3.4.3 Comparison with Mutual Information

The most significant death value is now compared with mutual information. Figure 3.20a shows the plot of mutual information versus delay for the harmonic oscillator. The first local minimum is marked on the graph. If the first local minimum is chosen as the delay, the reconstructed attractor collapses owing to redundancy. Similarly, the delay attaining the first local minimum of the mutual information is small for the limit cycle of the van der Pol system. Figure 3.20b shows the plot of the mutual information for this system.

However, the global minimum of the mutual information of both systems is about  $0.25T$  and this delay is suitable for the delay coordinate embedding where  $n = 2$ . Thus, it can be suggested that mutual information is not necessarily suitable for determining the delay of periodic signals in the cases where the embedding dimension is large.

As seen in Figure 3.20c, the mutual information suggests that the optimal delay is approximately  $0.2T$ . Figure 3.7 shows that this delay may be suitable for attractor reconstruction for embedding dimension equal to two or three.

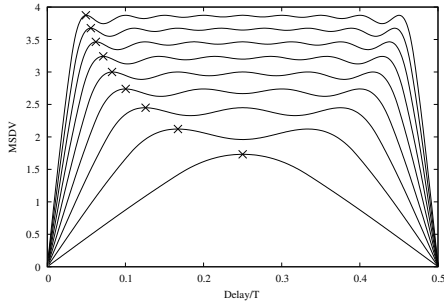


Figure 3.5: Most significant death values of the harmonic oscillator. The horizontal axis represents the delay divided by the period  $T = 628$ , and the vertical axis the most significant death values. The lowest line is the case of embedding dimension two. The embedding dimension is in an increasing order. The x marks plotted in the graph represent the points where  $a = \frac{1}{n} \frac{T}{2}$ . (Copyright©2019 IEICE, (Tsuji and Aihara, 2019a: Figure 9))

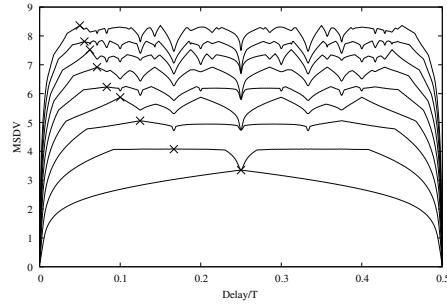


Figure 3.6: Most significant death values of the van der Pol system with  $\mu = 10$ . The horizontal axis represents the delay divided by the period  $T = 1908$ , and the vertical axis the most significant death values. The lowest line is the case of embedding dimension two. The embedding dimension is in an increasing order. The x marks plotted in the graph represent the points where  $a = \frac{1}{n} \frac{T}{2}$ . (Copyright©2019 IEICE, (Tsuji and Aihara, 2019a: Figure 10))

However, this delay may cause irrelevance for embedding dimension greater than three. We show the reconstructed attractors in higher dimension and with the delay  $0.2T$ . Figure 3.14 shows the reconstructed attractor of embedding dimension 5 with the delay 125, and Figure 3.15 shows the reconstructed attractor of embedding dimension 10 with the delay 125. This delay equals to  $0.2T$ . Although in the five dimensional case the reconstructed attractor seems to be formed well, in the ten dimensional case the reconstructed attractor tangles and there occurs the irrelevance.

Figure 3.20d shows the mutual information of the Lorenz attractor. The first local minimum is about  $0.34T$ . This value is too large even if the embedding dimension is two. For these two systems, the mutual information cannot estimate the appropriate delay for delay coordinate embeddings.

It can be seen in Figure 3.20e that the optimal delay for the Japanese vowel /a/, as determined by the mutual information, is approximately  $0.75T$ . It is can be said that this delay is appropriate for attractor reconstruction, because the most significant death value is sufficiently large in Figure 3.9.

Considering the discussion above, mutual information does not yield consistent results. The delay determined by mutual information is satisfactory for some systems and unsatisfactory for others. Although the mutual information is not so good, the maximum of the most significant death value yields too large delay for chaotic systems as seen in previous sections.

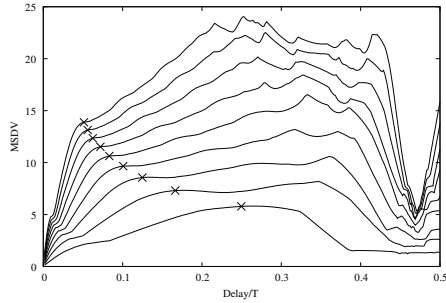


Figure 3.7: Most significant death values of the Rössler attractor. The vertical axis represents the delay divided by the characteristic period  $T = 625$ , and the horizontal axis the most significant death values. The lowest line is the case of embedding dimension two. The embedding dimension is in an increasing order. The x marks plotted in the graph represent the points where  $a = \frac{1}{n} \frac{T}{2}$ . (Copyright©2019 IEICE, (Tsuji and Aihara, 2019a: Figure 11))

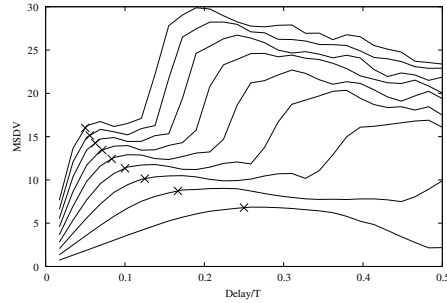


Figure 3.8: Most significant death values of the Lorenz attractor. The vertical axis represents the delay divided by the characteristic period  $T = 58$ , and the horizontal axis the most significant death values. The lowest line is the case of embedding dimension two. The embedding dimension is in an increasing order. The x marks plotted in the graph represent the points where  $a = \frac{1}{n} \frac{T}{2}$ . (Copyright©2019 IEICE, (Tsuji and Aihara, 2019a: Figure 12))

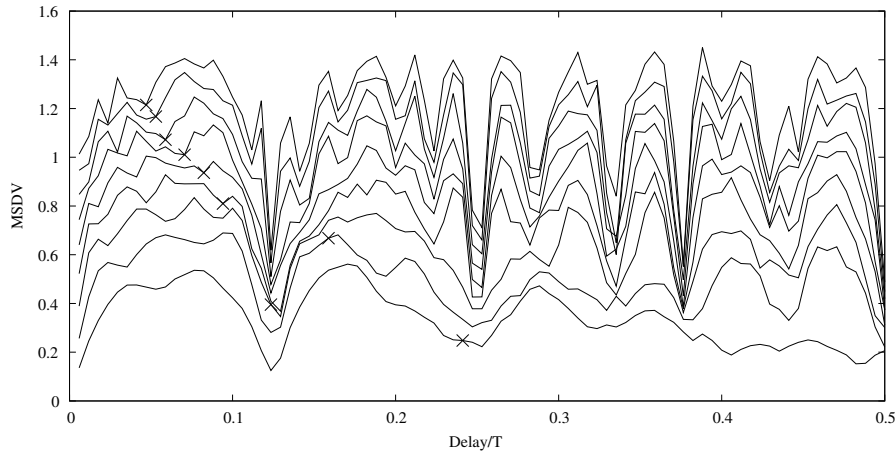


Figure 3.9: Most significant death values of the Japanese Vowel /a/. The horizontal axis is the delay divided by the characteristic period  $T = 170$ , and the vertical axis the most significant death values. The lowest line is the case of embedding dimension two. The embedding dimension is in an increasing order. The x marks plotted in the graph represent the points where  $a = \frac{1}{n} \frac{T}{2}$ . (Copyright©2019 IEICE, (Tsuji and Aihara, 2019a: Figure 13))

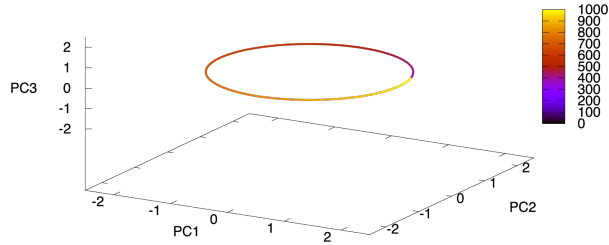


Figure 3.10: A reconstructed trajectory of the harmonic oscillator with delay time  $a = 62$  and embedding dimension  $n = 5$ . The axes of this plot represent principal components and the color scale indicates the time. This delay was chosen to satisfy the equation  $an = T/2$ . (Copyright©2019 IEICE, (Tsuiji and Aihara, 2019a: Figure 14))

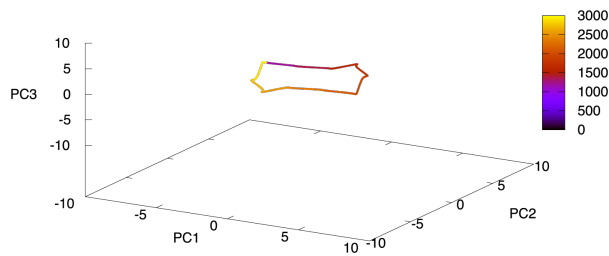


Figure 3.11: A reconstructed limit cycle of the van der Pol system with delay time  $a = 191$  and embedding dimension  $n = 5$ . The axes of this plot represent principal components and the color scale indicates the time. This delay was chosen to satisfy the equation  $a = T/2$ . (Copyright©2019 IEICE, (Tsuiji and Aihara, 2019a: Figure 15))

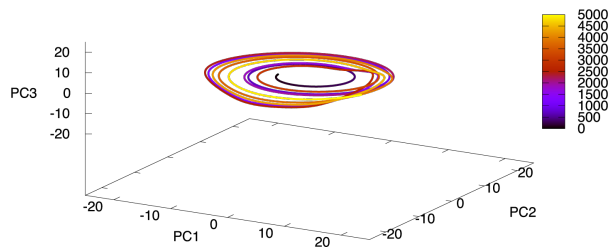


Figure 3.12: A reconstructed Rössler attractor with delay time  $a = 62$  and embedding dimension  $n = 5$ . The axes of this plot represent principal components and the color scale indicates the time. This delay was chosen to satisfy the equation  $an = T/2$ . (Copyright©2019 IEICE, (Tsuiji and Aihara, 2019a: Figure 16))

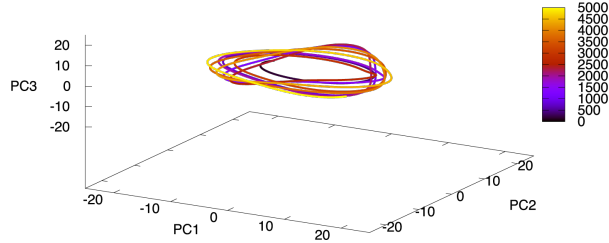


Figure 3.13: A reconstructed Rössler attractor with delay time  $a = 198$  and embedding dimension  $n = 5$ . The axes of this plot represent principal components and the color scale indicates the time. This delay attains the first peak of the graph. (Copyright©2019 IEICE, (Tsuji and Aihara, 2019a: Figure 17))

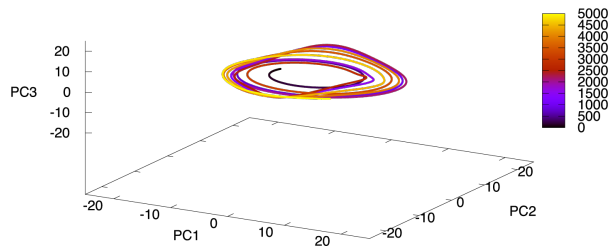


Figure 3.14: A reconstructed Rössler attractor with delay time  $a = 125$  and embedding dimension equal  $n = 5$ . The axes of this plot represent principal components and the color scale indicates the time. (Copyright©2019 IEICE, (Tsuji and Aihara, 2019a: Figure 18))

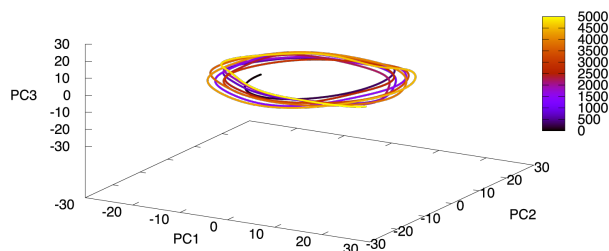


Figure 3.15: A reconstructed Rössler attractor with delay time  $a = 125$  and embedding dimension  $n = 10$ . The axes of this plot represent principal components and the color scale indicates the time. (Copyright©2019 IEICE, (Tsuji and Aihara, 2019a: Figure 19))

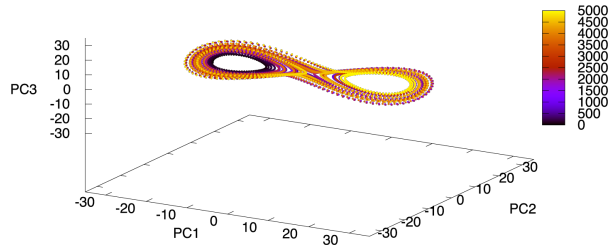


Figure 3.16: A reconstructed Lorenz attractor with delay time  $a = 6$  and embedding dimension  $n = 5$ . The axes of this plot represent principal components and the color scale indicates the time. This delay was chosen to satisfy the equation  $an = T/2$ . (Copyright©2019 IEICE, (Tsuiji and Aihara, 2019a: Figure 20))

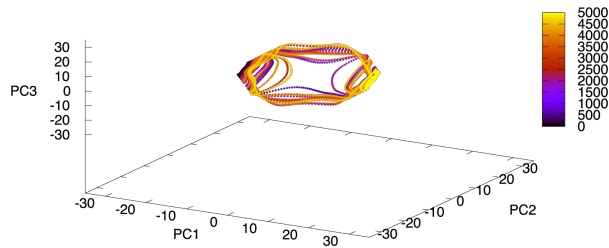


Figure 3.17: A reconstructed Lorenz attractor with delay time  $a = 22$  and embedding dimension  $n = 5$ . The axes of this plot represent principal components and the color scale indicates the time. This delay was chosen to the delay attains the maximum of the MSDV. (Copyright©2019 IEICE, (Tsuiji and Aihara, 2019a: Figure 21))

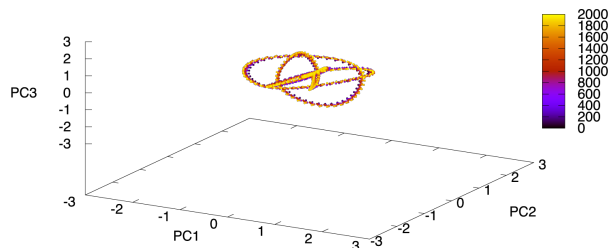


Figure 3.18: A reconstructed attractor of Japanese vowel /a/. The delay time was  $a = 12$  and the embedding dimension was  $n = 10$ . The axes of this plot represent principal components and the color scale indicates the time. This delay was chosen to maximize the most significant death value. (Copyright©2019 IEICE, (Tsuiji and Aihara, 2019a: Figure 22))

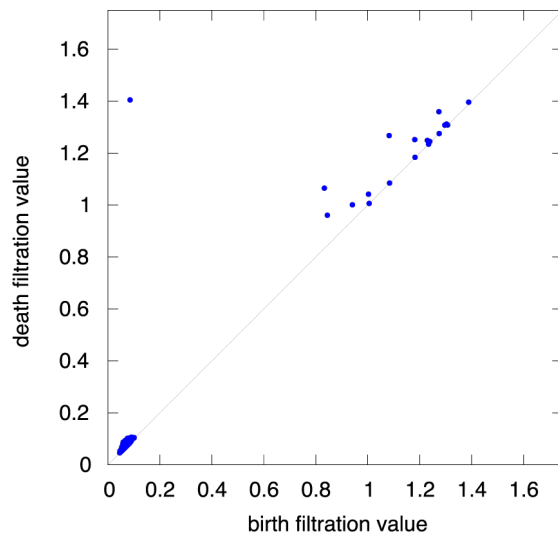
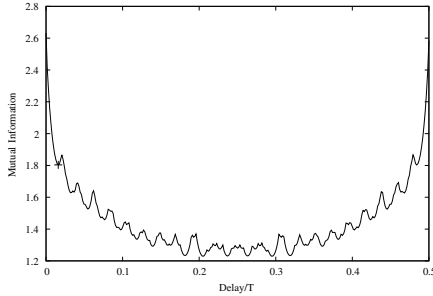
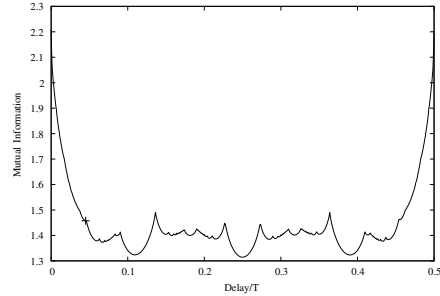


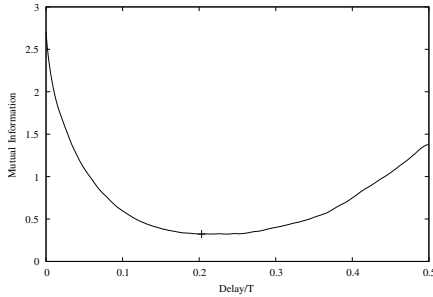
Figure 3.19: First persistence diagram of a reconstructed attractor of the Japanese vowel /a/. The delay time was  $a = 12$  and the embedding dimension was  $n = 10$ . This delay was chosen to maximize the most significant death value. The horizontal axis represents the birth filtration value and the vertical axis the death filtration value. (Copyright©2019 IEICE, (Tsuji and Aihara, 2019a: Figure 23))



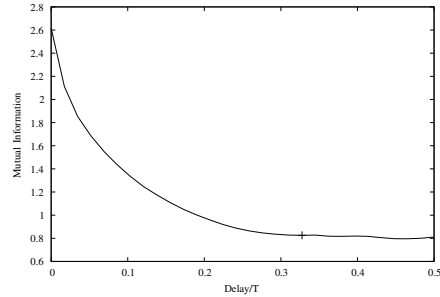
(a) Harmonic oscillator. (Copyright©2019 IEICE, (Tsuji and Aihara, 2019a: Figure 24))



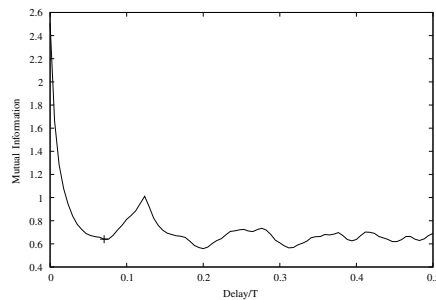
(b) The van der Pol equation. (Copyright©2019 IEICE, (Tsuji and Aihara, 2019a: Figure 25))



(c) The Rössler attractor. (Copyright©2019 IEICE, (Tsuji and Aihara, 2019a: Figure 26))



(d) The Lorenz attractor. (Copyright©2019 IEICE, (Tsuji and Aihara, 2019a: Figure 27))



(e) Japanese vowel /a/. (Copyright©2019 IEICE, (Tsuji and Aihara, 2019a: Figure 28))

Figure 3.20: Plots of mutual information versus delay. The horizontal axis represents the delay normalized by the period or the characteristic period and the vertical axis the mutual information between  $x(t)$  and  $x(t+a)$ . A “+” mark represents the first minimum on the graph.

## Chapter 4

# Vietoris-Rips Complex of Line Segments

While I was working on the study presented in Chapter 3, I suffered from the long computational time of persistent homology. For example, the input of five thousand points took one or two days to compute its persistent homology. Moreover, it required five or six hundred gigabytes of memory. Because the study presented in Chapter 3 needed computing the persistent homology of hundreds of data sets with varying the delay of delay-coordinates, it took me months to compute the persistent homology of all the data sets. It is possible to avoid this obstacle by subsampling or using the witness complex, but such methods sacrifice the precision of the persistent homology.

A simple way to make the computational time of persistent homology faster is to reduce the number of points from which the Vietoris-Rips complex is constructed. If the input is limited to continuous curves, it is possible to reduce the number of points. Line segments which approximate to a curve can represent the input points. The input points are assumed to be sampled from a continuous curve.

The proposed method that reduces the computational time of the persistent homology of a continuous curve has the following procedure. First cubic Bézier curves are fitted to the given curve. Second the fitted Bézier curves are divided into line segments. These line segments approximate to the given curve. Third the Vietoris-Rips complex is constructed from the line segments. It is done by the manner similar to the Vietoris-Rips complex constructed from points. Section 4.1 gives the explanation of the proposed method in detail.

Section 4.2 gives the method, the results and the discussion of the experiment. First the experiment measures the performance of the proposed method and compared it with the ordinary method. The ordinary method means the Vietoris-Rips complex from points. Second the experiment observed the bottleneck distance between the clean input and the noised input. The proposed method was compared with the ordinary method. Third the experiment compared the performance and the precision of the proposed method with those of the witness complex. The conclusion is presented in Chapter 5.

The study presented in Section 4.1, Section 4.2, and Chapter 5 is based on (Tsuji and Aihara, 2019b), which appeared in the 2019 IEEE International Con-

ference on Acoustics, Speech and Signal Processing The sentences, the figures, and the tables were reused from (Tsuji and Aihara, 2019b) under the permission of Institute of Electrical and Electronics Engineers.

## 4.1 Proposed Methods

This section describes the proposed method. The first description is of the method to acquire the line segments approximating to the given curve. The second description is of the definition and the construction method of the Vietoris-Rips complex of line segments.

### 4.1.1 Getting Approximating Line Segments

The input curve is given as a set of the sampling times and the sampled points:  $\{(t_i, \mathbf{x}_i) \mid t_i \in \mathbb{R}, \mathbf{x}_i \in \mathbb{R}^d\}_{i=1}^N$ . Suppose that the samples are contiguous, which means that the  $i$ -th sample  $(t_i, \mathbf{x}_i)$  was sampled immediately after the  $(i-1)$ -th sample  $(t_{i-1}, \mathbf{x}_{i-1})$ . The samples are separated into groups which contain around  $l$  points, where  $l$  is an integer.

A cubic Bézier curve is fitted to a group of the samples. The least squares method explained in Section 2.3 fits cubic Bézier curves.

The fitted Bézier curves are divided into line segments. A Bézier curve is divided into  $r$  line segments, where  $r$  is the number of segments. The parameter of a Bézier curve, which is a unit interval, is divided into  $r$  closed intervals of the same length. Let  $[s_0, s_1], [s_1, s_2], \dots, [s_{r-1}, s_r]$  be the closed intervals where  $s_i = i/r$  for  $i = 0, 1, \dots, r$ . The boundaries of the intervals are mapped onto the Bézier curve. The mapped points are  $\beta(s_0), \beta(s_1), \dots, \beta(s_r)$ , where  $\beta$  denotes the Bézier curve. The mapped points are connected to the contiguous points:  $\overrightarrow{\beta(s_i)\beta(s_{i+1})}$ . The line segments  $\overrightarrow{\beta(s_0)\beta(s_1)}, \overrightarrow{\beta(s_1)\beta(s_2)}, \dots, \overrightarrow{\beta(s_{r-1})\beta(s_r)}$  are obtained from the Bézier curve.

### 4.1.2 Vietoris-Rips Complex of Line Segments

The line segments that approximate to the given curve have been obtained by the procedure above. The Vietoris-Rips complex of line segments will be built.

The Vietoris-Rips complex of line segments is constructed in a way similar to the Vietoris-Rips complex of points. The distances between line segments are substituted for the distances between points.

**Definition 4.1.1** (distance between line segments). *Let  $\overrightarrow{p_0p_1}$  and  $\overrightarrow{q_0q_1}$  be line segments. The distance between line segments is defined as*

$$d(\overrightarrow{p_0p_1}, \overrightarrow{q_0q_1}) = \min_{p \in \overrightarrow{p_0p_1}, q \in \overrightarrow{q_0q_1}} d(p, q). \quad (4.1.1)$$

The distance between line segments is calculated by minimizing a function  $f$ . Suppose that  $\overrightarrow{p_0p_1}$  is parametrized as  $p(s) = (1-s)p_0 + sp_1$  and  $\overrightarrow{q_0q_1}$  is parametrized as  $q(t) = (1-t)q_0 + tq_1$ . The function  $f : [0, 1] \times [0, 1] \rightarrow \mathbb{R}$  is defined as

$$f(s, t) = \|p(s) - q(t)\|^2, \quad (4.1.2)$$

where  $\|\cdot\|$  is the Euclidean norm. The minimum of the function  $f$  is the distance between line segments.

## 4.2 Results and Discussion

The proposed method was tested with a trajectory of an irrational flow on 2-torus and the Japanese vowel signal data. In the following experiments, the Ripser (Bauer, 2019) was used for computing the persistent homology of Vietoris-Rips complex and the computer used for experiments has 2.40GHz Xeon E5-4640 and 1TiB of memory. The upper dimension of the persistent homology was set to 2.

### 4.2.1 Irrational Flow on 2-torus

The irrational flow on 2-torus (Poincaré, 1885: Ch. XV) is defined as

$$\frac{du}{dt} = \alpha t \pmod{1}, \quad \frac{dv}{dt} = \beta t \pmod{1}, \quad (4.2.1)$$

where  $(u, v) \in [0, 1] \times [0, 1]$  and the ratio  $\alpha/\beta$  is irrational. It is known that the solution of Equation (4.2.1) covers  $[0, 1] \times [0, 1]$  densely after sufficiently long time. In this experiment, the parameters were set to  $\alpha = 1$  and  $\beta = \sqrt{2}$ . Then the trajectory of the irrational flow is mapped into 3-dimensional Euclidean space. The mapping is defined as

$$\begin{cases} x_1 &= R \cos u + r \cos u \cos v, \\ x_2 &= R \sin u + r \sin u \cos v, \\ x_3 &= r \sin v, \end{cases} \quad (4.2.2)$$

where  $R$  and  $r$  are positive real values and they satisfy  $R > r$ . The parameters were set to  $R = 2$  and  $r = 1$ .

The trajectory was developed from  $t = 0$  to  $t = 50\pi$  and it was sampled in  $n = 2000, 3000$  and  $4000$  points. Then cubic Bézier curves were fitted to each series of sampled points; the number of points in each group was about 30. Finally each fitted Bézier curve was divided into line segments. The number of line segments was set to  $r = 3, 6$  and  $10$ .

The first experiment was performance comparison. The performance of computing the persistent homology of the ordinary Vietoris-Rips complex was compared with the performance of computing the persistent homology of the Vietoris-Rips complex of line segments. The comparison of the computational time is shown in Figure 4.1a and that of the computational space is shown in Figure 4.1b.

Figure 4.1a shows the plot of computational time versus the number of points of the trajectory. Figure 4.1b shows the plot of computational memory versus the number of points of the trajectory. The order of time and space complexity approximates to  $O(n^{3.25})$ . Even the case of  $r = 10$  requires about 45 times shorter and 30 times smaller than the case of the ordinary Vietoris-Rips complex. Because  $l \simeq 30$  and  $r = 10$  in this case, the number of points that construct the Vietoris-Rips complex was reduced to about  $10/30 = 1/3$ . It is natural that the computational time and memory were reduced to about  $(1/3)^{3.25} \simeq 35$ . The cases of  $r = 3$  and  $r = 6$  require shorter time and smaller memory similarly.

The ordinary Vietoris-Rips complex required about 630 GiB of memory when the number of points was 4000. This value is too large to use persistent homology in practical use. However the proposed method with  $r = 3$  and that with  $r = 6$

required less than 10 GiB of memory and less than 100 seconds of time. The proposed method enables us to use persistent homology in practice.

Second the proposed method was applied to noisy data. The noisy data was generated by adding 10% gaussian noise of the root mean squares of the trajectory of the irrational flow. The number of the points in each group was set to  $l \simeq 30$ . Each fitted Bézier curve was divided into  $r = 6$  segments.

The bottleneck distance between the persistent homology of the ordinary Vietoris-Rips complex of the original data and that of the Vietoris-Rips complex of the segments fitted to the noisy data were calculated. The bottleneck distance between that of the original data and that of the noisy data were also calculated. To simplify the description, let  $T_n$  be the original torus, where  $n$  is the number of sampled points. Let  $N_n$  be the noisy torus and  $S_n$  be the segments obtained by fitting. Paraphrasing the first two sentences, calculated were  $W_\infty(\text{Dgm}_q(T_n), \text{Dgm}_q(S_n))$  and  $W_\infty(\text{Dgm}_q(T_n), \text{Dgm}_q(N_n))$  for  $q = 0, 1, 2$  and  $n = 2000, 3000, 4000$ . Let  $d_{\text{segment}}(q, n)$  be the former distance and  $d_{\text{point}}(q, n)$  the latter. The comparison of  $d_{\text{segment}}(q, n)$  with  $d_{\text{point}}(q, n)$  is shown in Figure 4.2.

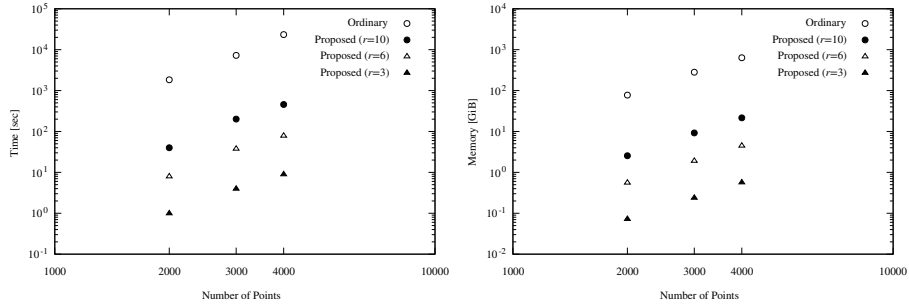
Figure 4.2 compares the distances  $d_{\text{point}}(q, n)$  with  $d_{\text{segment}}(q, n)$ . The graphs in Figure 4.2 show the distances of  $q = 0, q = 1$  and  $q = 2$  from left to right. The blank bars show the distances  $d_{\text{point}}(q, n)$  and the hatched bars show the distances  $d_{\text{segment}}(q, n)$ . For every value of  $q$  and  $n$ , the distance  $d_{\text{segment}}(q, n)$  is less than  $d_{\text{point}}(q, n)$ . It means that the proposed method has smoothing effect and it can compute more precise persistent homology under the noisy observation.

## 4.2.2 Japanese Vowels

The proposed method was also applied to the signals of Japanese vowels. The data was obtained from the Vowel Database: Five Japanese Vowels of Males, Females and Children Along With Relevant Physical Data (Ohyama et al., 2011). The chosen data was the utterance of 27-year-old female speaker. The utterance was recorded in 44.1 kHz, 16 bits PCM format and contains the signals of five Japanese vowels /a/, /e/, /i/, /o/ and /u/. The signals were rescaled to range from -1 to 1. The signals of these vowels were embedded into the delay-coordinate space of 10 dimension with delay of 10 steps. Then the 1100 steps, almost equal to 125 milliseconds, of each embedded signal were extracted. Each embedded signal was divided into the groups of  $l \simeq 10$  points and a cubic Bézier curve was fitted to each group of points, and then each Bézier curve was divided into  $r = 2$  segments. Therefore the number of the segments approximates to 220.

The witness complexes of the speech signals were also constructed for comparison in the manner explained in (de Silva and Carlsson, 2004: Section 2.4). and their persistent homology was analyzed with the Ripser. The number of the landmarks was 220 and they were chosen by the maxmin selection. The results are shown in Table 4.1 and Table 4.2.

Table 4.1 shows the comparison between the ordinary method and the proposed method applied to compute the persistent homology of the speech signals. It also shows the comparison with the witness complex. The proposed method and the witness complex were about 300 times faster than the ordinary method and took 100 times smaller memory than it. Table 4.2 shows the bottleneck

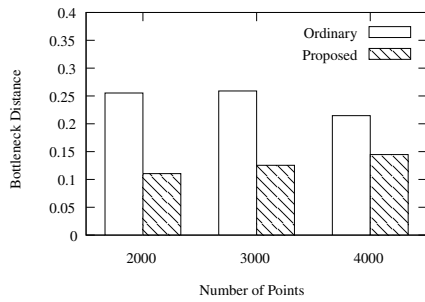


(a) Plot of computational time of persistent homology of 2-torus ©2019 IEEE.

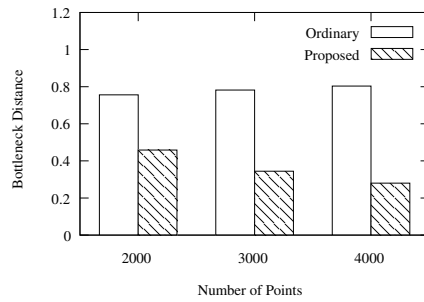
(b) Plot of computational memory of persistent homology of 2-torus ©2019 IEEE.

Figure 4.1: Comparison of the performance of the ordinary method and the proposed method.

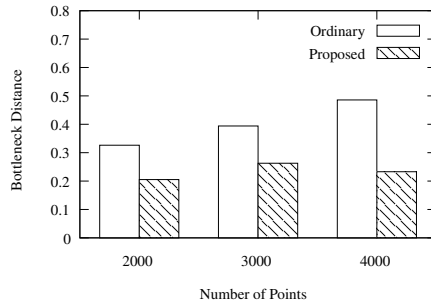
distance between the persistent homology computed with the ordinary method and that with the proposed method. It also shows the comparison with the witness complex. The distances of the proposed method took small values except the 1st persistent homology of the vowel /a/. The maximum of the filtration value is  $\sqrt{10} \simeq 3.16$  because the space is the ten times product of  $[-1, 1]$ . These distances took the value of 0.131 at most. This value is about 4% of the maximum filtration value. However, the distance of the 1st persistent homology of the vowel /a/ was 0.644; this value is about 20% of the maximum filtration value. The reason of this result may be the original data was noisy and the noise was smoothed out but it cannot be proven. In contrast the distances of the 1st persistent homology of the witness complex were much larger than the proposed method.



(a) 0th persistent homology



(b) 1st persistent homology



(c) 2nd persistent homology

Figure 4.2: Bottleneck distance between the original data of 2-torus and the noised data of that. The left-side blank bars show the distances between the original and the ordinary Vietoris-Rips complex of the noised data. The right-side hatched bars show the distances between the original and the Vietoris-Rips complex of the segments fitted to the noised data ©2019 IEEE.

Table 4.1: Performance comparison of computing the persistent homology of speech signals ©2019 IEEE.

(a) Computational Time			
Vowel	Ordinary	Proposed	Witness
/a/	290 sec	< 1 sec	< 1 sec
/e/	312 sec	< 1 sec	< 1 sec
/i/	268 sec	< 1 sec	< 1 sec
/o/	291 sec	< 1 sec	< 1 sec
/u/	277 sec	< 1 sec	< 1 sec

(b) Computational Memory			
Vowel	Ordinary	Proposed	Witness
/a/	12.5 GiB	0.11 GiB	0.14 GiB
/e/	11.5 GiB	0.09 GiB	0.09 GiB
/i/	11.5 GiB	0.09 GiB	0.10 GiB
/o/	11.5 GiB	0.09 GiB	0.09 GiB
/u/	11.5 GiB	0.09 GiB	0.09 GiB

Table 4.2: The comparison of the bottleneck distances between the ordinary method and the proposed method (left) and those between the ordinary method and the witness complex (right) ©2019 IEEE.

Vowel	Proposed Method			Witness Complex		
	0th	1st	2nd	0th	1st	2nd
/a/	0.064	0.644	0.131	0.126	0.645	0.177
/e/	0.029	0.032	0.047	0.026	0.217	0.038
/i/	0.026	0.027	0.014	0.018	0.292	0.034
/o/	0.021	0.068	0.011	0.022	0.279	0.069
/u/	0.016	0.032	0.020	0.015	0.332	0.029

## Chapter 5

# Conclusion

This chapter concludes the studies. The second and the third paragraphs present the conclusion of the study of attractor reconstruction and persistent homology. They are reused from (Tsuji and Aihara, 2019a). The fourth and the fifth paragraphs present the conclusion of the study of the Vietoris-Rips complex of line segments. The former paragraph is reused from (Tsuji and Aihara, 2019b).

The most significant death value can determine the delay that maximizes the hole width of reconstructed attractors of several examples of periodic signals shown in this paper. However, for chaotic signals, the maximum of the most significant death value yields irrelevance. The criterion of Perea and Harer, that the delay  $a$  satisfies  $a = \frac{1}{n} \frac{T}{2}$ , is also good for the Rössler attractor and the Lorenz attractor. The variable  $T$  is the period or a characteristic period of the given signal. Nevertheless, the criterion of Perea and Harer is not suitable for the signal of Japanese vowel /a/, which is periodic with harmonics. For this signal, the maximum of the most significant death value yields good delay for attractor reconstruction. Compared with the most significant death value, the mutual information was found not good for attractor reconstruction. It sometimes returns too small delay, and the delay is only suitable for too low-dimensional embeddings.

Multiple delays may be suitable for practical applications, as the optimal delay depends on the period of the signals, and the period cannot always be assumed. The vineyards (Cohen-Steiner, Edelsbrunner, and Morozov, 2006), which is a continuous set of persistence diagrams, may be useful for applications. However, there is the problem of the computational cost of the persistent homology.

A method that makes computing the persistent homology of time series data faster and smooths the observation noise out was proposed. The proposed method enables practical use of the combination of persistent homology and attractor reconstruction. Moreover, the proposed method brings noise robustness to it. There is an issue whether the classification performance will be improved with the proposed method. More experiments are necessary to show the advantages.

In addition, the sophistication of the method is required. The fitted Bézier curves are not continuous in the present situation. The degrees of the Bézier curves are fixed. It is better that the fitted Bézier curves are continuous and the degrees are chosen automatically.

# Bibliography

- Ali, S., Basharat, A., and Sha, M. (2007). "Chaotic invariants for human action recognition," *2007 IEEE 11th International Conference on Computer Vision*, pp.1-8.
- Baudo, P., Tapia, M., Bennequin, D., and Goillard, J.-M. (2019). "Topological information data analysis," *Entropy*, vol.21, 869.
- Bauer, U. (2019). "Ripser: efficient computation of Vietoris-Rips persistence barcodes", preprint.
- Birman, J.S. and Williams, R.F. (1983). "Knotted periodic orbits in dynamical systems—I: Lorenz's equation," *Topology*, vol. 22, pp. 47-82.
- Borsuk, K. (1948). "On the imbedding of systems of compacta in simplicial complexes," *Fundamenta Mathematicae*, vol.35(1), pp.217-234.
- Buzug, T.M., Reimers, T., and Pfister, G. (1990). "Optimal reconstruction of strange attractors from purely geometrical arguments," *Europhysics Letters*, vol.17, no.7, pp.605-610.
- Buzug, T.M. and Pfister, G. (1992). "Optimal delay time and embedding dimension for delay-time coordinates by analysis of the global static and local dynamical behavior of strange attractors," *Physical Review A*, vol.45, no.10, pp.7073-7084.
- Casdagli, M., Eubank, S., Farmer, J.D., and Gibson, J. (1991). "State space reconstruction in the presence of noise," *Physica D*, vol. 51, pp. 52-98.
- Chazal, F., de Silva, V., and Oudot, S. (2014). "Persistence stability for geometric complexes," *Geometricae Dedicata*, vol. 173(1), pp. 193-214.
- Cohen-Steiner, D., Edelsbrunner, H., and Morozov, D. (2006). "Vines and vineyards by updating persistence in linear time," *Proceedings of the Twenty-second Annual Symposium on Computational Geometry*, pp. 119-126.
- Cohen-Steiner, D., Edelsbrunner, H., Harer, J., and Mileyko, Y. (2010). "Lipschitz functions have  $L_p$ -stable persistence," *Foundations of Computational Mathematics*. vol.10, pp.127-139.
- De Silva, V. and Carlsson, G. (2004). "Topological estimation using witness complexes." In *Proceedings of the First Eurographics Conference on Point-Based Graphics*, Aire-la-Ville, Switzerland, Eurographics Association, pp. 157-166.

- De Silva, V., Morozov, D., and Vejdemo-Johansson, M. (2011a). "Persistent cohomology and circular coordinates," *Discrete and Computer Geometry*, vol.45, pp.737-759.
- De Silva, V., Morozov, D., and Vejdemo-Johansson, M. (2011b). "Dualities in persistent (co)homology," *Inverse Problems*, vol.27, 124003.
- Edelsbrunner, H. and Harer, J.L., (2008). "Persistent homology - a survey." In J. E. Goodman, J. Pach, & R. Pollack (Eds.), *Contemporary Mathematics: Vol. 453. Surveys on Discrete and Computational Geometry*. American Mathematics Society.
- Edelsbrunner, H. and Harer, J.L., (2010). *Computational Topology: An Introduction*, Providence, Rhodeisland, United States, American Mathematical Society.
- Edelsbrunner, H., Letcher, D., and Zomorodian, A. (2002). "Topological persistence and simplification," *Discrete & Computer Geometry*, vol.28(4), pp.511-533.
- Efrat, A., Itai, A., and Katz, M.J., (2001). "Geometry helps in bottleneck matching and related problems," *Algorithmica*, vol.31(1) pp.1-28.
- Emrani, S., Gentimis, T., and Krim, H. (2014a). "Persistent homology of delay embeddings and its application to wheeze detection," *IEEE Signal Processing Letters*, vol.21(4), pp. 459-463.
- Emrani, S., Chintakunta, H., and Krim, H. (2014b). "Real time detection of harmonic structure: A case for topological signal analysis," *ICASSP 2014 - 2014 IEEE International Conference on Acoustics, Speech and Signal Processing (ICASSP)*, Florence, Italy, pp. 3445-3449.
- Fraser, A.M. and Swinney, H.L. (1986). "Independent coordinates for strange attractors from mutual information," *Physical Review A*, vol. 33, no. 32, pp. 1134-1140.
- Garland, J., Bradley, E., and Meiss, J.D. (2016). "Exploring the topology of dynamical reconstructions," *Physica D: Nonlinear Phenomena*, vol. 334, pp. 49-59.
- Grassberger, P., and Procaccia, I. (1983). "Characterization of strange attractors," *Physical Review Letters*, vol. 50, no. 3, pp.346-349.
- Hatcher, A., (2015). *Algebraic Topology*, electronic version.
- Hopcroft, J.E. and Karp, R.M. (1973). "An  $n^{5/2}$  algorithm for maximum matchings in bipartite graphs," *SIAM Journal on Computing*, vol.2(4), pp.225-231.
- Hughes, M.E., Hogenesch, J.B., and Kornacker K. (2010). "JTK\_CYCLE: An efficient nonparametric algorithm for detecting rhythmic components in genome-scale data sets," *Journal of Biological Rhythms*, vol.25, no.5, pp.372-380.
- Judd, K. and Mees, A. (1998). "Embedding as a modeling problem," *Physica D*, vol.120, no.3, pp.273-286.

- Kantz, H. (1994). "A robust method to estimate the maximal Lyapunov exponent of a time series," *Physics Letter A*, vol. 185(1), pp.77-87.
- Khasawneh, F.A. and Munch, E. (2016). "Chatter detection in turning using persistent homology," *Mechanical Systems and Signal Processing*, vol.70-71, pp.527-541.
- Liebert, W., Pawelzik, K., and Shuster, H.G. (1991). "Optimal embeddings of chaotic attractors from topological considerations," *Europhysics Letters*, vol.14, no.6, pp.521-526.
- Lomb, N.R. (1976). "Least-squares frequency analysis of unequally spaced data," *Astrophysics and Space Science*, vol.39, pp.447-462.
- Lorenz, E.N. (1963). "Deterministic nonperiodic flow," *Journal of the Atmospheric Sciences*, vol. 20, no. 5, pp. 130-141.
- McGill, W.J. (1954). "Multivariate information transmission," *Psychometrika*, vol.19, no.2, pp.97-116.
- Mittal, K. and Gupta, S. (2017). "Topological characterization and early detection of bifurcations and chaos in complex systems using persistent homology," *Chaos*, vol.27, 051102.
- Muldoon, M.R., MacKay, R.S., Huke, J.P., and Broomhead, D.S. (1993). "Topology from time series," *Physica D*, vol. 65, pp.1-16.
- Ohyama, G., Deguchi, T., and Kasuya, H. (2011). "Construction of Japanese vowel database uttered by native speakers over a wide range of age", *Proceedings of Spring Meeting of the Acoustical Society of Japan*, 2-P-15(a) [in Japanese].
- Pastva, T.A. (1998). *Bézier Curve Fitting*, (Master's thesis), Naval Postgraduate School, Monterey, California.
- Perea, J.A. and Harer, J. (2015). "Sliding windows and persistence: An application of topological methods to signal analysis," *Foundations of Computational Mathematics*, vol. 15, no. 3, pp. 799-838.
- Pereira, C.M.M. and de Mello, R.F. (2015). "Persistent homology for time series and spatial data clustering," *Expert Systems with Applications*, vol. 42, no. 15, pp. 6026-6038.
- Poincaré, H. (1885). "Sur les courbes définies par les équations différentielles (III)," *Journal de Mathématiques Pures et Appliquées, 4<sup>e</sup> série*, vol. 1, pp. 167-244.
- Reininghaus, J., Huber, S., Bauer, U., and Kwitt, R. (2015). "A stable multi-scale kernel for topological machine learning," In *Proceedings of the IEEE Conference on Computer Vision and Pattern Recognition*. pp. 4741-4748.
- Rosenstein, M.T., Collins, J.J., and de Luca, C.J. (1994). "Reconstruction expansion as a geometry-based framework for choosing proper delay times," *Physica D*, vol.73, no.1, pp.82-98.

- Rössler, O.E. (1976). "An equation for continuous chaos," *Physical Letter A*, vol. 57, no. 5, pp. 397-398.
- Saltzman, B. (1962). "Finite amplitude free convection as an initial value problem – I," *Journal of the Atmospheric Science*, vol. 19, no. 4, pp. 329-341.
- Scargle, J.D. (1982). "Studies in astronomical time series analysis. ii. statistical aspects of spectral analysis of unevenly spaced data," *Astrophysical Journal*, vol.263, pp.835-853.
- Sciamarella, D. and Mindlin, G.B. (1991). "Topological structure of chaotic flows from human speech data," *Physical Review Letters*, vol. 82, 1450.
- Sciamarella, D. and Mindlin, G.B. (2001). "Unveiling the topological structure of chaotic flows from data," *Physical Review E*, vol. 64, 036209.
- Seversky, L.M., Davis, S., and Berger, M. (2016). "On time-series topological data analysis: New data and opportunities," *CVPRW 2016 - 2016 IEEE International Conference on Computer Vision and Pattern Recognition Workshops*, Las Vegas, Nevada, United States, pp. 1014-1022.
- Shao, L. and Zhou, H. (1996). "Curve fitting with Bézier cubics," *Graphical Models and Image Processing*, vol. 58, no. 3, pp. 223-232.
- Sheehy, D. (2013). "Linear-size approximations to the Vietoris-Rips filtration," *Discrete and Computational Geometry*, vol.49, pp.778-796.
- Skraba, P., de Silva, V., and Vejdemo-Johansson, M. (2012). "Topological analysis of recurrent systems," In *NIPS 2012 Workshop on Algebraic Topology and Machine Learning, December 8th, Lake Tahoe, Nevada*, pp. 1-5.
- Small, M. and Tse, C.K. (2004). "Optimal embedding parameters: a modeling paradigm," *Physica D*, vol.194, no.3, pp.283-296.
- Strogatz, S.H. (2014). *Nonlinear Dynamics and Chaos*, Westview Press.
- Takens, F. (1981). "Detecting strange attractors in turbulence." In D. Rand & L.S. Young (Eds.), *Dynamical Systems and Turbulence*, Warwick 1980. *Lecture Notes in Mathematics*, vol 898. Springer, Berlin, Heidelberg.
- Tamura, I. (2015). *Topology*, Tokyo, Iwanami Shoten.
- Tsankov, T.D. and Gilmore, R. (2003). "Strange attractors are classified by bounding tori," *Physical Review Letters*, vol. 91, 134104.
- Tsankov, T.D. and Gilmore, R. (2004). "Topological aspects of the structure of chaotic attractors in  $\mathbb{R}^3$ ," *Physical Review E*, vol. 69, 056204.
- Tsuji, S. and Aihara, K. (2019a). "Criterion for determining the optimal delay of attractor reconstruction using persistent homology," *Nonlinear Theory and Its Applications*, vol. 10, no. 1, pp. 74-89.
- Tsuji, S. and Aihara, K. (2019b). "A fast method of computing persistent homology of time series data," *ICASSP 2019 - 2019 IEEE International Conference on Acoustics, Speech and Signal Processing (ICASSP)*, Brighton, United Kingdom, pp. 3462-3466.

- Umeda, Y. (2017). "Time series classification via topological data analysis," *Transactions of the Japanese Society for Artificial Intelligence*, vol. 32, no. 3, pp. 4150-4154.
- Vejdemo-Johansson, M. (2008). "Sketches of platypus: A survey of persistent homology and its algebraic foundations." In U. Tillmann, S. Galatius, & D. Sinha (Eds.), *Contemporary Mathematics: Vol. 620. Algebraic Topology: Applications and New Directions*. American Mathematics Society.
- Van der Pol, B. (1926). On "relaxation-oscillations", *The London, Edinburgh, and Dublin Philosophical Magazine and Journal of Science*, 2:11, pp. 978-992.
- Venkataraman, V. and Turaga, P. (2016a). "Shape distributions of nonlinear dynamical systems for video-based inference," *IEEE Transactions on Pattern Analysis and Machine Intelligence*. vol.38, no.12, pp.2531-2543.
- Venkataraman, V., Ramamurthy, K.N., and Turaga, P. (2016b). "Persistent homology of attractors for action recognition," *ICIP 2016 - 2016 IEEE International Conference on Image Processing (ICIP)*, Phoenix, Arizona, United States, pp. 4150-4154.